공학박사학위논문

Effect of substrate and processing parameter on the thermochromic properties of VO_2 thin film for smart window application

기판과 공정변수가 스마트 윈도우 적용을 위한 이산화바나듐 박막의 열변색 특성에 미치는 영향

2013년 8월

서울대학교 대학원

재료공학부

구 현

Effect of substrate and processing parameter on the thermochromic properties of VO_2 thin film for smart window application

지도교수 박 찬

이 논문을 공학박사 학위논문으로 제출함

2013년 8월

서울대학교 대학원

재료공학부

구 현

구현의 박사학위 논문을 인준함

2013년 8월

위 원 장	유 상 임	(인)
부 위 원 장	박 찬	(인)
위 원	박 은 수	(인)
위 원	장 세 홍	(인)
위 원	이 시 무	(인)

Abstract

Effect of substrate and processing parameter on the thermochromic properties of VO_2 thin film

Hyun Koo

Department of Materials Science and Engineering

The Graduate School

Seoul National University

Vanadium dioxide (VO_2) thin films were deposited by pulsed laser deposition method and radio frequency magnetron sputtering on various single crystal or buffered soda lime glass substrates in order to investigate the effect of the substrate and the processing parameter on the thermochromic properties of VO_2 thin film.

First, VO_2 thin films were deposited on c-cut sapphire and MgO (111) substrate using pulsed laser deposition method in order to investigate the effect of lattice

misfit between the thin film and the substrate on the transition temperature of VO_2 thin film. All vanadium dioxide thin films showed heteroepitaxial growth with (002) preferred orientation. VO_2/c-sapphire and VO_2/MgO(111) had different transition temperatures, regardless of the thickness, orientation, and deposition conditions of the thin film. These results suggest that considering lattice mismatch between thin film and substrate is another promising option for controlling transition temperature of VO_2 thin films.

Second, VO_2 thin films were deposited on soda lime glass substrates with silicon nitride sodium-diffusion barrier layer as diffusion barrier, in order to investigate the effect of sodium ion diffusion on the formation of VO_2. SiN_x layers with thicknesses over 30 nm were found to successfully prevent sodium ion diffusion in VO_2 thin film and also contribute to the formation of VO_2 thin film, which was confirmed by XRD spectra and XPS measurements. The change of infrared transmittance at 2500 nm wavelength with temperature change from room temperature to 80^{o}C was increased significantly, and the optical hysteresis width of the sample decreased by almost 6K as well. The results suggest that applying diffusion barrier can improve the thermochromic properties of the VO_2 films for energy-saving smart coatings, and silicon nitride can be one of the effective materials to prevent sodium ion diffusion.

Third, VO_2 thin films were deposited on soda lime glass substrates with ZnO,

TiO_2, SnO_2 and CeO_2 thin films applied as buffer layers between the VO_2 films and the substrates in order to investigate the effect of buffer layer on the formation and the thermochromic properties of VO_2 film. Buffer layers with thicknesses over 50 nm were found to affect the formation of VO_2 film, which was confirmed by XRD spectra. By using ZnO, TiO_2 and SnO_2 buffer layers, monoclinic VO_2 (VO_2(M)) film was successfully fabricated on soda lime glass at 370^{o}C. On the contrary, films of VO_2 (B) which is known to have no phase transition near room temperature was formed rather than VO_2 (M) when the film was deposited on CeO_2 buffer layer at the same film deposition temperature. The excellent thermochromic properties of the films deposited on ZnO, TiO_2 and SnO_2 buffer layers were confirmed from the temperature dependence of electrical resistivity from room temperature to 80^{o}C. Especially, due to the tendency of ZnO thin film to grow with high degree of preferred orientation on soda lime glass at low temperature, the VO_2 film deposited on ZnO buffer layer exhibits the best thermochromic properties compared to those on other buffer layer materials used in this study. These results suggest that deposition of VO_2 films on soda lime glass at low temperature with excellent thermochromic properties can be achieved by considering the buffer layer material having structural similarity with VO_2. Moreover, the degree of crystallization of buffer layer is also related with that of VO_2 film, and thus ZnO can be one of the most effective buffer layer materials.

Finally, the VO_2 films were deposited on fused silica with different sputtering power of 200W, 300W, and 400W. The grain size of each sample was calculated and measured using XRD, Scherrer's formula, and TEM analysis. As the sputtering power increases, the grain size of VO_2 film decreased. Hysteresis width can be affected by the grain size of the VO_2 film. Hysteresis width tends to decrease while increasing sputtering power. The results suggest that grain size can be controlled by changing sputtering power, and can effectively control the hysteresis width of the VO_2 film.

Keywords: Vanadium oxide, Thermochromic coatings, Thermochromism, Metal-insulator transition, Pulsed laser deposition, Radio frequency magnetron sputtering, Thermochromic properties, Lattice misfit; Transition temperature, Sodium ion diffusion, Diffusion barrier, Buffer layer, RF power, Grain size, Microstructure, Hysteresis width

Student Number: 2007-30801

Table of Contents

List of Figures

List of Tables

Chapter 1. General Introduction

Vanadium dioxide(VO_2) has been one of the most extensively studied material that shows a metallic-to-insulating phase transition since the first report in 1959 by F.J. Morin[1]. It is well-known that VO_2 shows first-order phase transition at a certain critical temperature(T_c).[2] At temperature higher than the critical temperature T_c which is 340K, it shows tetragonal-rutile structure(VO_2(R)) with high electrical conductivity, while below T_c, it shows monoclinic structure (VO_2(M)) with electrical insulating property. Through this reversible metal-to-insulator transition(MIT) near room temperature, VO_2 shows abrupt change in conductivity over three orders of magnitude.

VO_2 also undergoes an ultrafast (~ 10^2 femtoseconds) transition when excited by a laser, and it shows metallic behavior under application of high electric-field (~10^6 V/cm).[3,4,5] This first-order MIT of VO_2 near room temperature has been widely studied over the last fifty years, yet the physics behind this intriguing phenomenon is not fully understood. The characteristics associated with MIT in VO_2 are fascinating scientifically, letting VO2 to have immense technological importance

for potential applications in thermochromic windows, sensor and memory type applications.[6,7,8,9]

The MIT in VO_2 is generally characterized by sharpness of transition ΔS, over which electrical and optical property changes are completed, amplitude ΔA, and width of thermal hysteresis ΔH. These characteristics of VO_2 thin films, which will be described as thermochromic properties in this dissertation, have been known to be a strong function of microstructure (grain size, grain size distribution, and grain boundary characteristics) and chemistry (stoichiometry, dopant and/or other defects). However, the individual effect of these factors on the thermochromic properties is not well understood as films studied in most of these cases were either polycrystalline or had other oxide phases (e.g. V_2O_5 or V_2O_3) or dopants present in the films which can produce a combined effect of all these parameters in modification of thermochromic properties.[10,11,12,13]

The typical deposition temperature for the growth of high-quality VO_2 thin films with good thermochromic properties definitely exceeds the transition temperature which is close to 340K(68℃). Following the deposition at elevated temperatures, when films are cooled to ambient temperature, VO_2 crystal structure transforms from tetragonal ($P_{42/mnm}$) to monoclinic ($P_{21/c}$). It is important, therefore, to understand as to how the tetragonal unit cell arranges itself on the underlying template of substrate or buffer layer material. Understanding the details of epitaxy

is important from the fundamental understanding to develop methodology to tailor the thin film strain/stress, and as a result, MIT characteristics suited to a particular application. In this dissertation, a model for calculating lattice misfit of epitaxially grown VO_2 thin film is established on both sapphire and magnesium oxide single crystal substrate. With the use of atomic arrangements in the unit cells of tetragonal and monoclinic VO_2 and in both sapphire and magnesium oxide, change in MIT characteristics of VO_2 thin film has been explained.

The MIT in VO_2 involves a small lattice distortion along c-axis direction, which results in pairing of vanadium atoms and a distinct band structure in each phase. These distortions result in failure of VO_2 bulk single crystals when subjected to repeated heating and cooling cycles. Therefore, thin films and nanoparticles of VO_2, which are able to withstand these distortions and dissipate heat through the substrate, are critical to a variety of technological applications. Recent advances in expertise of thin films growth techniques have allowed to explore the technological potential that the multifunctional strongly-correlated materials, such as VO_2, have to offer. To date, most of the researches on VO_2 thin films have focused on growth of epitaxial films with controlled properties on Al_2O_3 and TiO_2 substrates[14,15,16,17]; however, implementation of VO_2-based devices is restricted by the limited use of single crystal substrates in the smart window industry. One of the essential prerequisites to the development of smart window based on thermal switching is

the development of methods that enable integration of VO_2 films on soda lime glass, which is the conventional substrate material in the glass industry. Though the epitaxial growth of VO_2 on single crystal substrate can be anticipated via domain matching epitaxy[18], in which integral multiples of planes match across the film-substrate interface, direct deposition of VO_2 on soda lime glass remains a technological challenge. One challenge associated with direct deposition of VO_2 on soda lime glass is the diffusion of alkali ions into the vanadium dioxide layers, which can lead to the formation of sodium vanadate that can decrease the switching behavior of VO_2 thin film.[19]

Therefore, there is a major challenge in producing VO_2 thin films of correct structure, stoichiometry and controlled microstructures, especially high-quality single crystal films, which can be used to establish comprehensive structure-property correlations. In this dissertation we have addressed the integration of highly crystallized VO_2 thin films with soda lime glass substrates by using various buffer layers. Silicon nitride was selected as a sodium ion diffusion barrier material. Oxide materials such as ZnO, TiO_2, SnO_2 and CeO_2 were selected as a buffer layer material in order to investigate the effect of buffer layer material on the formation and crystallization of VO_2 thin film, which can contribute to improve the thermochromic properties, e.g. T_c, ΔS, ΔA, and ΔH.

To establish the correlation of characteristics of grain boundaries, relative

orientation, grain size and defects within the grains with MIT of VO_2 thin films, films were deposited in the conditions of limiting other experimental conditions except the substrates (chapter 5), buffer layers (chapter 6,7), and the deposition power (chapter 8). It was shown that not only the thin film epitaxy but also the microstructure of VO_2 thin film can play critical role in determining the characteristics of the hysteresis and the nature of the MIT. Electrical and optical properties of VO_2 thin films were studied systematically to correlate MIT characteristics with microstructural properties of the films.

Rest of the thesis is organized into the following chapters:

Chapter 2: Background knowledge pertinent to this dissertation is presented.

Chapter 3: Reviews of previously reported literatures related with this study are introduced.

Chapter 4: Experimental techniques and characterization methods used in this dissertation are introduced.

Chapter 5: Details of epitaxial relationship between VO_2 thin films and c-sapphire or MgO substrates are presented.

Chapter 6: Study of the role of silicon nitride diffusion barrier and the thermochromic properties of VO_2 thin film on silicon nitride buffered soda lime glass are presented.

Chapter 7: Results from the effect of various oxide buffer layer on the formation of

VO_2 thin film are presented and correlated with MIT characteristics.

Chapter 8: Study of the effect of sputtering power on the thermochromic properties of VO_2 thin films has been presented.

Chapter 9: A brief summary of the present work is provided. Scope for future work is discussed.

1.1 References

[1] F.J. Morin, *Oxides which show a metal-to-insulator transition at the Neel temperature*, Phys. Rev. Lett. 3 (1959) 34

[2] J.B. Goodenough, *The two components of the crystallographic transition in VO_2*, J. Solid. State. Chem. 3 (1971) 490

[3] P. Jin and S. Tanemura, *Relationship between transition temperature and x in $V_{1-x}W_xO_2$ films deposited by dual-target magnetron sputtering*, Jpn. J. Appl. Phys. 34 (1995) 2459

[4] C.N. Berglund and A. Jayaraman, *Hydrostatic-pressure dependence of electronic properties of VO_2 near semiconductor-metal transition temperature*, Phys. Rev. 185 (1969) 1034

[5] A. Cavalleri, T. Dekorsy, H. H. W. Chong, J. C. Kieffer, R. W. Schoenlein, *Evidence for a structurally-driven insulator-to-metal transition in VO_2: A view from the ultrafast timescale*, Phys. Rev. B 70 (2004) 161102

[6] F. Chudnovskiy, S. Luryi, B. Spivak, *Future Trends in Microelectronics: The Nano Millennium*, In: S. Luryi, J. M. Xu, A. Zaslavsky (Eds), Wiley Interscience, New York (2002) 148–155

[7] D. M. Newns, J. A. Misewich, C. C. Tsuei, A. Gupta, B. A. Scott, A. Schrott, *Mott transition field effect transistor*, Appl. Phys. Lett. 73 (1998) 780

[8] H. Wang, X. Yi, S. Chen, X. Fu, *Fabrication of vanadium oxide micro-optical switches*, Sens. Actuators A Phys. 122 (2005) 108

[9] M. J. Lee, Y. Park, D.S. Suh, E.H. Lee, S. Seo, D.C. Kim, R. Jung, B.S. Kang, S.E. Ahn, C.B. Lee, D.H. Seo, Y.K. Cha, I.K. Yoo, J.S. Kim, B.H. Park, *Two Series Oxide Resistors Applicable to High Speed and High Density Nonvolatile Memory*, Adv. Mater. 19 (2007) 3919

[10] Y.L. Wang, M.C. Li, L.C. Zhao, *The effects of vacuum annealing on the structure of VO_2 thin films*, Surface and Coatings Technology 201 (2007) 15

[11] O. Ya. Berezina, A.A. Velichko, L.A. Lugovskaya, A.L. Pergament and G.B. Stefanovich, *Metal-semiconductor transition in nonstoichiometric vanadium dioxide films*, Inorganic Materials 43 (2007) 505

[12] W. Yin, S. Wolf, C. Ko, S. Ramanathan, and P. Reinke, *Nanoscale probing of*

electronic band gap and topography of VO_2 thin film surfaces by scanning tunneling microscopy, J. Appl. Phys. 109 (2011) 024311

[13] G. Fu, A. Polity, N. Volbers, B.K. Meyer, *Annealing effects on VO_2 thin films deposited by reactive sputtering*, Thin Solid Films 515 (2006) 2519

[14] D.H. Youn, H.T. Kim, B.G. Chae, Y.J. Hwang, J.W. Lee, S.L. Maeng, and K.Y. Kang, *Phase and structural characterization of vanadium oxide films grown on amorphous SiO_2/Si substrates*, J. Vac. Sci. Technol. A22 (2004) 719

[15] Z. Yang, C. Ko, and S. Ramanathan, *Metal-insulator transition characteristics of VO_2 thin films grown on Ge(100) single crystals*, J. Appl. Phys. 108 (2010) 073708

[16] Y. Muraoka and Z. Hiroi, *Metal–insulator transition of VO_2 thin films grown on TiO_2 (001) and (110) substrates*, Appl. Phys. Lett. 80 (2002) 583

[17] K. Nagashima, T. Yanagida, H. Tanaka, and T. Kawai, *Interface effect on metal-insulator transition of strained vanadium dioxide ultrathin films*, J. Appl. Phys. 101 (2007) 026103

[18] J. Narayan and B. C. Larson, *Domain epitaxy: A unified paradigm for thin film growth*, J. Appl. Phys. 93 (2003) 278

[19] G. Guzman, R. Morineau, J. Livage, *Synthesis of vanadium dioxide thin films from vanadium alkoxides*, Mat. Res. Bull. 29 (1994) 509.

Chapter 2. General background

2.1 Smart windows

The air conditioning in summer and heating systems in winter nowadays are applied in various ways that they have become very essential for mankind to maintain comfortable working and living environments. This leads to an increase in the use of electricity, a concurrent increase in carbon dioxide emissions and other atmospheric pollutants formed in the electricity generation process. The increased use of air conditioning and heating systems comes with the increase in the emission of greenhouse gases. Technology is thus required that can reduce the use of air conditioning and heating in commercial and residential buildings to help reduce the use of energy. Solar-control coatings on windows can help the windows in commercial/residential buildings to play an active role in the enhancement of energy efficiency of the buildings.[1]

Smart materials cover a wide range of technologies. A particular type of smart

material can be used for large area glazing in buildings, automobiles, planes, and electronic display. These technologies consist of electrically-driven media including electrochromism, light responding photochromism, and heat responding thermochromism. The detailed information of smart windows will be described in this chapter and the comparison between each type of smart window will be shown in Table 2-1.

2.1.1 Photochromics

Photochromic windows respond to changes in light, much like sunglasses that darken when you move from a dim light to a bright one (Figure 2-1). While this type of technology may seem like a good idea, it has its drawbacks for saving energy. Photochromic windows work well to reduce glare from the sun, however, they cannot control heat gain, mainly because the amount of light that strikes a window does not necessarily correspond to the amount of solar heat it absorbs. Because the sun is lower in the sky during the winter, for example, the rays may arrive to the window more intensely in the cold season than in the summer, when the sun is higher in the sky. In this case, a photochromic window would darken more in the winter than in the summer, although winter is the time when gaining solar heat would be beneficial. Another problem is that, while this technology

works fine on small, eyeglass-sized pieces of glass, it has yet to be done successfully on a large-scale, commercial level for window-sized pieces.

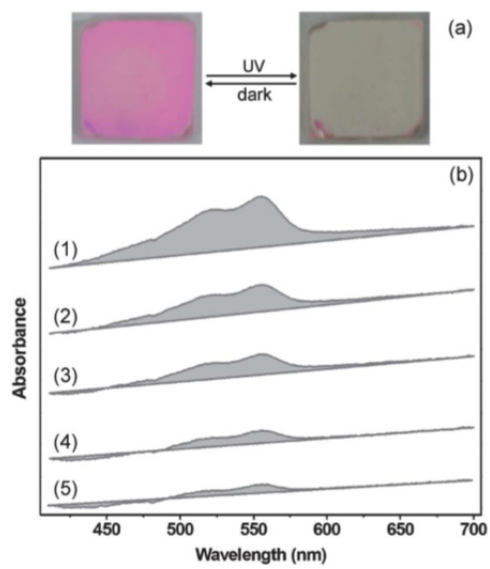

Figure 2-1 (a) Photographic images of the BSP/JUC-120 film with and without external UV irradiation, (b) UV-Vis spectra of the BSP/JUC-120 film before (1) and after the UV irradiation at different times ((2): 2 min, (3): 5 min, (4): 10 min, 5): 20 min).[2]

2.1.2 Electrochromics

Electrochromic devices are the most popular technology for large area switching devices. Since the first electrochromic devices made by Deb in 1969[3], electrochromic devices were being developed for displays and switchable mirrors in cars, which continue as a viable product to nowadays. Recently, several companies began developing devices for glazing applications, and the researches are still in progress.

Electrochromic materials, which change their optical properties in response to an electric field and can be returned to their original state by a field reversal, have major advantages as follows:

• A small switching voltage (1-5 V);

• Show specular reflection;

• Possess a gray scale;

• Require power only during switching;

Typical electrochromic devices have upper visible transmission of T_v = 70-50% and fully colored transmission of T_v = 25-10%. It is possible to lower the levels of transmittance as low as 1%. The range of shading coefficients (SC) for electrochromics is about 0.67-0.60 for the bleached state, and 0.30-0.18 for the fully colored state.

Electrochromic glazing has an interesting attractiveness, however, it has some

subtle complexities. The complexity comes from the fact that it has the structure of a transparent battery with a relatively thin large-area planar electrode. It differs from a battery in that the electrochromic is transparent, with very little optical scatter. Typically, coloration ions such as Li^+, H^+, and Ag^+ are used. An example of a Li^+ intercalation reaction for a cathodic coloring material is as follows:

WO_3 (colorless) + yLi^+ + ye^- ↔ Li_yWO_3 (blue)

A complementary anodic nickel vanadium oxide reaction is:

$Li_yNi_zV_{2-z}O_5$ - yLi^+ (light gray) - ye^- ↔ $Ni_zV_{2-z}O_5$ (colorless)

The electrochromic binary inorganic oxides which have generally used are WO_3 (the most commonly used), NiO, IrO_x, V_2O_5, and MoO_3.[4,5] An electrochromic glazing device must have an ion-containing material (electrolyte) in close proximity to the electrochromic layer, as well as transparent layers for setting up a distributed electric field. Electrochemical stability can be increased by using interfacial layers. Devices are designed to let ions move through the electrochromic layer back and forth with applied potential. Electrochromic glazing can be fabricated from five (or less) layers consisting of two transparent conductors, an electrolyte or ion conductor, a counter electrode, and an electrochromic layer, as shown in Figure 2-2.

Commercially, viologen derivatives are the most widely used organic electrochromics. Organic electrochromics tend to suffer from problems with

secondary reactions during switching, but more stable organic systems have been developed, in particular, by Gentex. Some other companies are now researching polymer materials and flexible films. Devices based on poly(3,4-ethylenedioxythiophene) or PEDOT have shown 60% luminous transmission change.[6]

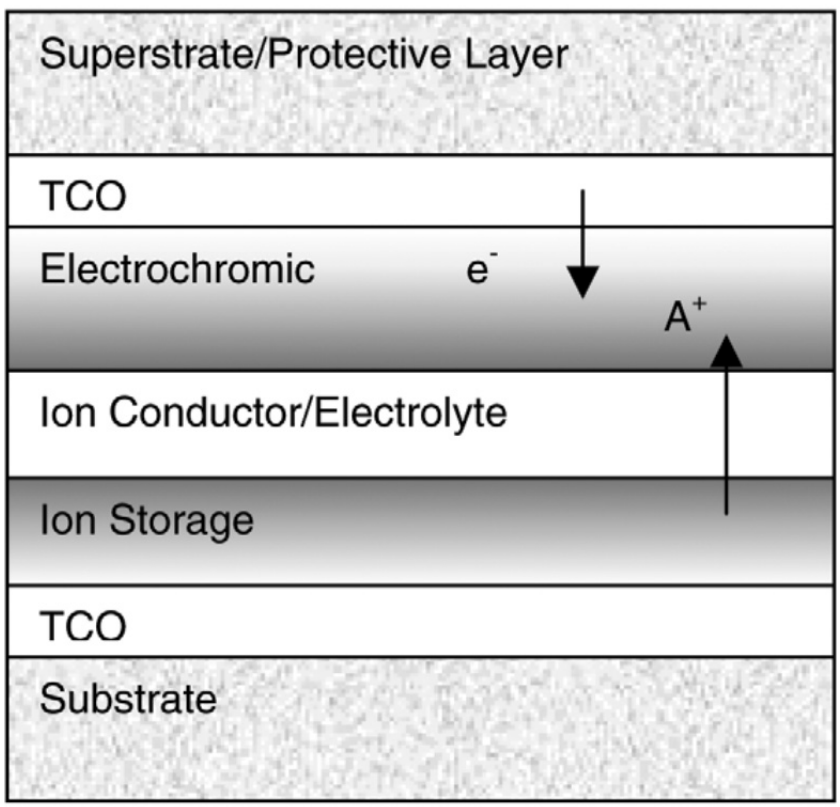

Figure 2-2. Schematic of the layer structure of an electrochromic window[7]

2.1.3 Thermochromics

The further development of smart window is thermochromism smart window, which can automatically change only its infrared optical transmittance/reflectance with temperature without consuming other extra energy. The term ‘thermochromic’ is generally used for referring both thermotropic and thermochromic. However, for convenience, thermochromic windows based on hydrogels and polymer blends will be called as thermotropic, whereas those based on oxide thin film will be called as thermochromic in this dissertation.

Thermotropics, which exhibit large physical changes at certain temperatures, have also been studied and developed for glazing. These materials appear clear at lower temperatures, but become opaque at higher temperatures. They can be used for skylights, inclined glazing, and upper windows where view is not important. They can be totally passive, changing with ambient temperature for solar heating. Some designs use a resistive heating layer made from thin film metals or transparent conductors, which enables electrical control of the physical change. Most thermotropics are based on hydrogels, and polymer blends have been studied for higher temperature performance. One example of a thermotropic polymer gel is polyether/ethylene oxide/carboxyvinyl. Figure 2-3 shows examples of thermotropic

windows in the off- and on-state. The technical problems with the hydrogels, however, are cyclic lifetime and inhomogeneity during switching.

For a thermochromic smart window, the thermochromic material would be coated on the glass surface, and then it works due to the thermochromism of the coating layer. The change of optical properties with temperature is usually related to a structural phase change on passing through a critical temperature, T_c. At temperature below T_c, the material is relatively transparent in visible light and infrared range. This allows most of the solar radiation to pass through the window maximizing the heating effect of the sunlight and blockbody radiation within the building, keeping the interior warm. At temperatures above T_c, the thermochromic coating becomes infrared reflective, preventing thermal radiation from excessively heating the building interior while remaining visually transparent, enabling the optimum use of natural light. Minimizing the use of internal lighting also reduces building maintenance costs.[1]

Many materials have such switching properties, and some of them are summarized in Table 2-2. By far, Vanadium dioxide(VO_2) has been the most widely studied, since the early demonstration of resistivity switching in bulk by Morin.[8] The near proximity of the transition temperature to room temperature, at 68℃, is the most important reason.

Figure 2-3. ThermoSEE thermotropic glazing. The off-state is shown on the left and the heated on-state is shown on the right. (Credit: F. Millett, Pleotint, USA.)[7]

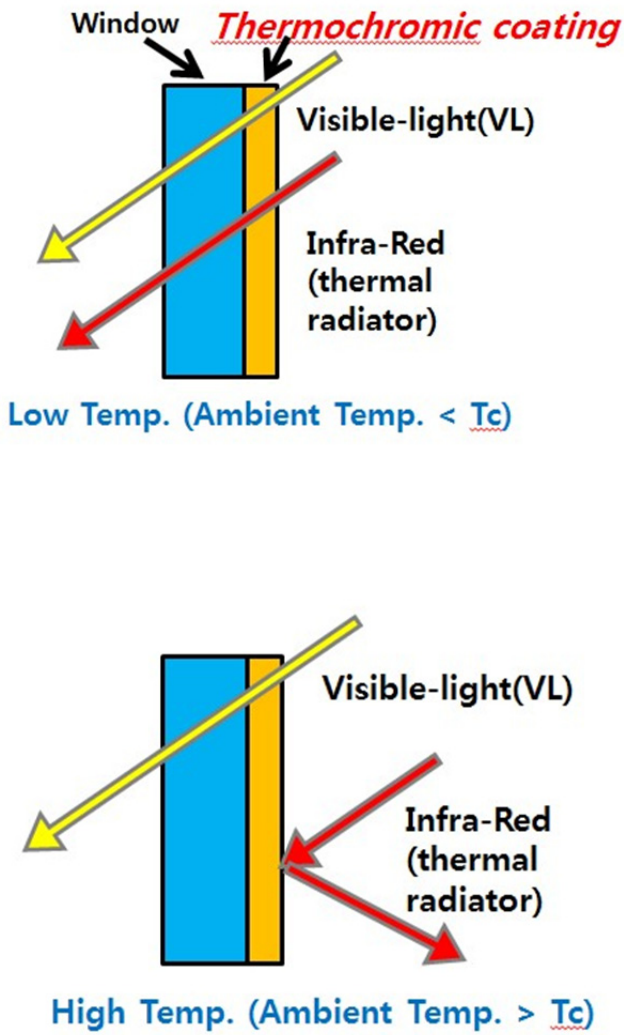

Figure 2-4 Schematic illustration of thermochromic smart window

Table 2-1. Comparison of various smart windows.

	Photo-chromic	**Electro-chromic**	**Thermo-chromic**
Source	Solar ray	Electric power	Heat
VIS Transparency	Changes Automatically	Changes Manually	Always Transparent
Operating Type	-	Manual	-
Weak Points	Not efficient during winter	Blocks VIS during Thermal Insulation	High IR Transmittance @High Temp.
Remarks	-	Requires Additional Energy	-

Table 2-2. Bulk solids and films exhibiting resistivity transitions[9]

Compound	Type of transition[a]	Form of compound	T_c[b] (°C)	Best ρ_{nm}/ρ_m[c]
VO_2	(Monoclinic/tetragonal)	Single crystal	68	10^4
		Film	68	10^4
V_2O_3	(Monoclinic/rhombohedral)	Single crystal and polycrystal	−123	10^7
		Film	≈ −134	10^6
Fe_3O_4	(Orthorhombic/cubic)	Single crystal and polycrystal	−154	10^2
Ag_2S	(Monoclinic/cubic)	Polycrystal	180	10^2-10^3
		Film (<2000 nm)	178	10^2-10^3
FeS	(Tetragonal/hexagonal)	Single crystal	157	10^3
NiS(hexagonal)	(Antiferromagnetic/paramagnetic)	Single crystal and polycrystal	−9	$<10^2$
$Sm_{1-x}Ln_x{}^{3+}S$	Sm^{2+}/Sm^{3+}	Well-crystallized bulk	[d]	—

[a]Expressed as the states at a low temperature/high temperature.
[b]Transition temperature.
[c]Ratio of the resistivity ρ_{nm} of the non-metallic state to the resistivity ρ_m of the metallic state.
[d]Dependent on the particular lanthanide and concentration.

2.2 Vanadium dioxide(VO_2)

Vanadium dioxide(VO_2) is well-known for its first-order phase transition at a certain critical temperature(T_c), as shown in Figure 2-5.[8] At temperature higher than the critical temperature T_c which is 340K, it shows tetragonal-rutile structure(VO_2(R)) with high electrical conductivity, while below T_c, it shows monoclinic structure (VO_2(M)) with electrical insulating property(Figure 2-6, 2-7).[10] Through this reversible metal-to-insulator transition(MIT) near room temperature, VO_2 shows abrupt change in conductivity over three orders of magnitude. Such property change made VO_2 to be considered as a material having high potentials for various applications, such as electronic switches, thermal sensors, and thermochromic smart windows.[11,12,13,14]

VO_2 also undergoes an ultrafast (~ 10^2 femtoseconds) transition when excited by a laser and exhibits metallic behavior under application of high electric-field (~10^6 V/cm).[15,16,17] This first-order MIT near room temperature has been widely studied over the last fifty years, yet the physics behind this intriguing phenomenon is not fully understood. The characteristics associated with MIT in VO_2 are fascinating scientifically, which let VO_2 have immense technological importance for potential applications in sensor- and memory-type applications.[18,19,20,21]

The MIT in VO_2 involves a small lattice distortion along c-axis direction, which results in pairing of vanadium atoms and a distinct band structure in each phase (Figure 2-7). These distortions result in failure of VO_2 bulk single crystals when subjected to repeated heating and cooling cycles.[22] Therefore, thin films and nanoparticles of VO_2, which are able to withstand these distortions and dissipate heat through the substrate, are necessary when applying VO_2 to various technologies.

The metal-to-insluator transition in VO_2 is characterized by abrupt orders of magnitude change in resistivity and increased reflectivity for infra-red light wavelengths (0.8-2.2 μm).[8,23,24] Being a transition-metal oxide with narrow d-electron bands, MIT in VO_2 is extremely sensitive to small changes in extrinsic parameters such as pressure or doping.[15,16] In bulk single crystals, the change in resistivity can be ~10^3-10^5, with a hysteresis width of ~1^{o}C.[8,25] On the other hand, hysteresis widths in thin films and in nanostructures are within the range of 3-10^{o}C and 30-35^{o}C, respectively.[26,27]

Thin films and nanoparticles tend to better withstand the repeated thermal cycling, and also the transition temperature can be lowered to room temperature by doping. Recent advances in thin film growth techniques and device fabrication methods have triggered numerous recommendations for technological applications of VO_2, such as, thermally activated optical switching and limiting,[28,29] thermal relays and

energy management devices,[30,31] sensors and actuators,[32] micro-bolometers,[33,34] electrochromic and photochromic memory and optical devices[35,36]. Two and three terminal devices utilizing the electric field induced switching of VO_2 is also an active area of research.[37,38] A recent study[39] has found that, materials synthesis, especially the VO_2/gate dielectric interface, plays an immensely important role in the response to the gate voltage, and thus controls the functioning of such electrically controlled devices.

Figure 2-8 shows the phase diagram for the vanadium-oxygen system.[40] It can be seen that there are as many as 15 to 20 other stable vanadium oxide phases, such as, V_6O_9, V_6O_{13}, V_7O_{13} and others that exhibit no semiconductor-to-metal transitions. The existence of these stable competing oxides presents a particular challenge to the growth of VO_2 in both bulk and thin film form. Therefore, to achieve optimum thermochromic properties, an elaborate synthesis procedure is required to ensure the formation of VO_2 and to avoid other undesirable vanadium oxide phases. Thin films of VO_2 have been deposited using several techniques, such as, reactive evaporation,[41,42] sputtering,[43,44] metal-organic chemical vapor deposition (MOCVD),[45,46] pulsed–laser deposition (PLD),[47,48] and sol-gel deposition.[49,50]

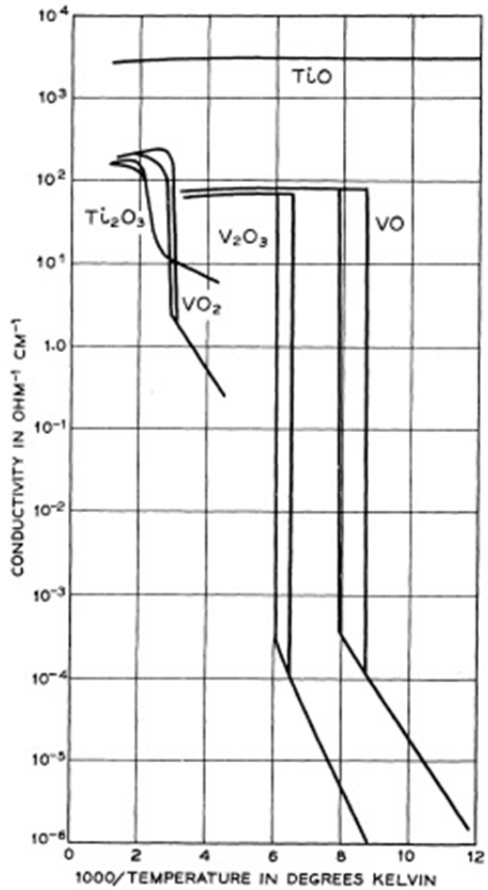

Figure 2-5 Conductivity as a function of reciprocal temperature for the lower oxides of titanium and vanadium.[8]

(a)

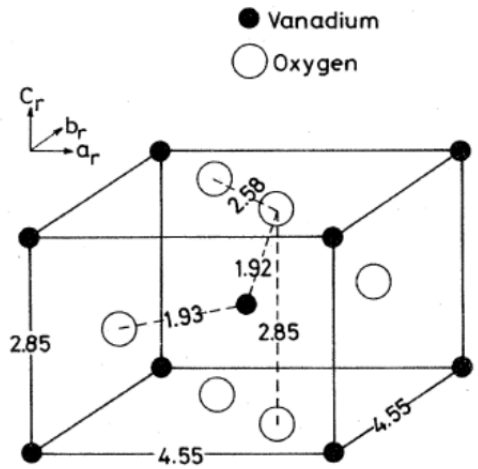

(b)

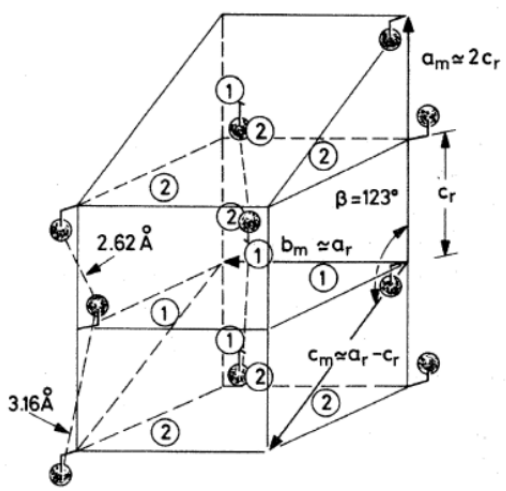

Figure 2-6. Schematic illustration of lattice of the two structural phases of VO_2: (a) tetragonal rutile, (b) monoclinic structure[51]

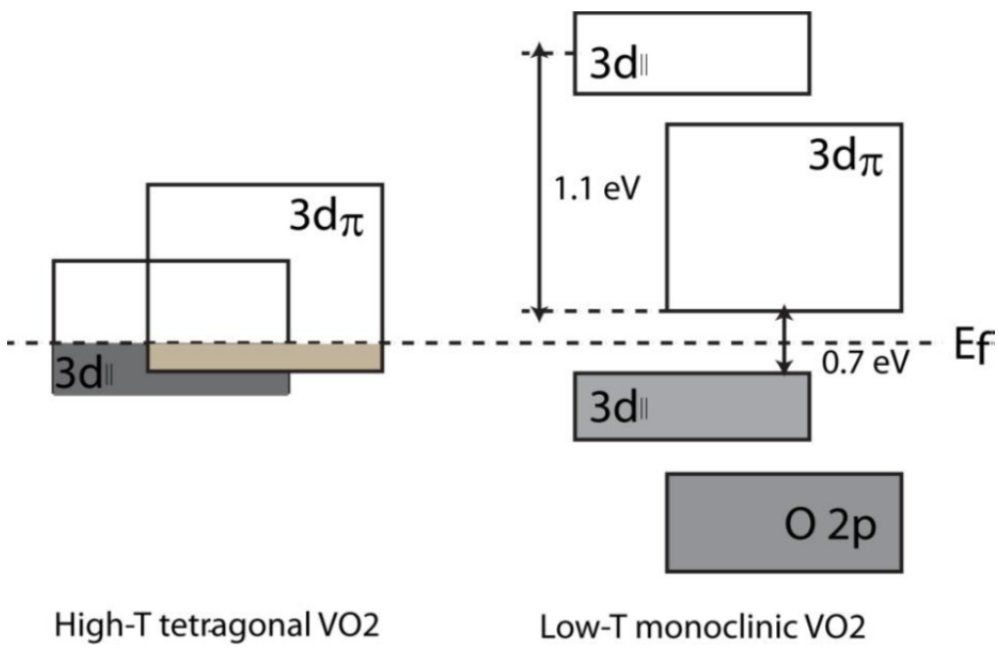

Figure 2-7. Schematic of one-electron band structure of tetragonal rutile (left) and monoclinic (right) VO_2[10]

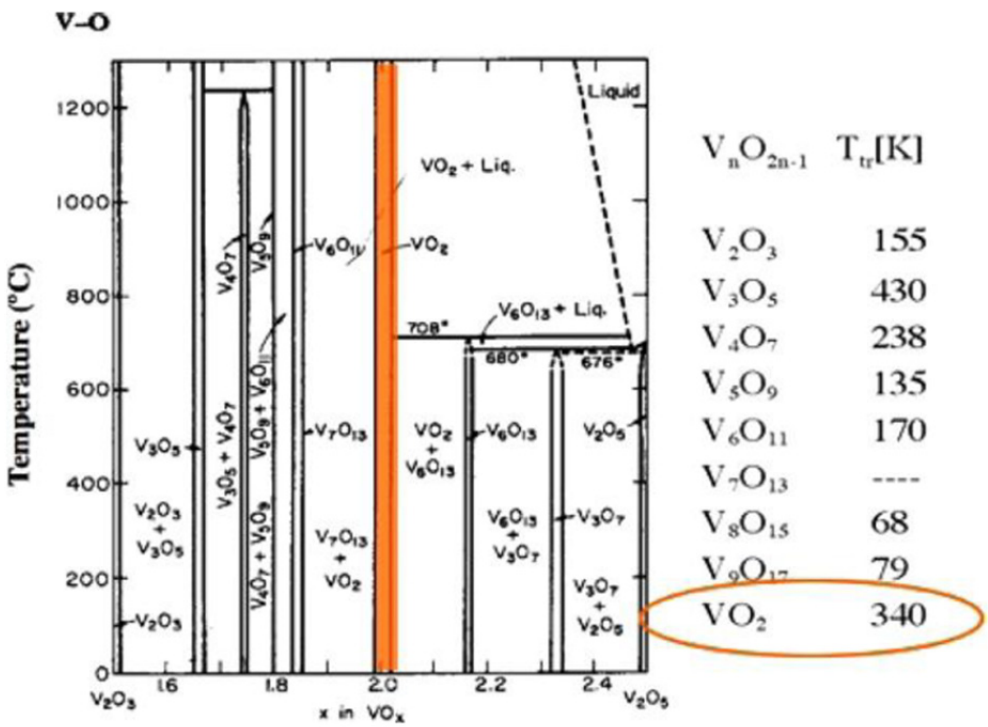

Figure 2-8. Phase diagram for the vanadium-oxygen system[40]

2.3 Thin film epitaxy

In lattice matching epitaxy, one-to-one matching of the lattice parameters (matching of unit cells) between the film and substrate occurs across the interface. This matching of lattice parameters takes place by means of strain in the films (and up to some extent in the substrate) as the films grow pseudomorphically, initially. The pseudomorphic growth of the film continues until a 'critical thickness' is reached. When the thickness is over the critical point, the strain energy becomes large enough to trigger the nucleation of dislocations to relax the strain. These dislocations are nucleated at the film surface and must glide to the interface to relieve the stain in the film. A schematic illustration of lattice matching epitaxy is presented in Figure 2-9. The critical thickness at which dislocation nucleation occurs is directly related to the misfit. In low misfit systems, the critical thickness for dislocation nucleation may be quite large and dislocation nucleation and therefore, strain relaxation may not be possible. Also, the obstacles to the glide of dislocations often results in a high threading dislocation density in the films, which is detrimental to the devices as these dislocations can act as charge carrier trap or recombination centers.

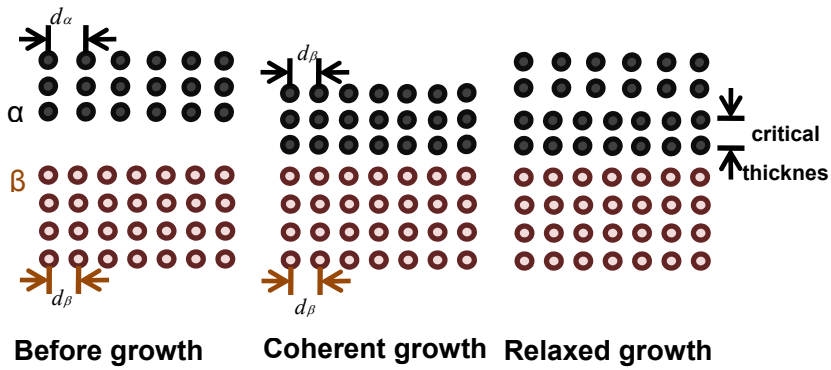

Figure 2-9. Schematic representation of lattice matching epitaxy, dc denoted the critical thickness.

2.4 References

[1] I.P. Parkin and T.D. Manning, *Intelligent thermochromic windows*, Journal of Chemical Education 83 (2006) 393

[2] F. Zhang, X. Zou, W. Feng, X. Zhao, X. Jing, F. Sun, H. Ren and G. Zhu, *Microwave-assisted crystallization inclusion of spiropyran molecules in indium*

trimesate films with antidromic reversible photochromism, J. Mater. Chem. 22 (2012) 25019

[3] S.K. Deb, *A novel electrophotographic system*, Appl. Opt. (1969) Suppl. 3, 193

[4] C.M. Lampert, *Electrochromic materials and devices for energy efficient windows*, Sol. Energy Mater. Sol. Cells 11 (1984) 1

[5] C.G. Granqvist, Handbook of Inorganic Electrochromic Materials, Elsevier (1995) Amsterdam

[6] L. Groenendaal1, F. Jonas1, D. Freitag1, H. Pielartzik1, J. R. Reynolds, *Poly(3,4-ethylenedioxythiophene) and Its Derivatives: Past, Present, and Future*, Adv. Mater. 12 (2000) 481

[7] C.M. Lampert, *Chromogenic smart materials*, Materialstoday (2004) 28

[8] F.J. Morin, *Oxides which show a metal-to-insulator transition at the Neel temperature*, Phys. Rev. Lett. 3 (1959) 34

[9] C.B. Greenberg, *Optically switchable thin films: a review*, Thin Solid Films 251 (1994) 81

[10] J.B. Goodenough, *The two components of the crystallographic transition in* VO_2, J. Solid. State Chem. 3 (1971) 490

[11] C.H. Griffiths, H.K. Eastwood, *Influence of stoichiometry on the metal-semiconductor transition in vanadium dioxide*, J. Appl. Phys. 45 (1974) 2201

[12] E.E. Chain, *The infulence of deposition temperature on the structure and optical properties of vanadium oxide films*, J. Vac. Sci. Technol. A4 (1986) 432

[13] A. Razavi, L. Bobyak, P. Fallon, *The effects of biasing and annealing on the optical properties of radio-frequency sputtered VO_2*, J. Vac. Sci. Technol. A8 (1990) 1391

[14] M. Fukuma, S. Zembutsu, S. Miyazawa, *Preparation of VO_2 thin film and its direct optical bit recording characteristics*, Applied Optics 22 (1983) 265

[15] P. Jin and S. Tanemura, *Relationship between transition temperature and x in $V_{1-x}W_xO_2$ films deposited by dual-target magnetron sputtering*, Jpn. J. Appl. Phys. 34 (1995) 2459

[16] C.N. Berglund and A. Jayaraman, *Hydrostatic-pressure dependence of electronic properties of VO_2 near semiconductor-metal transition temperature*, Phys. Rev. 185 (1969) 1034

[17] A. Cavalleri, T. Dekorsy, H. H. W. Chong, J. C. Kieffer, R. W. Schoenlein, *Evidence for a structurally-driven insulator-to-metal transition in VO_2: A view from the ultrafast timescale*, Phys. Rev. B 70 (2004) 161102

[18] F. Chudnovskiy, S. Luryi, B. Spivak, *Future Trends in Microelectronics: The Nano Millennium*, In: S. Luryi, J. M. Xu, A. Zaslavsky (Eds), Wiley Interscience, New York (2002) 148–155

[19] D. M. Newns, J. A. Misewich, C. C. Tsuei, A. Gupta, B. A. Scott, A. Schrott, *Mott transition field effect transistor*, Appl. Phys. Lett. 73 (1998) 780

[20] H. Wang, X. Yi, S. Chen, X. Fu, *Fabrication of vanadium oxide micro-optical switches*, Sens. Actuators A Phys. 122 (2005) 108

[21] M. J. Lee, Y. Park, D.S. Suh, E.H. Lee, S. Seo, D.C. Kim, R. Jung, B.S. Kang, S.E. Ahn, C.B. Lee, D.H. Seo, Y.K. Cha, I.K. Yoo, J.S. Kim, B.H. Park, *Two Series Oxide Resistors Applicable to High Speed and High Density Nonvolatile Memory*, Adv. Mater. 19 (2007) 3919

[22] C.N. Berglund and H.J. Guggenheim, *Electronic properties of VO2 near sumiconductor-metal transition*, Phys. Rev. 1 (1969) 1022

[23] A.S. Barker, H.W. Verleur, and H.J. Guggenheim, *Infrared optical properties of vanadium dioxide above and below the transition temperature*, Phys. Rev. Lett. 17 (1966) 1286

[24] H.W. Verleur, A.S. Barker, and C.N. Berglund, *Optical Properties of VO_2 between 0.25 and 5 eV*, Phys. Rev. 172 (1968) 788

[25] J. Narayan and V.M. Bhosle, *Phase transition and critical issues in structure-property correlations of vanadium oxide*, J. Appl. Phys. 100 (2006) 103524

[26] R. Lopez, L.C. Feldman, and R.F. Haglund Jr, *Size-Dependent Optical Properties of VO2 Nanoparticle Arrays*, Phys. Rev. Lett. 93 (2004) 177403

[27] R. Lopez, T.E. Haynes, L.A. Boatner, L.C. Feldman, and R.F. Haglund, *Size effects in the structural phase transition of VO_2 nanoparticles*, Phys. Rev. B 65 (2002) 224113

[28] M.F. Becker, A.B. Buckman, R.M. Walser, T. Lepine, P. Georges, and A. Brun, *Femtosecond laser excitation of the semiconductor-metal phase transition in VO_2*, Appl. Phys. Lett. 65 (1994) 1507

[29] M. Soltani, M. Chaker, E. Haddad, R. Kruzelecky, and J. Margot, *Micro-optical switch device based on semiconductor-to-metallic phase transition characteristics of W-doped VO_2 smart coatings*, J. Vac. Sci. Technol. A25 (2007) 971

[30] M. Soltani, M. Chaker, E. Haddad, and R.V. Kruzelesky, *Thermochromic vanadium dioxide smart coatings grown on Kapton substrates by reactive pulsed laser deposition*, J. Vac. Sci. Technol. A24 (2006) 612

[31] T.D. Manning, I.P. Parkin, R.J.H. Clark, D. Sheel, M.E. Pemble, and D. Vernadou, *Intelligent window coatings: atmospheric pressure chemical vapour deposition of vanadium oxides*, J. Mater. Chem. 12 (2002) 2936

[32] R.T. Rajendra Kumar, B. Karunagaran, D. Mangalaraj, S.K. Narayandass, P. Manoravi, M. Joseph, and V. Gopal, *Pulsed laser deposited vanadium oxide thin*

films for uncooled infrared detectors, Sensors Actuators A107 (2003) 62

[33] C. Chen, X. Yi, X. Zhao, and B. Xiong, *Characterizations of VO_2-based uncooled microbolometer linear array*, Sensors and Actuators A: Phy. 90 (2001) 212

[34] C.D. Reintsema, E.N. Grossman, and J.N. Koch, *Improved VO_2 microbolometers for infrared imaging: operation on the semiconducting-metallic phase transition with negative electrothermal feedback*, Proc. SPIE 3698 (1999) 190-200, Infrared Technology and Applications XXV

[35] G.V. Jorgenson and J.C. Lee, *Doped vanadium oxide for optical switching films*, Sol. Energy Mater. 14 (1986) 205

[36] J.S. Chivian, M.W. Scott, W.E. Case, and N.J. Krasutsky, *An improved scan laser with a VO_2 programmable mirror*, IEEE J. Quantum Electron. 21 (1985) 383

[37] C. Ko and S. Ramanathan, *Stability of electrical switching properties in vanadium dioxide thin films under multiple thermal cycles across the phase transition boundary*, J. Appl. Phys. 104 (2008) 086105

[38] Z. Yang, C.H. Ko, V. Balakrishnan, G. Gopalakrishnan, and S. Ramanathan, Dielectric and carrier transport properties of vanadium dioxide thin films across the phase transition utilizing gated capacitor devices, Phys. Rev. B 82 (2010) 205101

[39] D. Ruzmetov, G. Gopalakrishnan, C.H. Ko, V. Narayanamurti, and S. Ramanathan, *Three-terminal field effect devices utilizing thin film vanadium oxide*

as the channel layer, J. Appl. Phys. 107 (2010) 114516

[40] C.H. Griffith and H.K. Easwood, *Influence of stoichiometry on the metal-semiconductor transition in vanadium dioxide*, J. Appl. Phys. 45 (1974) 2201

[41] G. Golan, A. Axelevitch, B, Sigalov, and B. Gorenstein, *Metal–insulator phase transition in vanadium oxides films*, Microelectron. J. 34 (2003) 255

[42] M. Fukuma, S. Zembutsu, and S. Miyazawa, *Preparation of VO_2 thin film and its direct optical bit recording characteristics*, Appl. Opt. 22 (1982) 265

[43] J.A. Thornton, *Plasma-assisted deposition processes: theory, mechanisms and applications*, Thin Solid Films 107 (1983) 3

[44] F. Guinneton, L. Sauque, J.C. Valmalette, F. Cros, and J.R. Gavarri, *Optimized infrared switching properties in thermochromic vanadium dioxide thin films: role of deposition process and microstructure*, Thin Solid Films 446 (2004) 287

[45] T. Maruyama and Y. Ikuta, *Vanadium dioxide thin films prepared by chemical vapour deposition from vanadium (III) acetylacetonate*, J. Mater. Sci. 28 (1993) 5073

[46] M.B. Sahana, G.N. Subbanna, and S.A. Shivashankar, *Phase transformation and semiconductor-metal transition in thin films of VO_2 deposited by low-pressure metalorganic chemical vapor deposition*, J. Appl. Phys. 92 (2002) 6495

[47] M. Borek, F. Qian, V. Nagabushnam, and R.K. Singh, *Pulsed laser deposition of oriented VO_2 thin films on R-cut sapphire substrates*, Appl. Phys. Lett. 63 (1993) 3288

[48] A. Gupta, R. Aggarwal, P. Gupta, T. Dutta, R. J. Narayan, and J. Narayan, *Semiconductor to metal transition characteristics of VO_2 thin films grown epitaxially on Si (001)*, Appl. Phys. Lett. 95 (2009) 11915 (2009).

[49] C. B. Greenberg, *Undoped and doped VO_2 films grown from $VO(OC_3H_7)_3$*, Thin Solid Films 110 (1983) 73

[50] J. Livage, G. Guzman, F. Beteille, and P. Davidson, *Optical properties of sol-gel derived vanadium oxide films*, J. Sol–Gel Sci. Technol. 8 (1997) 857

[51] A. Zylbersztejn and N. Mott, *Metal-insulator transition in vanadium dioxide*, Physical Review B (1975) 4383

Chapter 3. Reviews of thermochromic VO_2 thin film

3.1 Problems of soda lime glass substrates

In order to apply VO_2 thin film in thermochromic smart window, the soda lime glass would be a good selection as substrate because of its low cost. Therefore, it is necessary to achieve pure VO_2 thin films with excellent thermochromic properties on soda lime glass substrate.

The existence of additives in soda lime glass (Table 3-1), which would cause the diffusion of alkali ions (mostly sodium), was considered as a main issue for the fabrication of VO_2 thin films. Alkali diffusion from the substrate is always observed when vanadium alkoxides are deposited onto a soda lime glass by sol-gel method, leading to crystalline phases such as NaV_3O_8, NaV_6O_{15} or $NaxV_2O_5$[1]. Takahashi et al [2] have reported fabrication of VO_2 thin film on fused silica, but suggested that films formed on borosilicate glass under the same fabrication condition did not correspond to any known vanadium oxide phases due to

contamination by sodium that diffused from the substrate. The sodium ion diffusion was confirmed in Wang's work [3] where VO_2 thin films were deposited on both soda lime glass and fused silica at 580℃ using RF sputtering. XPS was used in an attempt to determine the surface difference of films on different substrates. The XPS data reflected that the sodium was detected when VO_2 film was deposited on soda lime glass substrate (Figure 3-1).

Table 3-1. Chemical composition of soda-lime glass

Property	**Soda-lime glass for windows**
Chemical composition	SiO_2, Na_2O, CaO, MgO, Al_2O_3, K_2O, TiO_2, Fe_2O_3

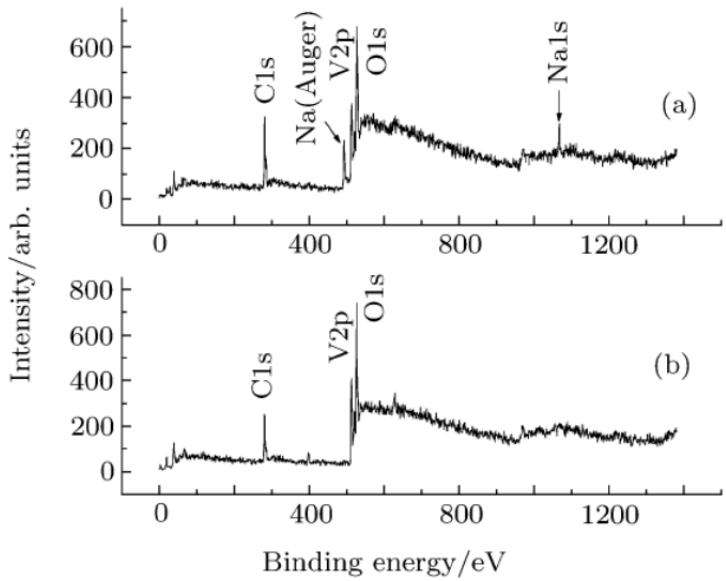

Figure 3-1 XPS scan of VO_2 films deposited on (a) soda-lime glass, and (b) fused silica [3]

Besides the sodium diffusion problem, the amorphous phase of soda lime glass is also a disadvantage for the fabrication of crystalline VO_2 thin films. Owing to the lack of epitaxial relationship with substrate, the growth of VO_2 thin films on glass depends on themselves. Consequently, the high deposition temperature and large thickness are usually required. Otherwise, VO_2 (B) would be formed instead of VO_2 (M) due to the deficiency of thermal energy. VO_2 (B) is a metastable compound of VO_2 and has no phase transition properties near room temperature. It has been found that an irreversible transformation from VO_2(B) to VO_2(R) can be obtained by annealing VO_2 (B) in an inert atmosphere at 400-500℃[4]. Moreover, the

crystallinity of VO_2 film would be poor if the thickness is small. Kato et al [5] found that there was no clear peak in XRD pattern when the thickness of VO_2 film, which was deposited on soda lime glass directly, was lower than 300nm. Wei et al [6] also suggested that VO_2 film with thickness of 80nm on glass substrate showed no obvious polycrystalline structure due to the small grain size. Moreover, with increasing thickness to 400nm, the clear polycrystalline structure of VO_2 (M) was confirmed. However, it was found that VO_2 thin films were easily deposited on single crystal substrates with high crystallinity. The high quality of VO_2 film with a large and sharp change in resistivity of $\Delta R \sim 10^3$ was achieved when VO_2 was deposited on TiO_2 single crystal substrate with thickness of only 10-15nm[7]. When VO_2 was deposited on sapphire substrate, the resistivity ratio was as high as 5 order and the hysteresis width was only 2℃[8]. On the other hand, high deposition temperature involves high heating cost which is not beneficial to industrialized mass production. Furthermore, the large thickness of VO_2 film is not accepted because of visible transmittance requirement for the realization of a VO_2-based thermochromic window. It is well known that the luminous transmittance of VO_2 is quite low due to the absorption in the short-wavelength range for both the semiconductor and the metallic phases. With increasing VO_2 thickness, the luminous transmittance was decreased [9]. Therefore, in order to achieve a reasonable transparency (transmittance, 40-60%) in the visible range and at the

same time an acceptable IR modulation efficiency, the VO_2 films must not exceed thickness in the order of 100-150nm[10]. Nevertheless, even though VO_2 films with high quality and small thickness can be deposited on single crystal substrate, the large area deposition and the expensive price of single crystal substrates are the obstacles.

3.2 Buffer layers for depositing VO_2 thin films on soda lime glass

Buffer layer is considered as one of good methods to solve the problem of successfult deposition of VO2 thin film on soda lime glass substrate, because it can modify the surface condition for the VO_2 films growth and can work as diffusion barrier as well. By using buffer layer, the lower deposition temperature and better thermochromic properties can be expected.

Buffer layer has been studied for different functions**.** The selection of buffer layer material was usually based on the application of VO_2 films and the property of substrates. For smart windows, several reports have been published. Kato et al [5] studied thermochromic VO_2 films grown on ZnO-coated glass substrates for “smart

windows". The VO_2 films were deposited on ZnO buffer layer at 400℃ using rf magnetron sputtering. It was found that VO_2 was hard to be crystallized until the VO_2 thickness was as high as 390nm when deposited on glass directly. However, by applying ZnO buffer layer, VO_2 (M) was easily deposited when the film thickness was only 90nm as shown in Figure 3-2. Therefore, the thermochromic transition was improved by using ZnO buffer layer. Figure 3-3 shows that there is no abrupt change in resistivity when VO_2 film was deposited on glass with thickness of 80nm, while the resistivity change of VO_2 was higher than two orders when deposited on ZnO buffer layer. Another research group had also investigated the effect of ZnO buffer layer. VO_2 films were deposited on ZnO buffer layer at 500℃ using PLD method[11].The VO_2 films were well grown with preferred orientation on ZnO buffer layer, which result is similar to that of Kato's work. However, the secondary phase was formed (Figure 3-4).

Besides ZnO, TiO_2 buffer layer was used for the enhancement in oxidization durability of VO_2 films. It is well known that VO_2 can be oxidized to high valence oxides when annealed at high temperature and in an oxygen-rich atmosphere. The insufficient oxidization durability leads to difficulties for further thermal treatments that are required for smart glazing, for example a toughening process. Zhang et al. [12] studied the effect of TiO_2 buffer layer on the improvement in the oxidization durability of VO_2 films. The VO_2 films were deposited on bare and TiO_2-buffered

fused quartz substrates via a solution based deposition. During gradual oxidization process, the VO_2 films deposited on bare quartz were transformed from VO_2 to V_2O_5, while transformation was prevented by applying TiO_2 buffer layer (Figure 3-5). It was also found that the incorporation of the TiO_2 buffer layer improved the film's crystallinity and hysteresis characteristics. However, Pure TiO_2 rutile structure requires substrate temperature as high as 800℃. Compared with fused silica, soda lime glass cannot sustain such high temperature because of its glass transition. It would be a problem when applying TiO_2 buffer layer for real smart windows.

Zhang et al [13] deposited VO_2 films on F-doped SnO_2 (FTO) glasses by the solution-based method. It was observed that the rutile-structured FTO substrate enhanced the crystallinity of the VO_2 films and lowered the synthesis temperature to ~ 390℃. However, the transmittance in the NIR region for the M and R states was greatly depressed by the strong absorption and reflection of FTO in this region (Figure 3-6). Such performance of transmittance change at NIR region was obviously not suitable for smart windows.

Literature survey revealed that research reports on the buffer layers for VO_2 thin film as smart windows are very limited so far. As shown previously, very few materials have been reported. Even though the buffer layers help the growth of VO_2

films, there are still problems which are yet to be solved as was already mentioned previously. Furthermore, there is no work carried out and reported about the comparison of the effect of different buffer layers on the thermochromic properties of VO_2 thin films. In the present work, several buffer layer materials will be involved to investigate the effect of different buffer layers on the thermochrmism of VO_2 films, and afterword the deposition of VO_2 film with excellent thermochromic properties on soda lime glass is expected.

In order to be applied as buffer layer for smart window, there are many criteria for the selection of buffer layer materials. The important requirement is that material has high visible transmittance whence buffer layers should be easily deposited on glass substrate. The most important is that buffer layer needs to effectively prevent the alkali ion diffusion. Buffer layers that were considered as candidates in this study are summarized in this study are shown in Table 3-2. Such materials are well known for diffusion barrier and most of them are applied usually for the glass coating.

It is well known that the glass possesses glass transition which would happen at the temperature higher than 520℃, therefore, we used deposition temperature below 500℃. In order for the buffer layer to effectively enhance the deposition of crystalline films, the buffer layers should be crystallized rather than remaining as

amorphous phase when deposited at lower temperature (<500℃). Among these materials, it was found that SiO_2, Al_2O_3, ZrO2 [14], when deposited on soda lime glass, showed amorphous phase. On the other hand, TiO_2, ZnO, SnO_2 and CeO_2 exhibited polycrystalline phase. TiO_2 and SnO_2 have the same rutile structure with VO_2, and so these two materials were selected as the candidates of buffer layer in this work. It has been investigated that VO_2 film was heteroepitaxially grown on sapphire substrate because of the similar oxygen arrangement. ZnO has the similar hexagonal crystal structure with sapphire and also its thin film is known to grow with the preferential orientation of [0001] even on glass substrate, which was why ZnO was also selected. Due to its high refractive index, CeO_2 was studied as an AR coating material for the improvement in visible transmittance of VO_2 film. Therefore, it is interesting to check if the buffer layer with high refractive index can improve the visible transmittance of VO_2 films. Consequently, TiO_2, SnO_2, ZnO and CeO_2 were selected as buffer layer materials in this study. By comparing the different structures of these buffer layer materials, the relationship between structural similarity and VO_2 growth was studied. And the improvement in thermochromic properties of VO_2 thin films can be expected by using buffer layers.

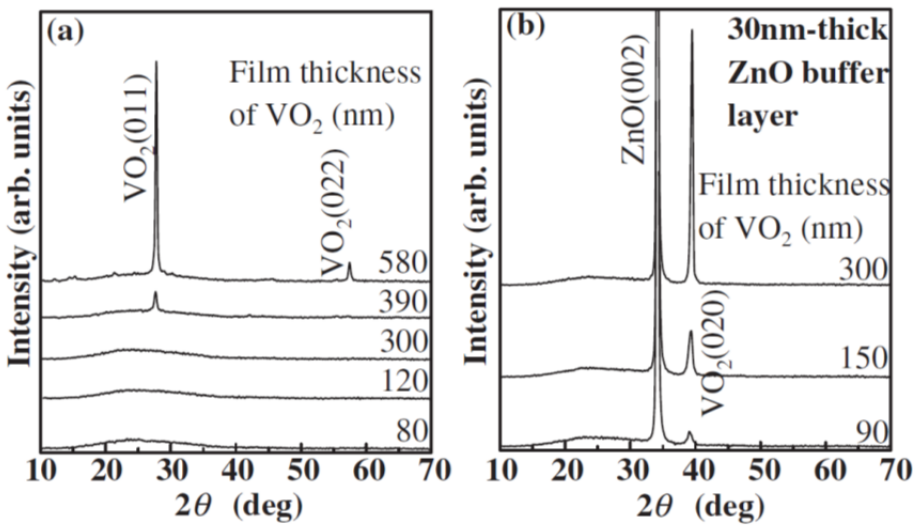

Figure 3-2. XRD patterns of VO2 films deposited on (a) glass directly, and (b) ZnO buffer layer with different thicknesses.[5]

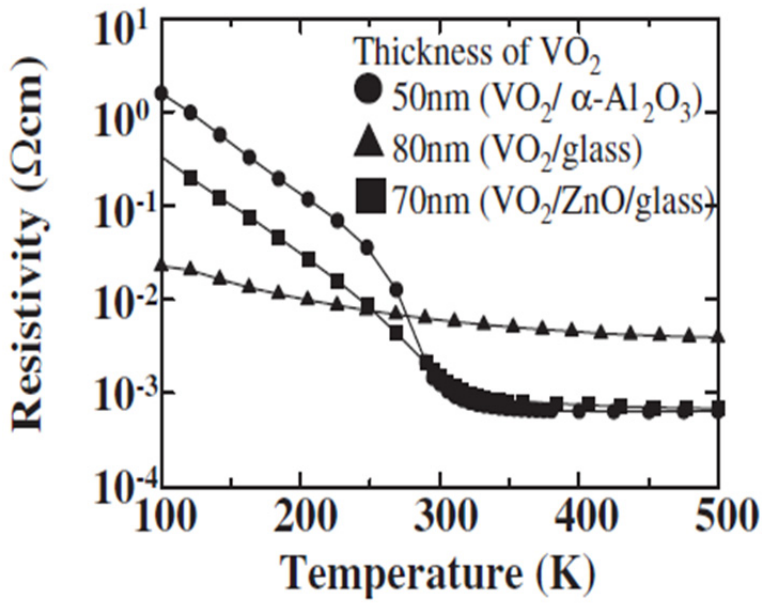

Figure 3-3. Resistivity of VO2/Al2O3, VO2/glass and VO2 deposited on 10nm-thick-ZnO-coated glass as a function of temperature from 100 to 500K [5]

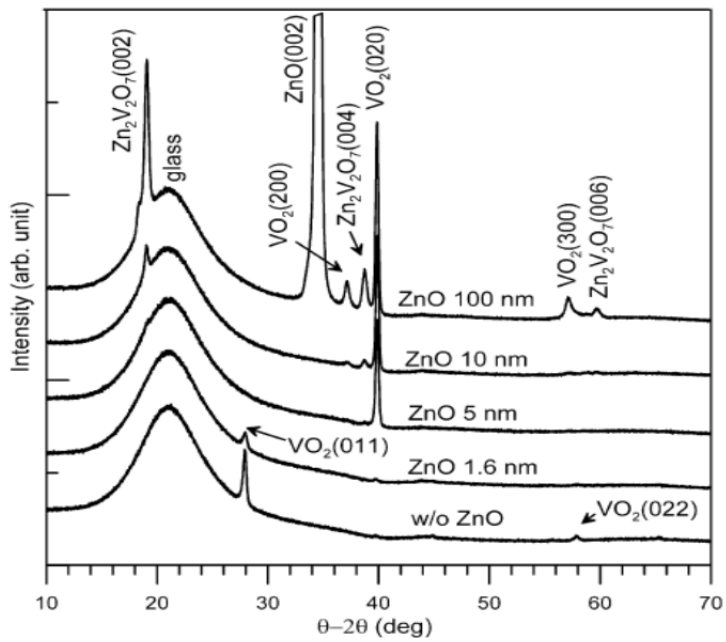

Figure 3-4. XRD spectra of VO_2 films deposited on ZnO buffer layer [11]

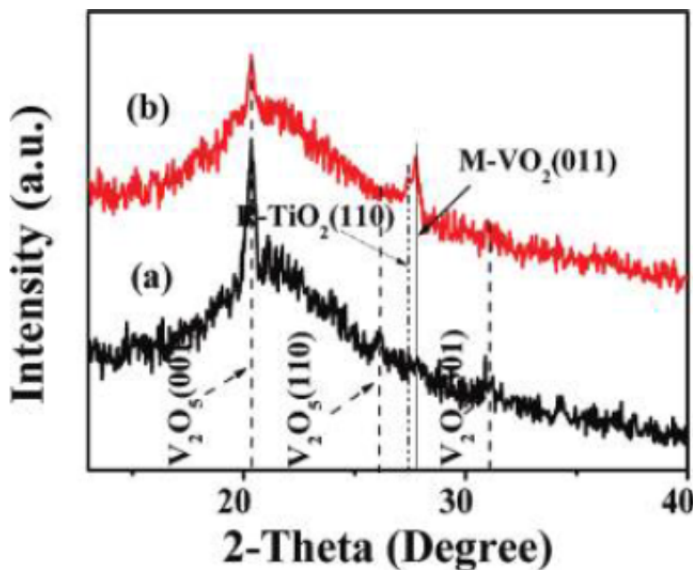

Figure 3-5 XRD patterns for postoxidization treated films grown on (a) fused silica and (b) R-phase TiO_2 buffered fused silica substrates [12]

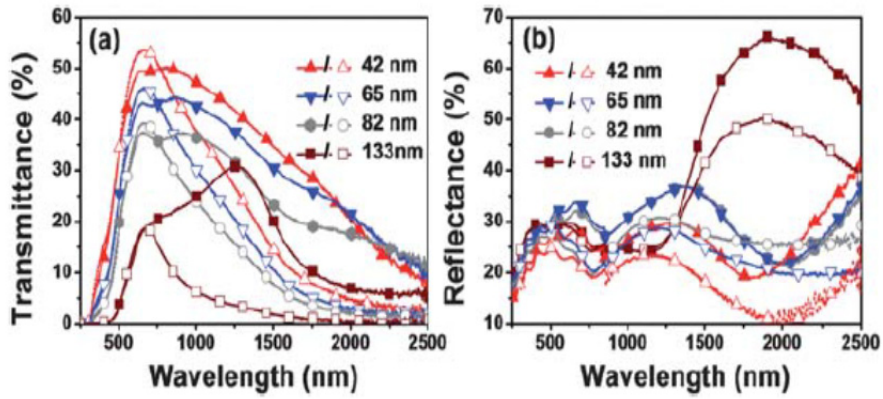

Figure 3-6 Transmittance (a) and reflectance (b) spectra for the VO_2/FTO/substrate double-layered films with different thicknesses. Lines with solid and open symbols are the spectra measured at 20℃ and 90℃, respectively [13]

Table 3-2 Candidates of buffer layer for smart window

Material	**Crystallization (≤500℃)**	**Structure**
SiO_2	amorphous	Hexagonal
TiO_2	polycrystalline	Rutile
Al_2O_3	amorphous	Hexagonal
ZnO	polycrystalline	Hexagonal
ZrO_2	amorphous	Monoclinic
SnO_2	polycrystalline	Rutile
CeO_2	polycrystalline	Cubic

3.3 Influence of oxygen pressure

The key parameter to obtain high quality VO_2 film is the oxygen pressure. The critical range of oxygen pressure to obtain high quality VO_2 film is in the range of 1 Pa–2.6 Pa (Figure 3-7, 3-8).[7,15,16] Oxygen pressure plays an important role in the final phase structure and microstructure of VO_2 film. High oxygen pressure tends to form coarse VO_2 (B) nanocrystals while low pressure favors a flat VO_2 (M) film epitaxial growth. It is reported that the oxygen pressure on the PLD setting will change the plume shape/profile greatly, which will affect the deposition rate and the nucleation behavior of VO_2 on sapphire substrate. For the low oxygen pressure condition, the plume is quite large and the ablated atoms/ions will be evaporated with higher kinetic energy, thus the condensed film will be deposited. While for the high oxygen pressure, the plume will be depressed to some extent. Since the distance between target and substrate is kept the same, the coarse and porous VO_2 (B) nanocrystals will be easily formed under the high oxygen pressure condition.

Moreover, it is reported that, when depositing VO_2 thin films by RF sputtering at a constant substrate temperature, the stoichiometry x of VO_x is dominated mainly by oxygen partial pressure and deposition rate, thus the deposition condition for obtaining VO_2 films is very narrow, and stable and reproducible deposition is

considered to be difficult at the temperature of 400°C.[17,18]

Due to the difficulties of control and the sensitive dependence of VO_2 formation, the value of oxygen pressure was fixed during the experiments performed in this dissertation

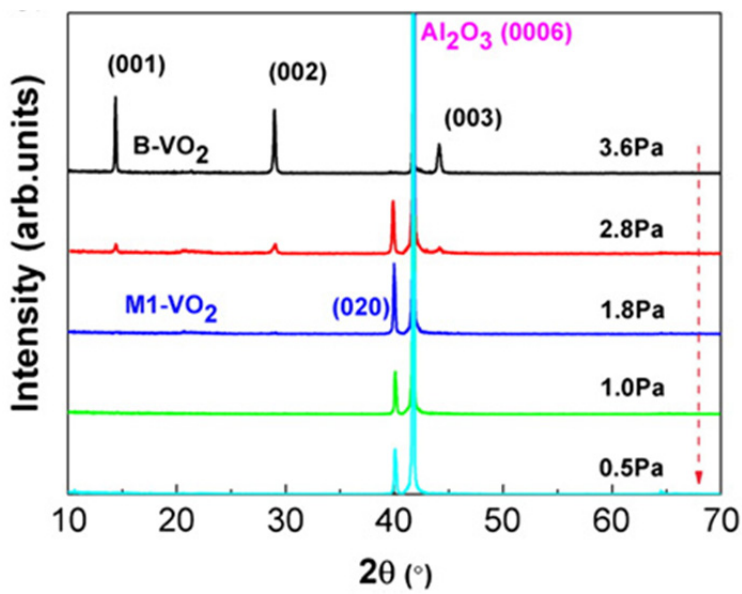

Figure 3-7. XRD patterns of different VO_2 films deposited on sapphire substrates[17]

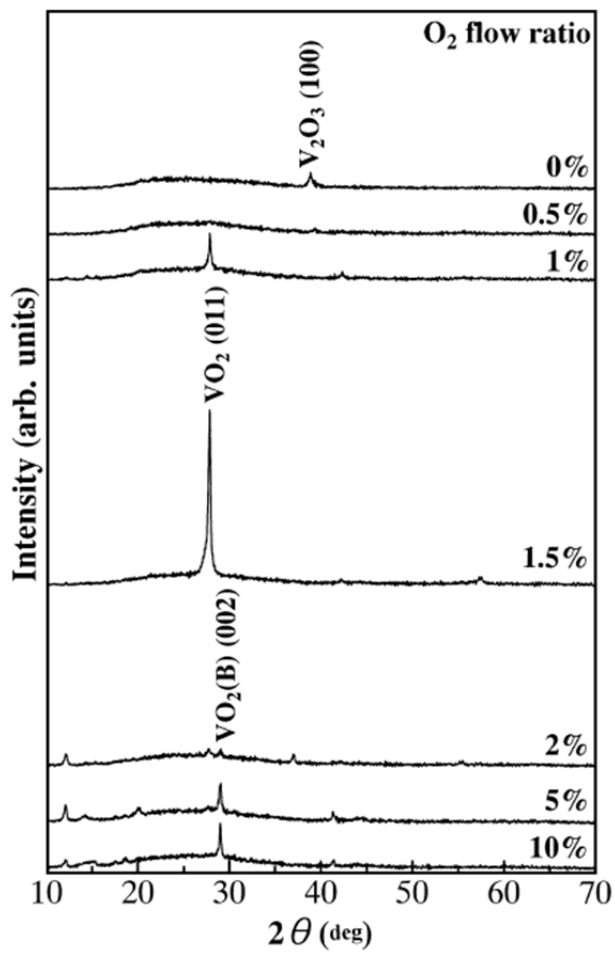

Figure 3-8. XRD patterns of the VO_x films at the various oxygen flow ratios $[O_2/(Ar+O_2)]$ deposited by rf magnetron sputtering using the V_2O_3 target.[18]

3.4 References

[1] G. Guzman et al., *Synthesis of Vanadium Dioxide Thin Films from Vanadium Alkaoxides*, Materials Research Bulletin 29 (1994) 209

[2] I. Takahashi et al., *Thermochromic $V_{1-x}W_xO_2$ thin films prepared by wet coating using polyvanadate solutions*, Jpn. J. of Appl. Phys. 35 (1996) 438

[3] X.J. Wang et al., *Surface oxidation of vanadium dioxide films prepared by radio frequency magnetron sputtering*, Chinese Physics B 17 (2008) 3512

[4] C. Leroux, et al., *From VO_2(B) to VO_2(R): Theoretical structures of VO_2 polymorphs and in situ electron microscopy*, Physical Review B 57 (1998) 5111

[5] K. Kato, et al., *Study on thermochromic VO_2 films grown on ZnO-coated glass substrates for "smart windows,"* Jpn. J. of Appl. Phys. Part 1- Regular Papers Short Notes Review Papers, 42 (2003) 6523

[6] X.B. Wei, et al., *Growth mode and texture study in vanadium dioxide thin films deposited by magnetron sputtering*, Journal of Physics D: Applied Physics, 41 (2008) 055303

[7] Y. Muraoka and Z. Hiroi, *Metal-insulator transition of VO_2 thin films grow on TiO_2 (001) and (110) substrates*, Appl. Phys. Lett. 80 (2002) 4

[8] D.H. Kim and H.S. Kwok, *Pulsed laser deposition of VO_2 thin films*, Appl. Phys. Lett. 65 (1994)

[9] G. Xu, et al., *Thickness dependence of optical properties of VO_2 thin film epitaxially grown on sapphire (0001)*, Appl. Surf. Sci. 244 (2005) 449

[10] C. Batista et al., Structural and Morphological Characterization of Magnetron Sputtered Nanocrystalline Vanadium Oxide Films for Thermochrmic Smart Surface, Journal of Nano Research, 2 (2008)

[11] T.W. Chiu, et al., Growth of b-axis orientated VO_2 thin films on glass substrates using ZnO buffer layer, Appl. Surf. Sci. 256 (2010) 6834

[12] Z.T. Zhang, et al., Effects of a TiO_2 buffer layer on solution-deposited VO2 films: Enhanced oxidization durability, Journal of Physical Chemistry C, 114 (2010) 22214

[13] Z.T. Zhang, et al, Solution-based fabrication of vanadium dioxide on F:SnO_2 substrates with largely enhance thermochromism and low-emissivity for energy-saving applications, Energy & Environmental Science, 4 (2011) 4290

[14] T. Ivanova et al., Effect of annealing temperatures on properties of sol-gel grown ZnO-ZrO_2 films, Crystal Research and Technology, 45 (2010) 1154

[15] T.H. Yang, S. Nori, H. Zhou, J. Narayan, *Defect-mediated room temperature*

ferromagnetism in vanadium dioxide thin films, Appl. Phys. Lett. 95 (2009) 102506.

[16] J.Y. Suh, R. Lopez, L.C. Feldman, R.F. Haglund Jr., *Semiconductor to metal phase transition in the nucleation and growth of VO_2 nanoparticles and thin films*, J. Appl. Phys. 96 (2004) 1209-1213

[17] L.L. Fan, Y.F. Wu, C. Si, C.W. Zou, Z.M. Qi, L.B. Li, G.Q. Pan, Z.Y. Wu, *Oxygen pressure dependent VO_2 crystal film preparation and the interfacial epitaxial growth study*, Thin Solid Films 520 (2012) 6124

[18] Y. Shigesato, M. Enomoto, H. Odaka, *Thermochromic VO_2 films deposited by RF magnetron sputtering using V_2O_3 or V_2O_5 targets*, Jpn. J. Appl. Phys. 39 (2000) 6016

Chapter 4. Experiments

In this chapter, experimental methods employed for the successful deposition and for the modification and characterization of VO_2 thin film are discussed. The thin films in this study were deposited by pulsed laser deposition method or radio frequency magnetron sputtering, and post annealing process was performed in order to enhance the crystallinity of the VO_2 thin film. The characteristics of deposited VO_2 thin films were analyzed by X-ray diffractometer, resistivity measurements, and UV-Vis-NIR spectrophotometer.

4.1 Deposition methods

4.1.1 Pulsed Laser Deposition

Pulsed laser deposition(PLD) method is a versatile non-equilibrium thin film growth technique based on physical vapor deposition. A high powered laser is

focused on a target to vaporize the material to be deposited. The interaction of the target material with the laser leads to localized evaporation of the material and the formation of a highly energetic plasma. This phenomenon is frequently referred to as laser ablation. The ablated material is ejected in a direction normal to the target surface in the form of a plume. The material in this plume is deposited on the substrate which is usually heated.

The PLD system consists of three main components; the laser, the vacuum chamber and the optics that control the laser. The schematic diagram of the PLD system used in the present study is shown in Figure 4-1. The peak power of most commercial lasers is inversely correlated with the duration of the laser pulse. Since ablation of most materials requires very high energy densities, typically nanosecond, and sometimes femtosecond, lasers are used for pulsed laser deposition. A laser emits coherent light, with a well defined wavelength, in a narrow and low divergent beam. Hence, lasers can be focused and directed effectively to be used for material processing. The most important lasers used for PLD are the KrF(248nm) excimer laser.

There are several advantages associated with PLD that make it a popular thin film deposition technique. Most advantages arise due to the high energy of the ablated species. The energy of the ablated species can be as high as 10 to 100 eV (*i.e.* about 100-1000 kT). In comparison, the energy of the ejected species in an

evaporation technique (thermal or e-beam) is about 0.1 eV at 1200 K. Listed below are some advantages and salient features of the PLD technique.

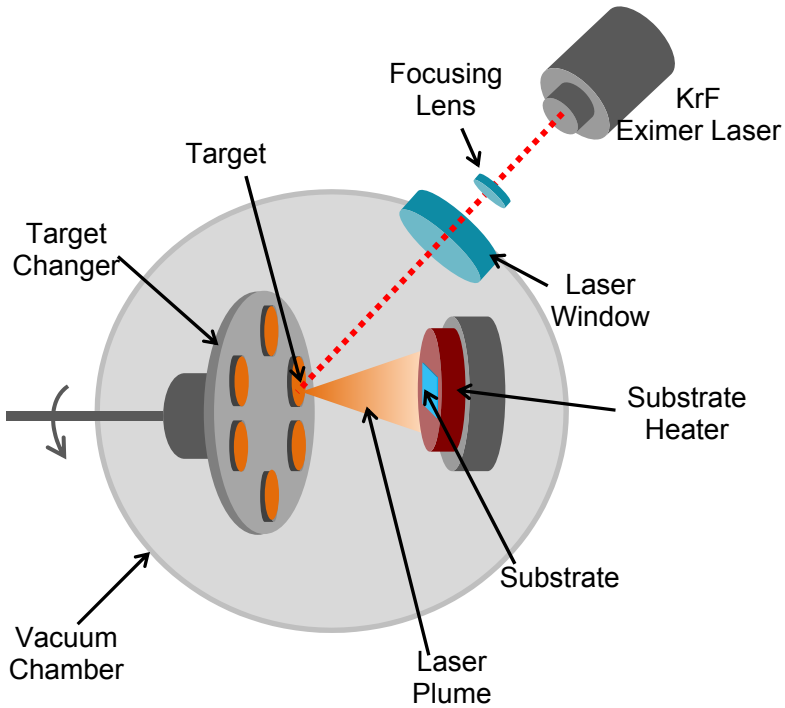

Figure 4-1. Schematic illustration of pulsed laser deposition system

1. PLD is a highly non-equilibrium processing technique due to high energy of the plume. Using PLD, complex metastable phases could be formed that would otherwise be difficult to form by typical equilibrium synthesizing routes.

2. In case of a multi-component system, the high energy and forward directed nature of the plume helps to reproduce the stoichiometry of the target in the film.[1] Due to the high energy density of the laser, the material removal from the target is so fast that vapor pressures of the individual components do not play a role.

3. The high energy of the plume helps reduce the required processing temperatures to achieve high quality films.

4. Multi-layered heterostructure thin films can easily be synthesized using PLD. The target carousel can be suitably manipulated to hold multiple targets (4 to 6 targets). This means multi-layered films can be deposited without breaking the vacuum.

5. Conceptually, any material can be ablated to form a thin film as long as it has a large enough absorption coefficient for the laser used.[2]

6. Depending on the repetition rate of the laser, the deposition rate of the film can be controlled. In fact, in PLD the number of nucleation sites can be controlled such that they are much higher than those formed in MBE or sputter deposition. By controlling the impingement rate and increasing nucleation site density, the smoothness of the film can be improved.[3]

7. It is important to realize that in the PLD system the energy source, which is the laser, is placed externally. The vacuum chamber in itself is devoid of filaments and other sources of contamination, thereby resulting in a clean process environment. The interaction between the laser and gas species in the vacuum chamber is minimal. This means that the dynamic range of deposition pressures could be high, resulting in less stringent vacuum requirements. Also, the spatial confinement of laser-solid interaction and the subsequent plume render PLD a clean process. The deposited films are thus relatively contamination free.[2]

On the other hand, PLD also suffers from some disadvantages. The area of deposited material obtained by PLD is relatively low (typically 1 cm x 1 cm). In the case of large substrates, non-uniformity in film thickness is observed due to the forward directed nature of the plume.[2] Deposition on larger substrates and uniformity of film thickness can be achieved to some extent by rastering the laser beam over a large target and/or rotation and translation of the substrate.[4] The other drawback of PLD is the formation of chunks during ablation, which can prove to be detrimental to the quality of the film.[5] Chunks are nothing but large (few microns) particulates or globules of molten material. These undesirable chunks are formed due to improper ablation that involves various mechanisms such as subsurface boiling, expulsion of the liquid layer by shock wave recoil and

exfoliation.[2,3,5] Chunk control is also possible by increasing the absorption coefficient and thermal conductivity of the target material. A compact target with better cohesion of the grains also reduces the emission of chunks. By careful manipulation of the laser parameters, the size and number of chunks can be minimized to some extent.[2,5]

Figure 4-2. Photograph of the vacuum chamber used in this work

4.1.2 Radio Frequency magnetron sputtering

Radio frequency magnetron sputtering (RFMS) is a thin-film deposition technique that can be used to deposit a wide range of dielectric and semiconductor materials. Figure 4-3 shows schematic of the magnetron/substrate arrangement used within this work. The magnetrons contain a symmetrical configuration of permanent magnets to which a disc of the desired target material is fixed. They are water cooled to prevent the targets from overheating. A summarized description of the sputtering process, from a single target, is as follows:

. The vacuum chamber is filled with a pressure (1 - 20 mTorr) of argon.

. An RF voltage (13.56 MHz) is applied across the substrate holder and the magnetron.

. Residual electrons, within the vacuum chamber, are accelerated by the voltage and confined to spiral paths around the magnetic field lines at the target surface.

. The Ar atoms within the region of the target surface are ionized by electrons, forming a plasma, and are accelerated towards the target. The motion of the Ar^+ ions is not influenced by the magnetic field because of their large mass, relative to electrons.

. Ar^+ ions that impact upon the target surface knock out neutrally charged species of target material which travel, with long mean free paths, until they encounter the substrate.

The use of an RF voltage is necessary for dielectric materials in order to overcome the build-up of positive charge at the target surface. Because of this, the growth rates associated with RFMS are typically half those of direct current magnetron sputtering (DCMS) as the Ar^+ ions spend as much time travelling away from the target as travelling towards it. In general, it is only possible to use DCMS to deposit from metallic targets where the high conductivity of the materials prevent a charge build-up.

The three key deposition parameters of RFMS are RF power, pressure and substrate temperature. Some general characteristics relating to the effect on the growth rate of varying these three parameters include:

. A linear increase in the growth rate of a material with RF power.

. An increase in growth rate with a reduction in pressure.

. A relatively small decrease in growth rate with increasing substrate temperature.

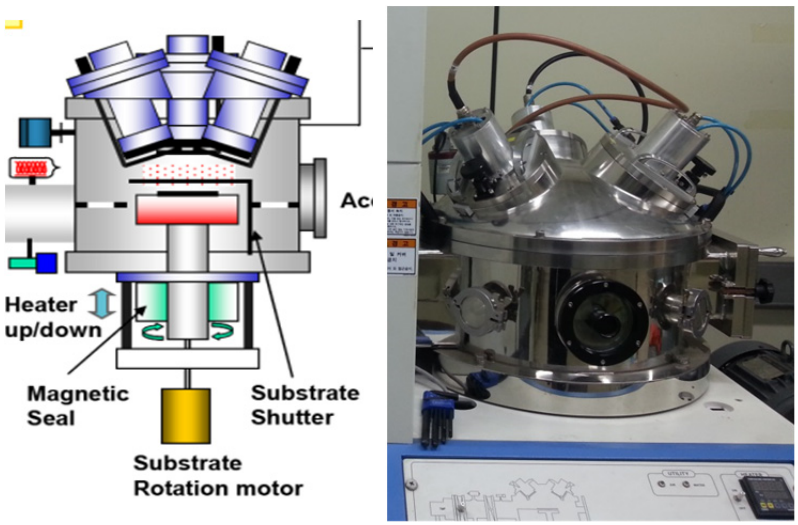

Figure 4-3. Schematic illustration(left) and photograph of RF magnetron sputtering system used in this study.

4.2 Post-annealing process

Epitaxial films are conventionally grown at higher temperatures,[6,7,8] to facilitate atom mobility at the surface during growth. For the case of VO_2 thin film deposition, when grown at high temperature, the film grows as stoichiometric, tetragonal VO_2, and transforms to monoclinic structure only during cooling, leading to stress-driven rearrangement; whereas during RT growth, initial

amorphous film growth is smooth, crystallizing to aligned grains of stoichiometric VO_2 during annealing.

Figures 4-5 (c) and (d) are high-resolution(HR) TEMs of grains and grain boundaries in RT-grown and HT-grown films, respectively. For RT-grown films, neighboring grains share grain boundaries and form sharp interfaces at the substrate. In the HT-grown films, on the other hand, the HRTEM and energy-dispersive spectroscopic measurements reveal an interdiffusion layer in which Al, V, and O are found in nonstoichiometric proportions.

These differences in morphologies, residual strains and orientations of the films lead to distinctive MIT characteristics seen in the transmission curves of Figure 4-5 (a) and (b). The RT-grown films have lower critical temperature and higher contrast than HT-grown films. The asymmetric hysteresis evident in the HT-grown film can be attributed to the stress in the film.[9]

J.Y. Suh et al.[10] found that the ΔH became larger when the grains grew in size. This contradiction was explained by the hypothesis that MIT in VO_2 can be described on the model of a martensitic transformation in which the density of heterogeneous nucleation centers, such as structural defects or oxygen vacancies, grain boundaries as well, plays the essential role in the phase transformation. Therefore, the ΔH becomes narrow in the films with small granules because the phase transition can easily occur in this highly defective structure. Moreover, a

clear relationship between ΔH and degree of misorientation has also been observed. The degree of crystallographic misorientation between adjacent grains has been reported to be related to the sharpness of the transition. [11] Metallic regions can be effectively propagated without additional energy loss when the grain boundary misorientation angles are small, which can lead to narrow ΔH.

Therefore, in order to prevent the formation of interdiffusion layer and improve thermochromic properties of VO_2 thin films, most of the samples were deposited at room temperature and crystallized by post-annealing process under following conditions;

Oxygen pressure: 10mTorr

Annealing temperature: 500~550^{o}C

Annealing time: 30 minutes

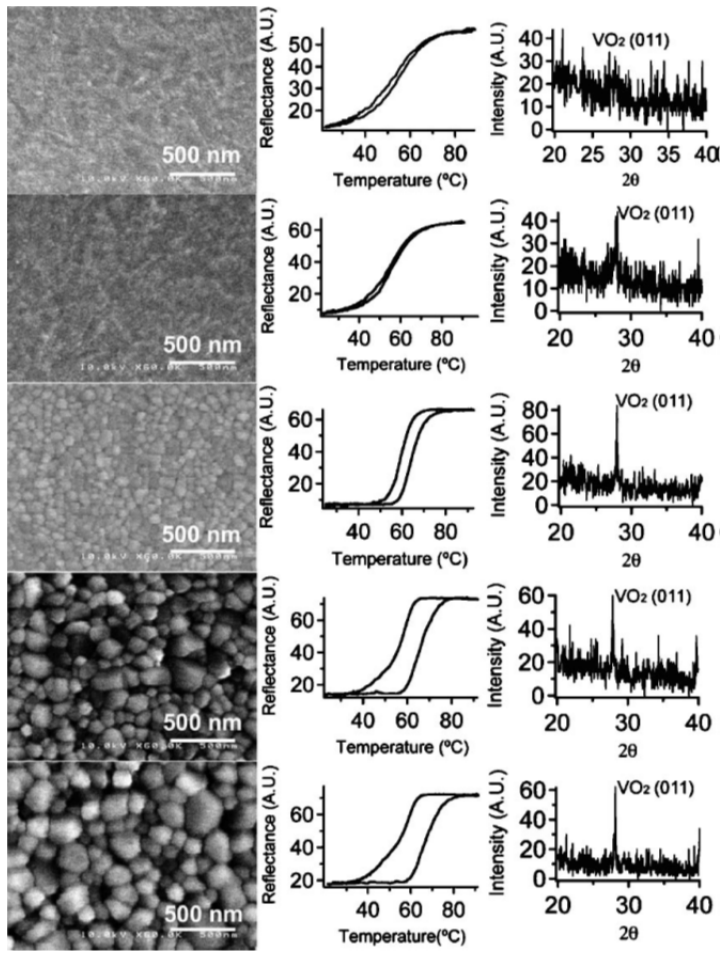

Figure 4-4. Scanning electron micrographs of nanoparticle and thin film morphology, relative IR (l5980 nm) switching curves through the structural phase transition; and x-ray diffraction θ/2θ vs annealing time for pulsed laser deposited vanadium oxide films of 100 nm thickness fabricated at 450 °C in 250 mTorr of O_2 to crystallize them into VO_2. From top to bottom 5, 10, 20, 40, and 80 min of annealing time.[10]

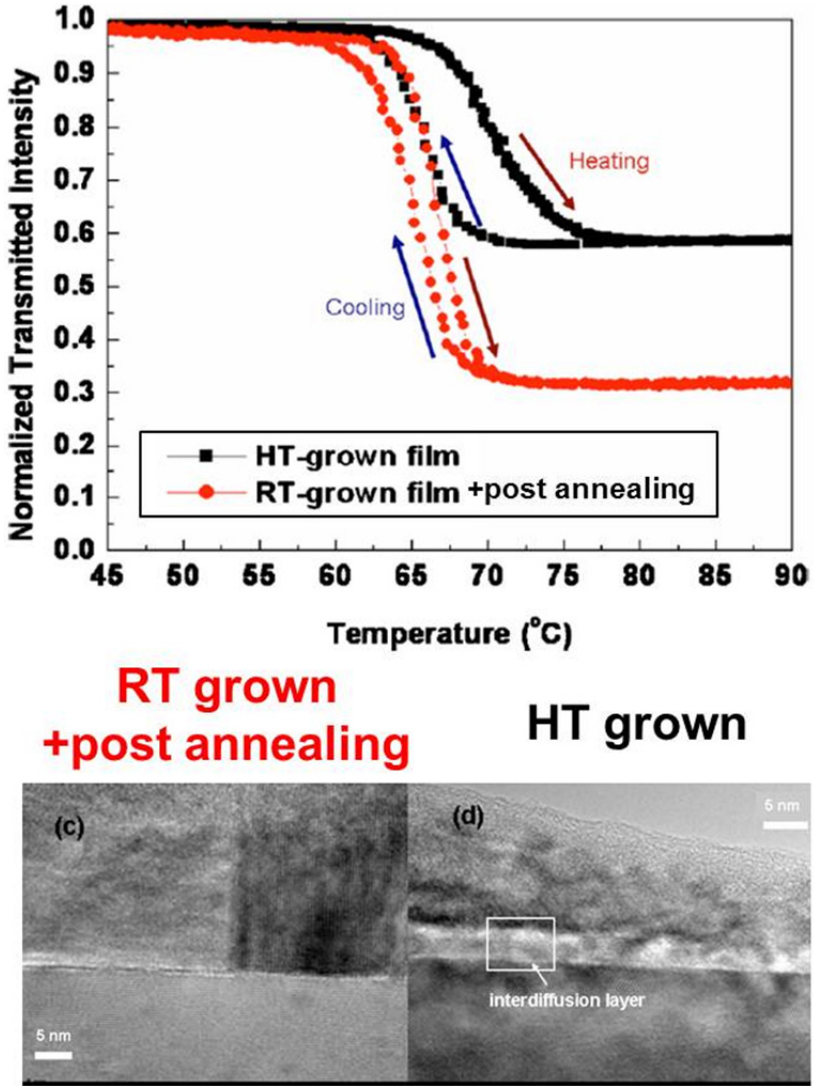

Figure 4-5. White light transmission as a function of temperature for (a) RT-grown and (b) HT-grown film. TEM images of (c) RT-grown film and (d) HT-grown film[12]

4.3 X-ray diffraction analysis

X-ray diffraction (XRD) was used to study the crystal structure and orientation of the samples. This technique also provides information about the phase composition, lattice parameter, grain size and lattice strain. The XRD technique is based on diffraction governed by the Bragg's law.[13] Diffraction typically occurs when waves interact with a periodic structure. It is important to realize that the wavelength of the wave should be about the same as the repeat distance of the periodic structure for diffraction to occur.[13] Inter-atomic distances are of the order of a few angstroms. X-rays have wavelengths of the same order and hence they are used to investigate the structyre of crystals. When an X-ray beam is incident on a crystal it interacts with the parallel plane of atoms either constructively or destructively depending upon the path difference. Bragg's law is satisfied when the waves interfere constructively and the following condition is met.[13]

$$n\lambda = 2d \sin\theta$$

Where n is an integer indicating the order of reflection, λ is the wavelength of the X-ray beam, d is the inter-planar spacing and θ is the incident angle. In the present work θ-2θ scans were performed using Bruker D8 Advance diffractometer with Cu Kα radiation(Figure 4-6, 4-7). This instrument is a two-circle diffractometer in

which the sample can be rotated along one of the axis (θ-axis) and also the detector can be rotated independently (2θ-axis). This diffractometer is based on Bragg-Brentano parafocusing diffraction geometry. In this geometry, the detector is at 2θ and the sample surface is at θ angle to the incident beam. The incident beam, normal to sample surface and detector are in the same plane. Since the diffracted beam always lies in the plane containing the incident beam and plane normal, and due to the restricted rotation of the sample only along θ-axis, this diffractometer can be used to access diffraction information only from the planes which are parallel to surface of the sample.

In the present study the Bruker D8 Advance system was used to perform θ/2θ scans for phase identification and low angle 2θ scans for crystallite size calculation using Scherrer's formula. In order to minimize the intensity representing the phases of substrates, low-angle 2θ scans were performed in this dissertation.

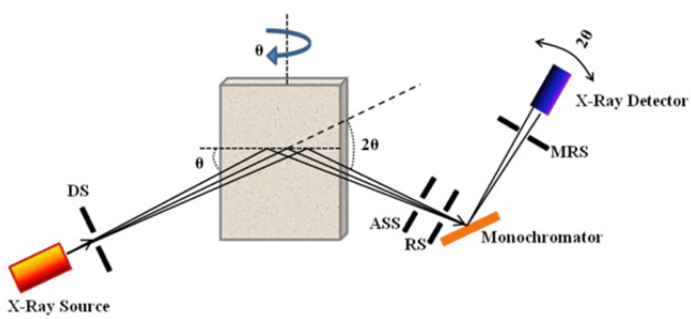

Figure 4-6. A schematic diagram of X-ray diffractometer used for θ-2θ scans.

Figure 4-7. Photograph of Bruker D8 Advance X-ray diffractometer.

4.4 Electrical/Optical property measurements

4.4.1 Van der Pauw method

The van der Pauw technique[14, 15] allows the sheet resistance of a square sample to be measured. Two characteristic resistances, R_A and R_B, are measured using square contact geometry as shown in Figure 4-8, where

$$R_A = \frac{R_A^+ + R_A^-}{2} = \frac{{}^{V_{43}}/_{I_{12}} + {}^{V_{34}}/_{I_{21}}}{2}$$

$$R_B = \frac{R_B^+ + R_B^-}{2} = \frac{{}^{V_{23}}/_{I_{14}} + {}^{V_{32}}/_{I_{41}}}{2} \qquad \text{(Eq. 4-1)}$$

The subscripts for I denote the contacts into which current is injected, e.g. for I_{12} the current flows into contact 1 and out of contact 2. Similarly, the subscripts for V denote the contacts across which the corresponding voltage is measured. Two source meters were used separately to apply a current to the sample and measure the corresponding voltage. The subscripts `+' and `-' denote the resistances measured when the current was applied in positive and negative directions respectively. The sheet resistance was calculated by iteratively solving the following relation for $R_{\square}$:

$$exp^{\frac{-\pi F_A}{R_{\square}}} + exp^{\frac{-\pi F_B}{R_{\square}}} = 1 \qquad \text{(Eq. 4-2)}$$

The error associated with this sheet resistance value was calculated as the standard deviation between a minimum of three repeated measurements. For further reviews on resistance measurements using the van der Pauw technique the reader is directed to the following references.[16,17]

All measurements were made using custom built equipment and software. A contact relay was used to automatically swap the orientation of the contacts for each measurement. This eliminated the need to manually disconnect and reconnect the contacts. Also, by ensuring that contacts were not moved throughout the measurement, the systematic error associated with changes in contact position was

avoided. Note that for the measurement of R_A and R_B to be reliable, an Ohmic contact was required, otherwise equations 4-1 and 4-2 were not applicable. For films with larger R_2 values the quality of the contacts was improved by applying a small amount of silver or indium paste to the sample corners.

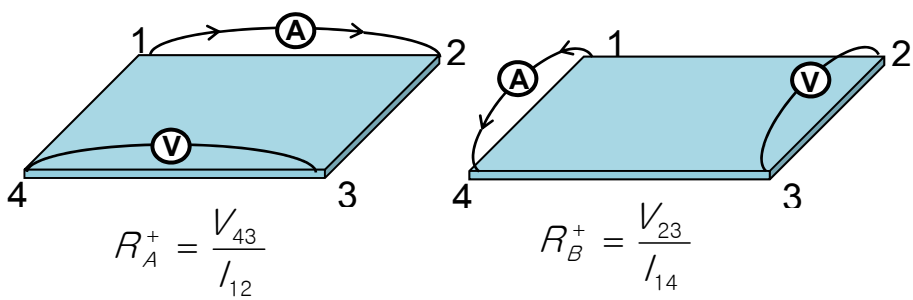

Figure 4-8. Contact configuration for van der Pauw resistivity measurement.

Figure 4-9. Photograph of Hall measurement system used in this study. The resistivity measurement is based on van der Pauw method.

4.4.2 UV-Vis-NIR spectrophotometer

The Varian CARY5000 UV-Vis-NIR spectrophotometer that was used in this work consists of a light source, a sample holder with a self-made heating stage, a detector, and a data acquisition computer. The sample holder is located between the light source and the detector. The self-made heating stage, which heats samples using thermoelectric module, can heat up the sample to 150^{o}C and cool down to -5^{o}C by applying reversible voltages. The spectrophotometer was allowed to create a baseline which removes background from the data to be collected. The beam light

was directed to the sample and the detector detects the amount of light that is transmitted through the sample.

The data was generated and captured by the computer. The measurements were taken with changing the measuring temperature. The wavelength range of the spectrophotometer used in this work was 180-3300nm. The data collected was used to plot the graphs of transmittance as a function of wavelength. The UV-VIS spectra were used to investigate the optical switching property of the deposited vanadium oxide films.

Figure 4-10. Photograph of Varian CARY5000 UV-Vis-NIR spectrophotometer.

4.5 References

[1] P. Macquart, F. Bridou, and B. Pardo, *Carbon/tungsten multilayers for X-ray-UV optics deposited by laser evaporation: Preparation and interface characterization*, Thin Solid Films 203 (1991) 77

[2] *Pulsed Laser Deposition of Thin Films*, edited by D. B. Chrisey and G. K. Hubler, Wiley-Interscience, New York (1994)

[3] R.K. Singh and J. Narayan, *Pulsed-laser evaporation technique for deposition of thin films: Physics and theoretical model*, Phys. Rev. B 41 (1990) 8843

[4] J.A. Greer and M.D.J. Tabat, *Large-area pulsed laser deposition: Techniques and applications*, Vac. Sci. Technol. A 13 (1995) 1175

[5] R.K. Singh, D. Bhattacharya, and J. Narayan, *Subsurface heating effects during pulsed laser evaporation of materials*, Appl. Phys. Lett. 57 (1990) 2022

[6] J. Narayan and V. M. Bhosle, *Phase transition and critical issues in structure-property correlations of vanadium oxide*, J. Appl. Phys. 100 (2006) 103524

[7] Z.P. Wu, S. Yamamoto, A. Miyashita, Z.J. Zhang, K. Narumi, and H. Naramoto, *Single-crystalline epitaxy and twinned structure of vanadium dioxide thin film on (0001) sapphire*, J. Phys.: Condens. Matter 10, (1998) L765

[8] J. Nag and R. F. Haglund, *Synthesis of vanadium dioxide thin films and nanoparticles*, J. Phys.: Condens. Matter 20 (2008) 264016

[9] V. A. Klimov, I. O. Timofeeva, S. D. Khanin, E. B. Shadrin, A. V. Ilinskii, and F. Silva-Andrade, *Hysteresis loop construction for the metal-semiconductor phase transition in vanadium dioxide films*, Tech. Phys. 47 (2002) 1134

[10] J.Y. Suh, R. Lopez, L.C. Feldman, R.F. Haglund Jr., *Semiconductor to metal phase transition in the nucleation and growth of VO_2 nanoparticles and thin films*, J. Appl. Phys. 96 (2004) 1209

[11] J.F. De Natale, P.J. Hood, A.B. Harker, *Formation and characterization of grain-oriented VO_2 thin films*, J. Appl. Phys. 66 (1989) 5844

[12] J. Nag, E.A. Payzant, K.L. More, and R.F. Haglund, *Enhanced performance of room-temperature-grown epitaxial thin films of vanadium dioxide*, Appl. Phys. Lett. 98 (2011) 251916

[13] B.D. Cullity, *Elements of X-Ray diffraction*, Addison-Wesley Publishing Co. Inc. (1982)

[14] L. van der Pauw, *A method of measuring specific resistivity and Hall effect of discs of arbitrary shape*, Philips Res. Rep. 13 (1958) 1

[15] L. van der Pauw, *A method of measuring the resistivity and Hall coefficient on*

lamellae of arbitrary shape, Philips Technical Review 20 (1958) 220

[16] G. Rietveld, C. Koijmans, L. Henderson, M. Hall, S. Harmon, P. Warnecke, B. Schumacher, *DC conductivity measurements in the Van der Pauw geometry*, IEEE T. Instrum. Meas. 52 (2003) 449

[17] D. K. Schroder. Semiconductor Material and Device Characterization. John Wiley & Sons, New York (1998)

Chapter 5. Effect of lattice misfit on the transition temperature of VO_2 thin film

5.1 Introduction

Vanadium dioxide(VO_2) is well-known for its first-order phase transition at a certain critical temperature(T_c).[1] At temperature higher than the critical temperature T_c which is 340K, it shows tetragonal-rutile structure(VO_2(R)) with high electrical conductivity, while below T_c, it shows monoclinic structure (VO_2(M)) with electrical insulating property.[2] Through this reversible metal-to-insulator transition(MIT) near room temperature, VO_2 shows abrupt change in conductivity over three orders of magnitude. Such property change made VO_2 to be considered as a material having high potentials for various applications, such as electronic switches, thermal sensors, and thermochromic smart windows.[3]-[6]

However, for the practical application of VO_2, controlling T_c to have appropriate value for each application is needed. Doping transition metal ions has been widely studied in order to control T_c of VO_2.[7]-[10] Although doping tungsten on VO_2 is

known to be the most effective method to change T_c with a decreasing rate of approximately 25K/%[7], in thin film, the T_c of pure VO_2 can be changed by engineering the thermal stress applied to the VO_2 thin film. It was reported that thermal stress between the film and the substrate can affect T_c of VO_2, caused by the anisotropy in the thermal expansion of VO_2.[11] Also, VO_2 thin films with less than 100nm thickness can have lower T_c compared to the bulk VO_2.[12] VO_2 thin film on sapphire substrate is widely studied and known to have T_c of 340K when the film is thicker than 200nm.[12],[13] However, many research groups have reported that VO_2 thin films on sapphire substrate can have T_c lower than 340K when the film is thinner than 100nm. It was reported that T_c was lowered to 325K for VO_2 thin film sputter deposited on c-cut sapphire substrate.[14] Similar result has been reported for VO_2 thin film on TiO_2 substrate.[15] These results suggest that the T_c of VO_2 can be controlled by stress along the c axis of VO_2(R). In this study, in order to investigate the effect of lattice misfit between the film and the substrate on the T_c, VO_2 thin films with same preferred orientation were pulsed laser deposited on different substrates which can induce different amount of stress.

5.2 Experimental procedure

VO_2 thin films were prepared by pulsed laser deposition(PLD) method, using 1"Φ V_2O_5 pellet as the target material. 99.99% V_2O_5 powder(Kojundo Chemical Laboratory Co., Ltd) was used for target manufacturing process, which includes 24 hours of ball milling, 4 hours of calcinations at 550℃, and 12 hours of sintering at 600℃ with a temperature increasing rate of 5℃/min. For the substrates, c-cut sapphire and MgO(111) single crystals were used. The size of each substrate was 10mm x 10mm with 0.5mm thickness. The substrates were cleaned prior to the deposition process by washing with acetone, ethanol, and distilled water in ultrasonic bath for 10 minutes each and then blown with nitrogen. For the uniform thickness of the samples, deposition time for each sample was 4 minutes with 5Hz of repetition rate and $2J/cm^2$ of energy density, using Lambda Physik excimer laser(KrF) source. To minimize the variation of the amount of crystallinity in the samples, substrate temperature of 400℃ and oxygen pressure of 10mTorr were maintained during deposition with a base pressure of 1×10^{-6}Torr, which was the optimized condition to obtain VO_2 thin films on both sapphire and MgO substrates. After deposition, the films were cooled down naturally to room temperature.

The X-ray diffraction patterns were obtained from Bruker D8Advance θ-2θ diffractometer using Cu-Kα radiation and Ge111 monochromator. Film thickness

was determined by FE-SEM, observing a distinct edge between the film and the substrate. The temperature dependence of resistivity was measured using Hall measurement system based on the 4 probe stage and van der Pauw method with additional heating stage attached. In order to determine T_c of each sample accurately, the temperature during resistivity measurement was calibrated by attaching thermocouple on the surface of each substrate. T_c value of VO_2 thin film has been obtained by calculating the middle point of the total integrated area of the hysteresis loop. In order to confirm the epitaxial growth of the films, high resolution transmission electron microscope(HR-TEM) measurements were carried out using JEM-3000F JEOL microscope operated at 300kV. XPS measurement of each sample was carried out by a K-alpha ESKA System with a monochromatic Al Kα source.

5.3 Results & discussion

Figure 5-1 shows the θ-2θ XRD patterns of the VO_2 thin films deposited on c-sapphire and MgO(111) substrates, respectively. Both samples had high intensity regardless of the thin VO_2 layer, showing preferred oriented growth of 2θ position near 39.9º which can come from diffractions at (002) or (020) plane of VO_2(M)

phase. Many research groups reported results assuming this peak to be (020) plane.[12],[16],[17] However, recent report has clarified that the orientation of heteroepitaxially grown VO_2 film on c-sapphire is (002).[18],[19] Thus, here we will assume the orientation of this plane to be (002). Since the VO_2 films should have preferred in-plane orientation to induce the misfit strain, pole figure was plotted to confirm the heteroepitaxy between the VO_2 thin films and the substrates, as shown in figure 5-2. The results show that the films have clear in-plane orientations, indicating that the VO_2 thin film on each substrate was deposited epitaxially.

HR-TEM analyses were performed for both VO_2/MgO(111) and VO_2/c-sapphire samples. All VO_2 films had thickness of 25~30nm with epitaxial growth, showing distinct interface without any interdiffusion layer observed.(Figure 5-3 (a), (c)) Films may not have full or nearly full crystallinity when they are very thin. The XRD data and HR-TEM images at the interface, however, showed that the films with only 25~30nm thicknesses deposited in this work are highly crystallized. To confirm the composition similarity of each sample, XPS quantitative analysis was performed. The V:O ratios were 1.61 and 1.78 for VO_2/c-sapphire and VO_2/MgO(111) respectively. Considering general error rate of XPS quantitative analysis which is ±10%, both samples can be considered to have similar ratio of V and O elements. Selected area electron diffraction(SAED) patterns of VO_2 films and substrates are shown in Figure 5-3 (b) and (d). The diffraction subpattern

shows reflections from [100] zone axis for VO_2/MgO(111) and [010] zone axis for VO_2/c-sapphire, meaning that VO_2 films have in-plane orientation which is nearly parallel with the substrates: VO_2(M)[100]||MgO[011], and VO_2(M)[010]||Al_2O_3[2$\bar{1}\bar{1}$0] for VO_2(001) plane of each sample. These results are well matched with previous reports performed by other research groups.[18],[19]

Combining the results obtained by XRD and SAED pattern, the [100] and [010] in-plane orientation of (001) oriented VO_2(M) thin film is parallel to [011] of (111) oriented MgO and [2$\bar{1}\bar{1}$0] of (0001) oriented Al_2O_3 substrate, respectively. Since the [010] of VO_2(M) // [100] of VO_2(R), applying stress along [010] of VO_2(M) refers stress along [100] of VO_2(R) as well, which can decrease the lattice parameter c of VO_2(R). The relation between the lattice parameter c and the T_c of VO_2 on TiO_2 substrate has been reported.[15],[20] However, due to the inaccuracy of determining lattice parameter of thin film samples, misfit ratios of oxygen-oxygen distance along [001] of VO_2(R), which corresponds with the lattice parameter c of VO_2(R), were calculated and presented instead of obtaining residual strain of the thin films in Figure 5-4. The misfit ratio of oxygen-oxygen distance between VO_2/MgO(111) was approximately 4.3% with tensile strain applied, whereas that of VO_2/c-sapphire was 5.7% with compressive strain applied. VO_2 films with thickness smaller than 100nm were reported to have low T_c values[14],[15],[20], compared to those of thicker films, which can result from the presence of

compressive strain along [001] of VO_2(R). It was also confirmed in this study that, with less than 100nm thickness, T_c had lower values as the film thickness decreased. Therefore, VO_2/c-sapphire was expected to have lower transition temperature than that of bulk VO_2[14], and VO_2/MgO(111) to have higher transition temperature than that of VO_2/c-sapphire and bulk VO_2 as well.

The resistivity measured at temperature from room temperature to 360K is shown in Figure 5-5 for (a) VO_2/c-sapphire and (b) VO_2/MgO(111). Regardless of the high crystallinity of VO_2 thin film as shown in XRD data(Figure 5-1), the resistivity of VO_2/c-sapphire showed gentle slope and low resistivity at low temperature compared to those of VO_2/MgO(111). This phenomenon is not clearly explained, but it seems that the resistivity at low temperature tends to have lower value compared to that at high temperature, which can be observed from VO_2 thin films with low T_c[10],[14],[20] in other reported data. The T_c of thin film for each sample was determined by calculating the mid-point of integrated hysteresis loop area. VO_2/c-sapphire had lower T_c of 318K compared to 331K of VO_2/MgO(111), as expected. However, VO_2/MgO(111) sample showed lower T_c than that of bulk VO_2(340K[1]). This can be explained by thermal stress applied by the thermal expansion coefficient difference between the thin film and the substrate. F.C. Case[11] reported that VO_2 thin films with 300nm thickness which were deposited on different substrates have different T_c values, suggesting that the tensile stress applied on the

film by thermal stress can cause T_c change with a linear relationship between T_c and thermal stress.[11] The thermal stress was calculated using the following equation:

$$S = (\Delta\alpha)\Delta T E \quad [11],[21] \qquad (1)$$

where S: thermal stress,

$\Delta\alpha$: difference between linear thermal expansion coefficients,

ΔT: difference between deposition temperature and room temperature,

E=Young's modulus of VO_2 (=2 x 10^{11} N/m^2).

Based on the calculated thermal stress using equation 1 and the data of F.C. Case[11], estimated T_c of VO_2 on each substrates was obtained when considering thermal stress only, 330K and 337K for VO_2/MgO(111) and VO_2/c-sapphire, respectively.(Table 5-1) Since the thermal stress of VO_2/MgO(111) has smaller value than that of VO_2/c-sapphire, the T_c of VO_2/MgO(111) should be lower than that of VO_2/c-sapphire when considering thermal stress effect only. Considering both misfit strain and thermal stress, these results can lead to the following conclusions: 1. Because of the thermal stress, both VO_2/MgO(111) and VO_2/c-sapphire samples can have lower T_c than that of bulk VO_2(340K[1]), 2. VO_2/MgO(111) can have higher T_c than that of VO_2/c-sapphire due to the strain by lattice misfit between the film and the substrate.

5.4 Summary

VO_2 thin films were deposited on c-cut sapphire and MgO (111) substrate using pulsed laser deposition method, in order to investigate the effect of lattice misfit on the transition temperature of VO_2. All VO_2 thin films showed heteroepitaxial growth with (002) preferred orientation. By XRD and TEM measurements, the in-plane orientations of VO_2 thin films on each substrate material were confirmed. VO_2/c-sapphire and VO_2/MgO(111) had different transition temperatures which depend on the amount of lattice misfit between thin films and substrates. The decrement of T_c for VO_2/c-sapphire and VO_2/MgO(111) were approximately 318K, and 331K respectively. These results suggest that considering lattice mismatch between thin film and substrate is another promising option for controlling transition temperature of VO_2 thin films.

5.5 References

[1] F.J. Morin (1959) Oxides which show a metal-to-insulator transition at the Neel temperature. Phys Rev Lett 3:34. doi:10.1103/PhysRevLett.3.34

[2] J.B. Goodenough (1971) The two components of the crystallographic transition

in VO2. J Solid State Chem 3:490.

[3] C.H. Griffiths, H.K. Eastwood (1974) Influence of stoichiometry on the metal-semiconductor transition in vanadium dioxide. J Appl Phys 45:2201. doi:10.1063/1.1663568

[4] E.E. Chain (1986) The influence of deposition temperature on the structure and optical properties of vanadium oxide films. J Vac Sci Technol A 4:432. doi:10.1116/1.573897

[5] A. Razavi, L. Bobyak, P. Fallon (1990) The effects of biasing and annealing on the optical properties of radio-frequency sputtered VO2. J Va Sci Technol A 8:1391. doi:10.1116/1.576887

[6] M. Fukuma, S. Zembutsu, S. Miyazawa (1983) Preparation of VO2 thin film and its direct optical bit recording characteristics. Applied Optics 22:265

[7] C. Tang et al (1985) local atomic and electronic arrangements in WxV1-xO2. Physical Review B 31:1000.

[8] J.B. Macchesney and H.J. Guggenheim (1969) Growth and electrical properties of vanadium dioxide single crystals containing selected impurity ions. J Phys Chem Solids 30:225.

[9] G.V. Jorgenson and J.C. Lee (1986) Doped vanadium oxide for optical

switching films. Solar Energy Materials 14:205.

[10] K.L. Holman et al (2009) Insulator to correlated metal transition in V1-xMoxO2. Physical Review B 79:245114. doi:10.1103/PhysRevB.79.245114

[11] F.C. Case (1984) Modifications in the phase transition properties of predeposited VO2 films. J Vac Sci Technol A 2:1509. doi:10.1116/1.572462

[12] A. Gupta, J. Narayan, and T. Dutta (2010) Near bulk semiconductor to metal transition in epitaxial VO2 thin films. Appl Phys Lett 97:151912. doi:10.1063/1.3503632

[13] K. Okimura, J. Sakai, and S. Ramanathan (2010) In situ x-ray diffraction studies on epitaxial VO2 films grown on c-Al2O3 during thermally induced insulator-metal transition. J Appl Phys 107:063503. doi:10.1063/1.3327422

[14] G. Xu, P. Jin, M. Tazawa, and K. Yoshimura (2005) Thickness dependence of optical properties of VO2 thin films epitaxially grown on sapphire (0001). Applied Surface Science 244:449.

[15] Y. Muraoka and Z. Hiroi (2002) Metal–insulator transition of VO2 thin films grown on TiO2 (001) and (110) substrates. Appl Phys Lett 80:583. doi:10.1063/1.1446215

[16] J. Nag, E.A. Payzant, K.L. More, R.F. Haglund Jr. (2011) Enhanced

performance of room-temperature-grown epitaxial thin films of vanadium dioxide. Appl Phys Lett 98:251916. doi:10.1063/1.3600333

[17] K. Kato, P.K. Song, H. Odaka, and Y. Shigesato (2003) Study on thermochromic VO2 films grown on ZnO-coated glass substrates for "smart windows". Jpn J Appl Phys 42:6523.

[18] T.H. Yang, C. Jin, R. Aggarwal, R.J. Narayan, and J. Narayan (2010) On growth of epitaxial vanadium oxide thin film on sapphire (0001). J Mater Res 25:422. doi:10.1557/JMR.2010.0059

[19] G.J. Kovács, D. Bürger, I. Skorupa, H. Reuther, R. Heller, and H. Schmidt (2011) Effect of the substrate on the insulator–metal transition of vanadium dioxide films. J Appl Phys 109:063708. doi:10.1063/1.3563588

[20] K. Nagashima, T. Yanagida, H. Tanaka, and T. Kawai (2007) Interface effect on metal-insulator transition of strained vanadium dioxide ultrathin films. J Appl Phys 101:026103. doi:10.1063/1.2424321

[21] T.H. Courtney (2000) Mechanical Behavior of Materials. 2nd edn. McGraw-hill, New York

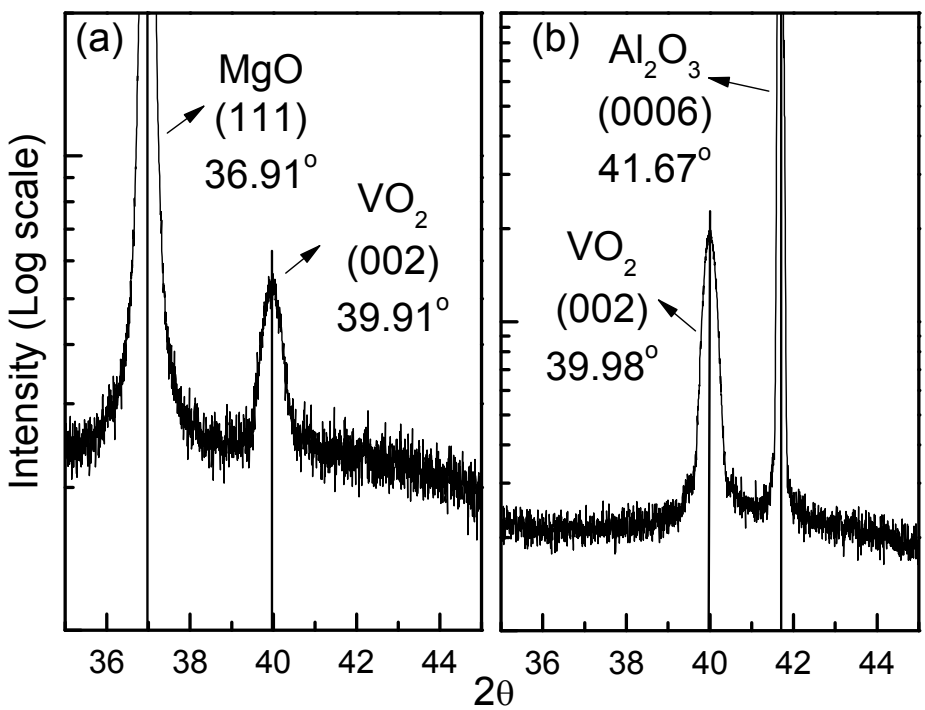

Figure 5-1. XRD phase analysis results of vanadium dioxide thin films deposited on c-cut sapphire and MgO(111).

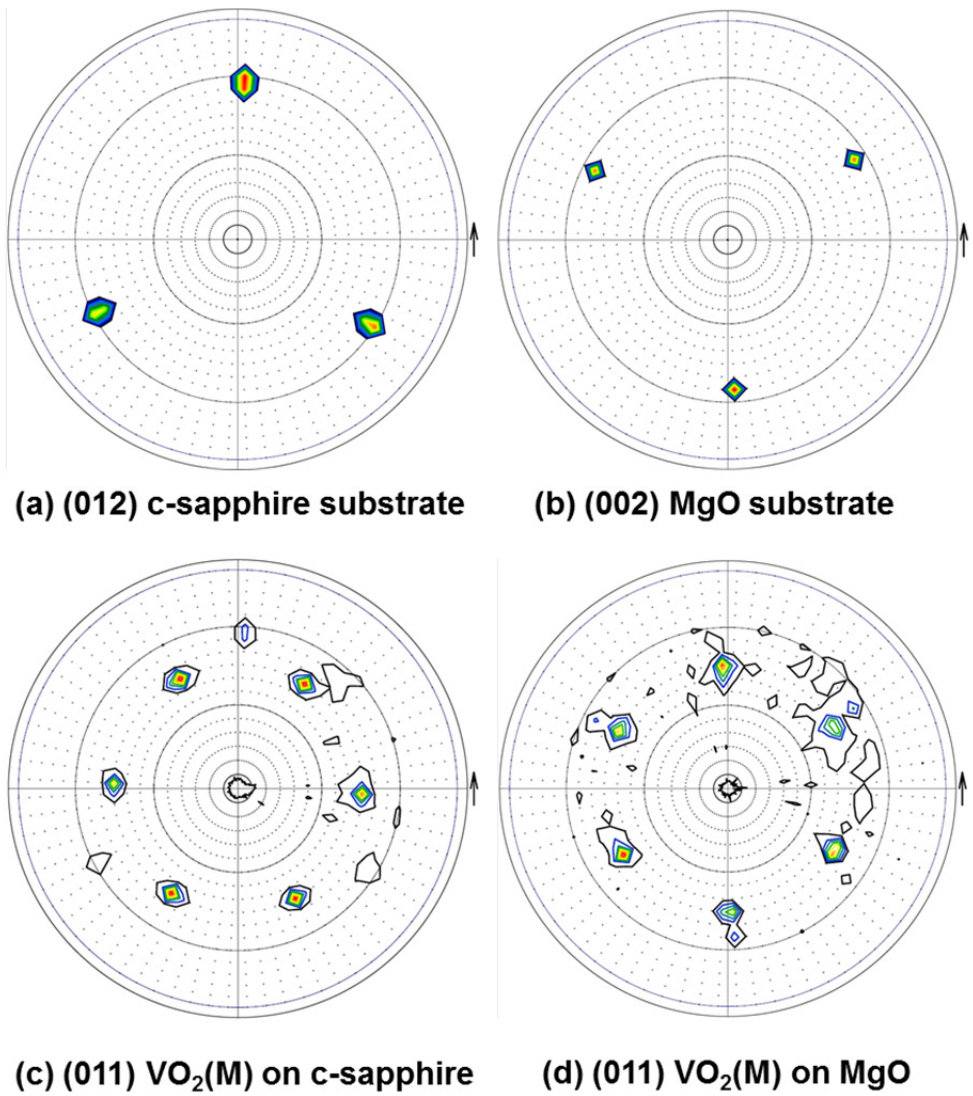

Figure 5-2. Pole figures of substrates;(a) c-sapphire, (b) MgO, and vanadium dioxide films on (c) c-sapphire, (d) MgO.

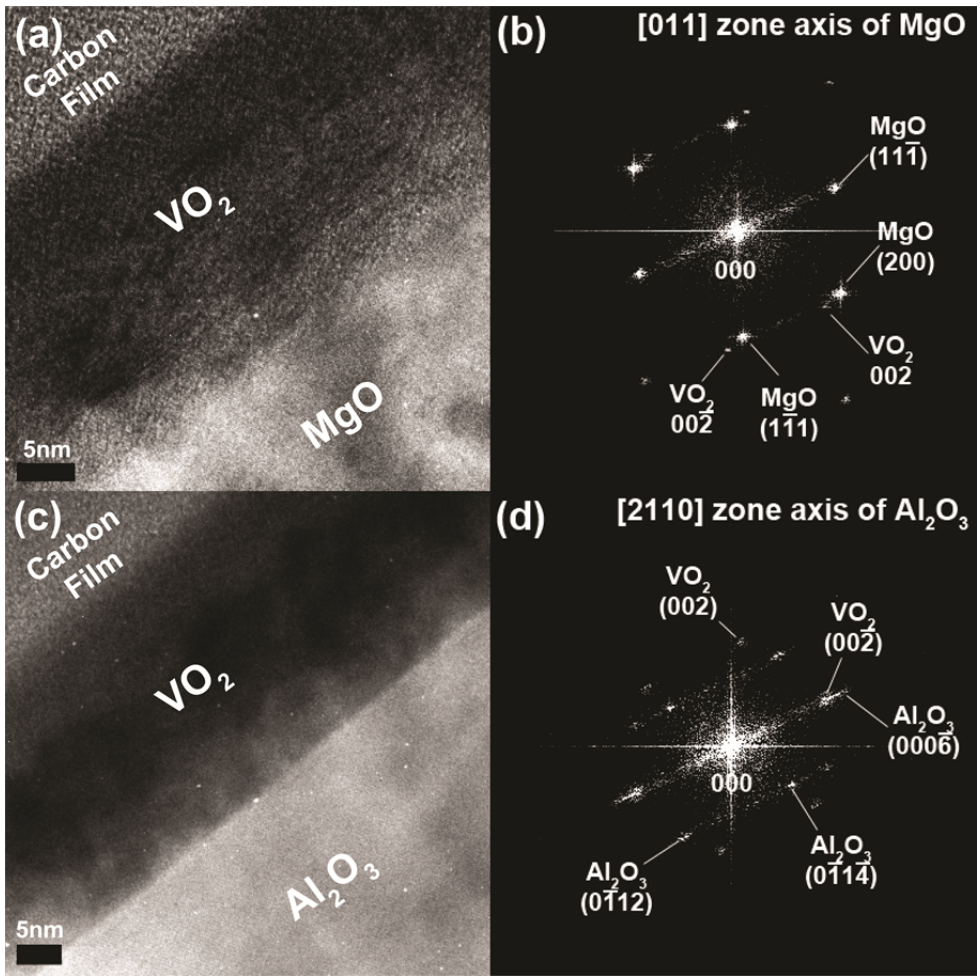

Figure 5-3. High resolution transmission electron microscope(HR-TEM) image and selected area electron diffraction(SAED) patterns of VO_2 thin films;

(a) HR-TEM image of VO_2/MgO(111), (b) SAED pattern of VO_2/MgO(111), (c) HR-TEM image of VO_2/c-sapphire, and (d) SAED pattern of VO_2/ c-sapphire

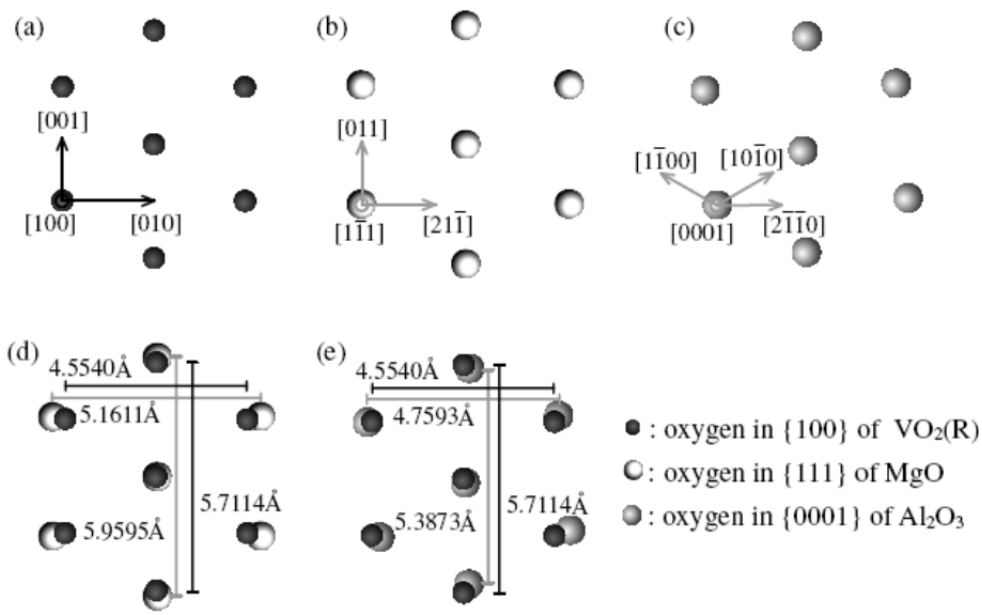

Figure 5-4. Schematic illustrations of oxygen in (a) {100} of VO_2(R), (b) {111} of MgO, and (c) {0001} of Al_2O_3. The lattice mismatch between VO_2 thin films and (e) MgO(111) and (f) Al_2O_3(0001) are shown.

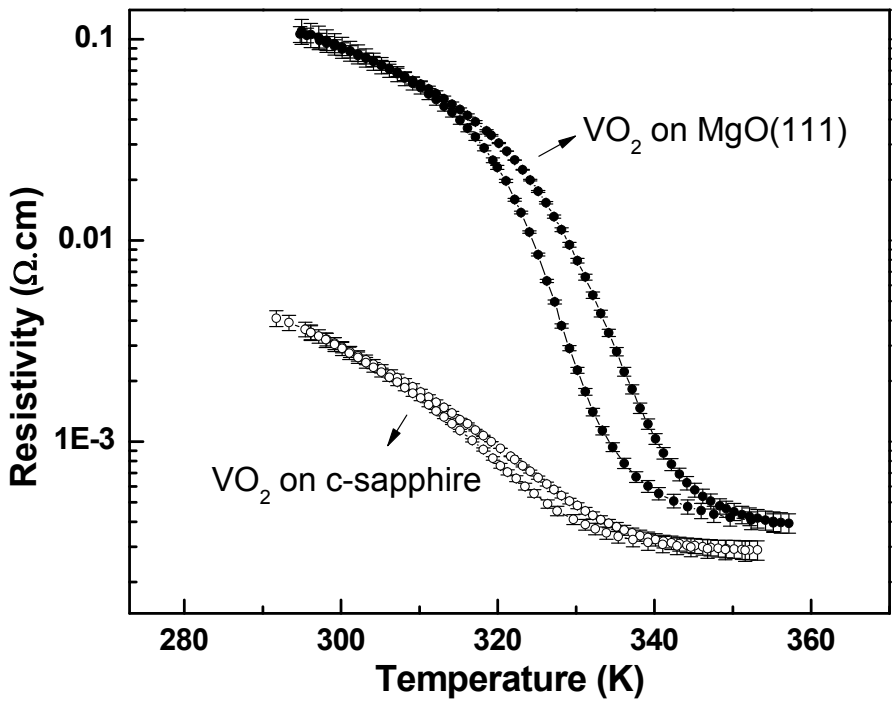

Figure 5-5 Resistivity change of VO_2 thin films

Table 5-1. Comparison of thermal stress and mismatch between VO_2/MgO(111) and VO_2/c-sapphire

	Calculated thermal stress	Lattice mismatch	Estimated T_c considering thermal stress only	T_c
VO_2/MgO(111)	0.98Gpa	4.3% (tensile)	330K	331K
VO_2/c-sapphire	1.25Gpa	5.7% (compressive)	337K[11]	318K

6. Thermochromic Properties of VO_2 thin film on SiN_x buffered glass substrate

6.1 Introduction

As the global warming became one of the greatest social issues, the efforts to control energy loss (or to use energy more efficiently) have been made by various approaches.[1],[2] Among them, applying smart coatings that can control the transmittance of the solar rays through windows in buildings has been studied widely.[3]-[5]

Thermochromic smart coating, which changes infrared transmittance with temperature, is one of the promising idea for improving energy efficiency in buildings. For the materials, vanadium dioxide(VO_2) is studied widely due to its abrupt change of reflectance in the infrared range near room temperature.[6],[7] At temperatures higher than the critical temperature T_c which is ~340K, it shows tetragonal-rutile structure(VO_2(R)) with high electrical conductivity accompanied by high infrared reflectance, while below T_c, it shows monoclinic structure

(VO_2(M)) with electrical insulating property accompanied by high infrared transmittance.[6] Through this reversible metal-to-insulator transition(MIT) near room temperature, VO_2 is considered as a material having high potentials for various applications other than thermochromic smart coatings, which include electronic switches and thermal sensors.[8]-[12]

In order to use VO_2 thin film in practical smart coating application, there are several properties to be controlled. First of all, transition temperature(T_c) of VO_2 must be made closer to room temperature. Also, visible light transmittance should be improved. But most of all, the VO_2 thin film should be easily grown on conventional soda lime glass with good optical properties.

There are many reports on controlling the T_c of VO_2 thin film, either by doping[13] or applying stress[14]. It is reported that the visible light transmittance of VO_2 thin film can be improved by designing multi-layer structure, due to the anti-reflection effect[15]. However, most of the previous studies were based on single crystal or fused silica substrates, since those were focused on the properties of VO_2 thin film.[14],[16],[17]

As mentioned, the thin film should be easily deposited on conventional soda lime glass with good optical properties. Unfortunately, depositing VO_2 thin film with good optical properties on conventional soda lime glass is difficult task due to the

sodium ion diffusion from the substrate during the deposition process.[18]-[20] Several research groups have been reported the results of direct deposition of VO_2 film on soda-lime glass, yet most of the results were not good enough practical application for smart windows.[20],[21] Although the VO_2 film showed metal-insulator transition, the resistivity and transmittance change of VO_2 thin film were small compared to those of highly crystallized VO_2. Considering these previous reports, in order to deposit VO_2 thin films with good electrical and optical properties on soda lime glass, the use of buffer layer is essential.

Introducing buffer layer between VO_2 film and the substrate have been carried out using various oxide materials, yet their purpose was heteroepitaxial growth of the VO_2 thin films[22], successful deposition on amorphous substrates[23], or improving visible light transmittance by anti-reflection effect[24]. In this work, a buffer layer was introduced in order to prevent sodium ion diffusion on the VO_2 thin film on soda-lime glass. Due to the well-known properties of high stability and strong adsorptivity with high optical transmittance in the visible light range[25], which are mostly required properties for buffer layer material in smart window application, amorphous silicon nitride(SiN_x), one of the most popular materials for diffusion barrier application, was applied between VO_2 thin film and soda lime glass in this experiment for the first time. Also, the thermochromic properties of the VO_2 based thin film has been optimized by investigating the effect of SiN_x layer thickness on

the properties.

6.2 Experimental procedure

VO_2 based multilayer thin films were deposited on 10mm x 10mm sized conventional soda lime glass. To observe and clarify the sodium ion diffusion phenomenon, VO_2 thin film was deposited on fused silica as well. The substrates were cleaned prior to the deposition process by washing with acetone, ethanol, and distilled water in ultrasonic bath for 10 minutes each which was followed by blowing with nitrogen. In order to prevent the diffusion of sodium ions, silicon nitride(SiN_x) layer was introduced between the VO_2 thin film and soda lime glass substrate. To determine the critical thickness needed for SiN_x layer to work as a diffusion barrier, 10, 30, 50, and 100nm SiN_x films were deposited by plasma-enhanced chemical vapor deposition(PECVD)(Plasmalab800Plus, Oxford, England) at 250℃. Over the substrates, VO_2 thin films were deposited by RF sputtering using 3" Φ V_2O_5 target, with 300W of RF power applied at room temperature for 20minutes. During the deposition process, argon(Ar) gas was injected with 100sccm flow rate, maintaining 20mTorr of pressure in the chamber. The deposited

films were post annealed at 550℃ with oxygen pressure of 10mTorr for 30 minutes.

After the annealing process, X-ray diffraction(XRD) patterns were obtained from Bruker D8-Advance θ-2θ diffractometer using Cu-Kα radiation and Ge111 monochromator. The thickness of each layer was determined by field emission scanning electron microscope(FE-SEM), observing a distinct edge between the film(s) and the substrate. In order to identify the existence of sodium ions in VO_2 layer, X-ray photoelectron spectroscopy(XPS) depth profile and surface analysis were carried out using a Thermo Scientific K-Alpha XPS spectrometer with a monochromatic Al Kα source.

The optical transmittance of the thin film samples was measured by VARIAN CARY5000 UV-VIS-NIR spectrometer with additional home-made heating stage. In order to determine T_c of each sample accurately, the temperature during the measurement was calibrated by attaching a thermocouple on the surface of each substrate. T_c value of VO_2 thin film has been obtained by calculating the middle point of the total integrated area of the hysteresis loop.

6.3 Results & discussion

Sodium ion was observed on the film surface by XPS surface analysis when soda lime glass was used as a substrate, whereas film on fused silica substrate did not have any sodium ion, as shown in Figure 6-1. As a result, film on soda lime glass showed no specific peak in the XRD phase analysis result(Figure 6-2(b)), meaning that the VO_2 film deposited directly on soda lime glass was not fully crystallized. Therefore, in order to deposit VO_2 thin film on soda lime glass successfully, SiN_x buffer layer was introduced between the film and the substrate. Three sets of VO_2 thin films were fabricated on soda lime glass substrates with each set having SiN_x layer between the VO_2 film and the substrate with three different thicknesses. In all samples the VO_2 thin films had uniform thickness of 75±5nm, while SiN_x layers with thicknesses of 10, 30, and 100nm were introduced between VO_2 layer and soda lime glass substrate.

Figure 6-2 shows the X-ray diffraction patterns of the VO_2 thin films deposited on conventional soda lime glass with or without SiN_x buffer layer. As mentioned above, the sample without SiN_x layer did not have any clear diffraction peak, indicating that the VO_2 film deposited directly on soda lime glass was not fully crystallized. The samples with SiN_x layer, however, had a diffraction peak with high intensity, showing (011) preferred oriented growth of VO_2(M) phase near 2θ=27.8º. These results are in good agreement with previous reports[20],[21], showing difficulties of depositing well-cyrstallized VO_2 thin film directly on soda lime glass

substrate and that the SiN_x buffer layer has contributed to the formation of VO_2(M/R) film.

Although the XRD analysis results have shown that SiN_x layer has contributed to the formation of VO_2(M/R) phase, clarifying the prevention of sodium ion diffusion is necessary. Even when no sodium ions were detected on the surface, the sodium ions may exist in the VO_2 layer. Therefore, in order to clarify the existence of sodium ions in the VO_2 layer, quantitative XPS depth profiling of each sample was carried out as shown in Figure 6-3. Clear peaks representing sodium ions were detected in the VO_2 thin film deposited directly on pure soda lime glass. The amount of diffused sodium ions in VO_2 layer decreased to zero as the thickness of SiN_x layer increased to 30nm. From the results of XRD and XPS measurements, it is clear that SiN_x layer over 30nm has successfully prevented sodium ion diffusion in VO_2 thin film, and has contributed to the formation of VO_2 thin film.

To compare the amount of diffused sodium ions and the optical properties of each sample, the percentage of diffused sodium ions in VO_2 layer were calculated by taking the average values in the entire thickness range of VO_2 layer and plotted in Figure 6-4(a). The change of optical transmittance with temperature was measured for each thin film as well.(Table 6-1 & Figure 6-4(b), (c)) The change of T_c was small when SiN_x layer was introduced, which can be attributed to the inhomogeneous distribution of T_c in the sample due to the spatial inhomogeneity in

the distribution of the factors responsible for the change of T_c of the VO_2 thin film.[26] However, the change of infrared transmittance at 2500nm wavelength with temperature from room temperature to 80°C($\Delta T_{\lambda=2500nm,\ 80°C\text{-}RT}$) has been significantly increased when the SiN_x layer was introduced, as shown in Figure 6-4(b). Comparing Figure 6-4(a) and Figure 6-4(b), when the sodium ion diffusion was prevented, the change of infrared transmittance was increased. However, since the infrared transmittance of SiN_x is not 100%, as the thickness of SiN_x layer was increased, $\Delta T_{\lambda=2500nm,\ 80°C\text{-}RT}$ showed slight decrement when the thickness of SiN_x was over 50nm.

The optical hysteresis width of the sample was decreased by almost 6K when the SiN_x layer was applied as shown in Figure 6-4(c). Considering the reports of the relation between crystallinity and hysteresis width of VO_2 film[26],[27] and the result of XRD phase analysis shown in Figure 6-2, the prevention of sodium ion diffusion led to the improvement of crystallinity of the film, which in turn resulted in the decrease of the hysterisis width. However, despite the similar crystallinities, the hysteresis widths of VO_2 on SiN_x buffered soda lime glass were larger than that of the VO_2 on fused silica. Since the hysteresis width can also be affected by grain size and residual stress[28], the difference between the substrate material can affect the grain size and/or residual stress, resulting to the difference of optical properties of each sample as well.

By considering both results of Figure 6-4(b) and (c), the optimized thickness of SiN_x layer was determined to be 30nm in this experiment. The optical transmittance of VO_2 on soda lime glass, 30nm SiN_x buffered soda lime glass, and fused silica are plotted in Fig. 5. The optical transmittance in the visible light range has been decreased when the SiN_x layer was introduced due to the improved homogeneity in the VO_2 layer by preventing sodium ion diffusion. However, by introducing 30nm thick SiN_x layer, the optical transmittance change in the near-infrared region significantly increased, which is almost the same value with that of VO_2 on fused silica, thus, enhancing the thermochromic properties of the VO_2 films for energy-saving smart coatings.

6.4 Summary

VO_2 thin films were successfully deposited on soda lime glass substrates with different thickness of SiN_x buffer layer by RF sputtering and PECVD method. SiN_x layer thicker than 30nm has successfully prevented sodium ion diffusion in VO_2 thin film and contributed to the formation of VO_2 thin film, which was confirmed by XRD spectra and XPS measurements. The transition temperature had small change when SiN_x layer was introduced, which can be due to the improved

crystallinity of the VO_2 thin film. However, the infrared transmittance change of 2500nm wavelength with temperature from room temperature to $80^oC(\Delta T_{\lambda=2500nm,80°C-RT})$ has been increased significantly. The optical hysteresis width of the sample decreased by almost 6K as well. These results suggest that applying diffusion barrier can improve the thermochromic properties of the VO_2 films for energy-saving smart coatings, and silicon nitride can be one of the effective materials which can prevent sodium ion diffusion and improve optical properties as well.

6.5 References

[1] B. O'Regan, M. Grätzel, A low-cost, high-efficiency solar cell based on dye-sensitized colloidal TiO_2 films, Nature 353 (1991) 737.

[2] O.J. Kwon, W. Jo, S. Yoon, D. Shin, H. You, K. Choi, J.S. Kim, C. Park, Relation between Seebeck Coefficient and Lattice Parameters of $(Ca_{2y}Sr_yCoO_3)_xCoO_2$, J. Elec. Mat. 41 (2012) 1513-1518

[3] H.W. Heuer, R. Wehrmann, S. Kirchmeyer, Electrochromic Window Based on Conducting Poly(3,4-ethylenedioxythiophene)±Poly(styrene sulfonate), Adv. Funct.

Mater. 12 (2002) 89-94.

[4] K.I. Jensen, J.M. Schultz, F.H. Kristiansen, Development of windows based on highly insulating aerogel glazings, J. Non-Cryst. Sol. 350 (2004) 351-357.

[5] J. Wu, X. Wei, N.P. Padture, P.G. Klemens, M. Gell, E. Garcia, P. Miranzo, M.I. Osendi, Low-Thermal-Conductivity Rare-Earth Zirconates for Potential Thermal-Barrier-Coating Applications, J. Am. Ceram. Soc. 85 (2002) 3031-3035.

[6] F.J. Morin, Oxides which show a metal-to-insulator transition at the Neel temperature, Phys Rev Lett 3 (1959) 34

[7] J.B. Goodenough, The two components of the crystallographic transition in VO_2, J. Solid State Chem. 3 (1971) 490

[8] C.H. Griffiths, H.K. Eastwood, Influence of stoichiometry on the metal-semiconductor transition in vanadium dioxide, J. Appl. Phys. 45 (1974) 2201.

[9] E.E. Chain, The infulence of deposition temperature on the structure and optical properties of vanadium oxide films, J. Vac. Sci. Technol. A4 (1986) 432.

[10] A. Razavi, L. Bobyak, P. Fallon, The effects of biasing and annealing on the optical properties of radio-frequency sputtered VO_2, J. Vac. Sci. Technol. A8 (1990) 1391.

[11] M. Fukuma, S. Zembutsu, S. Miyazawa, Preparation of VO_2 thin film and its direct optical bit recording characteristics, Applied Optics 22 (1983) 265.

[12] I.P. Parkin, T.D. Manning, Intelligent Thermochromic Windows, J. Chem. Edu. 83 (2006) 3.

[13] C. Tang, P. Georgopoulos, M.E. Fine, J.B. Cohen, M. Nygren, G.S. Knapp, A. Aldred, Local atomic and electronic arrangements in $W_xV_{1-x}O_2$, Physical Review B 31 (1985) 1000.

[14] H. Koo, S. Yoon, O.J. Kwon, K.E. Ko, D. Shin, S.H. Bae, S.H. Chang, C. Park, Effect of lattice misfit on the transition temperature of VO_2 thin film, J. Mater. Sci. 47 (2012) 6397

[15] C.G. Granqvist, S. Green, G.A. Niklasson, N.R. Mlyuka, S. von Kræmer, P. Georén, Advances in chromogenic materials and devices, Thin Solid Films 518 (2010) 3046.

[16] K. Okimura, J. Sakai, S. Ramanathan, In situ x-ray diffraction studies on epitaxial VO_2 films grown on c-Al_2O_3 during thermally induced insulator-metal transition, J. Appl. Phys. 107 (2010) 063503.

[17] D.H. Youn, J.W. Lee, B.G. Chae, H.T. Kim, S.L Maeng, K.Y. Kang, Growth optimization and electrical characteristics of VO_2 films on amorphous SiO_2/Si

substrates, J. Appl. Phys. 95 (2004) 1407.

[18] X.Wang, J. Xu, Y. Fei, D.Li, T. Li, Y. Nie, K.Feng, N. Wu, Preparation of Thermochromic VO_2 Thin Films on Fused Silica and Soda-lime Glass by RF Magnetron Sputtering, Jpn. J. Appl. Phys. 41 (2002) 312.

[19] H. Yuan, K. Feng, X. Wang, C. Li, C. He, Y. Nie, Effect of nonstoichiometry on Raman scattering of VO_2 films, Chinese Physics 13 (2004) 82.

[20] X.J. Wang, C.J. Liang, K.P. Guan, D.H Li, Y.X. Nie, S.O Zhu, F. Huang, W.W. Zhang, Z.W. Cheng, Surface oxidation of vanadium dioxide films prepared by radio frequency magnetron sputtering, Chinese Physics B 17 (2008) 3512.

[21] G. Guzman, R. Morineau, J. Livage, Synthesis of vanadium dioxide thin films from vanadium alkoxides, Mat. Res. Bull. 29 (1994) 509.

[22] A. Gupta, J. Narayan, and T. Dutta, Near bulk semiconductor to metal transition in epitaxial VO_2 thin films, Appl. Phys. Lett. 97 (2010) 151912.

[23] K. Kato, P.K. Song, H. Odaka, and Y. Shigesato, Study on Thermochromic VO2 Films Grown on ZnO-Coated Glass Substrates for “Smart Windows”, Jpn J Appl Phys 42 (2003) 6523-6531.

[24] P. Jin, G. Xu, M. Tazawa, K. Yoshimura, Design, formation and characterization of a novel multifunctional window with VO_2 and TiO_2 coatings,

Appl. Phys. A 77 (2003) 455-459.

[25] H. Ohsaki, Y. Tachibana, K. Kadowaki, Y. Hayashi, K. Suzuki, Bendable and temperable solar control glass, J. Non-Cryst. Sol. 218 (1997) 223-229.

[26] P. Jin, S. Tanemura, Formation and Thermochromism of VO_2 Films Deposited by RF Magnetron Sputtering at Low Substrate Temperature, Jpn. J. Appl. Phys. 33 (1994) 1478-1483.

[27] J.Y. Suh, R. Lopez, L.C. Feldman, R.F. Haglund Jr., Semiconductor to metal phase transition in the nucleation and growth of VO_2 nanoparticles and thin films, J. Appl. Phys. 96 (2004) 1209-1213.

[28] K.Y. Tsai, T.S. Chin, H.Shieh, and C.H. Ma, Effect of as-deposited residual stress on transition temperatures of VO_2 thin films, J. Mater. Res. 8 (2004) 2306-2314.

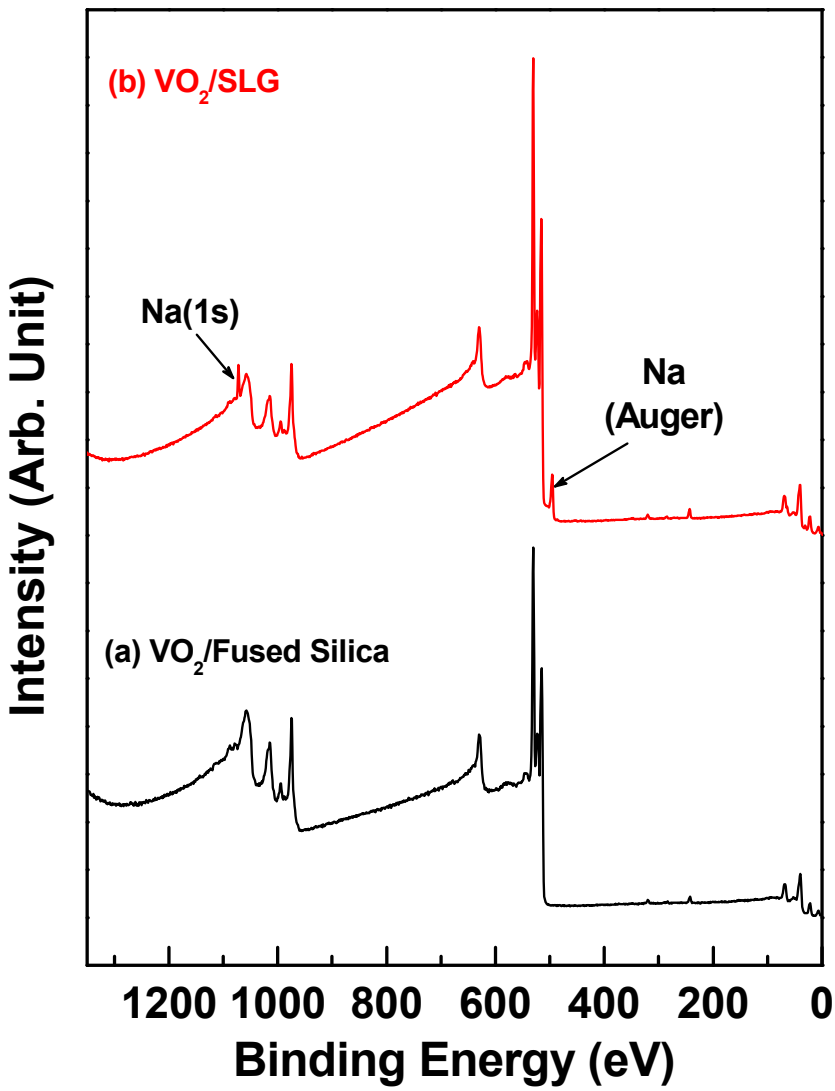

Figure 6-1. XPS surface analysis of VO_2 thin films on (a) fused silica and (b) soda lime glass.

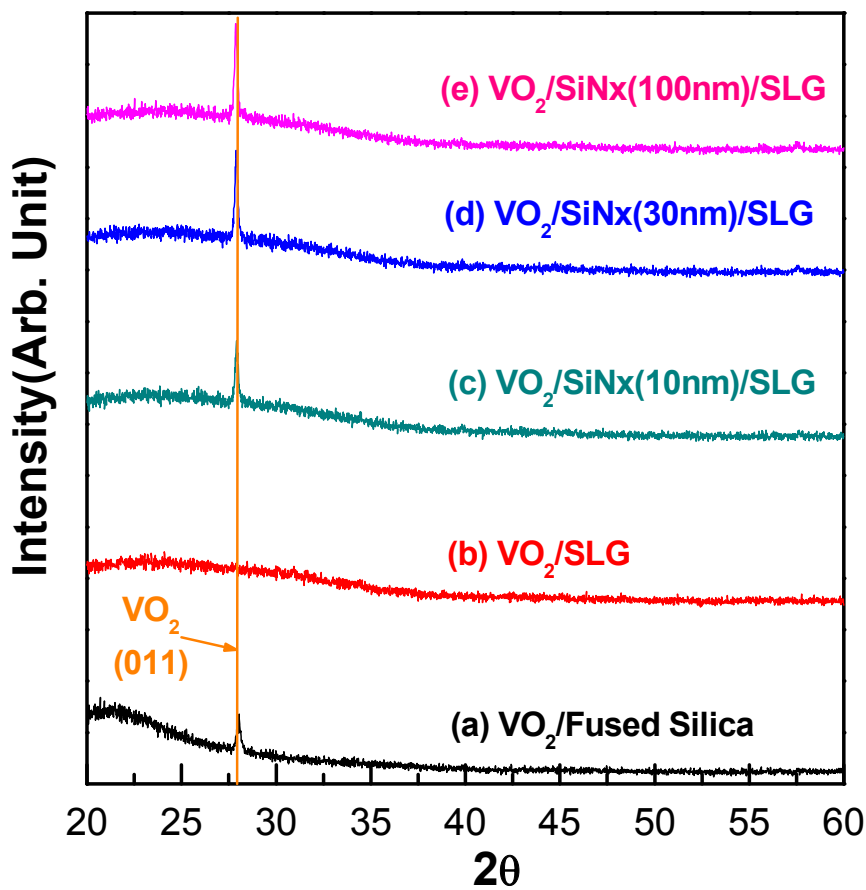

Figure 6-2. XRD phase analysis results of vanadium dioxide thin films deposited on (a) fused silica, (b) soda lime glass, and (c) 10nm, (d) 30nm (e) 100nm thick silicon nitride buffered soda lime glass.

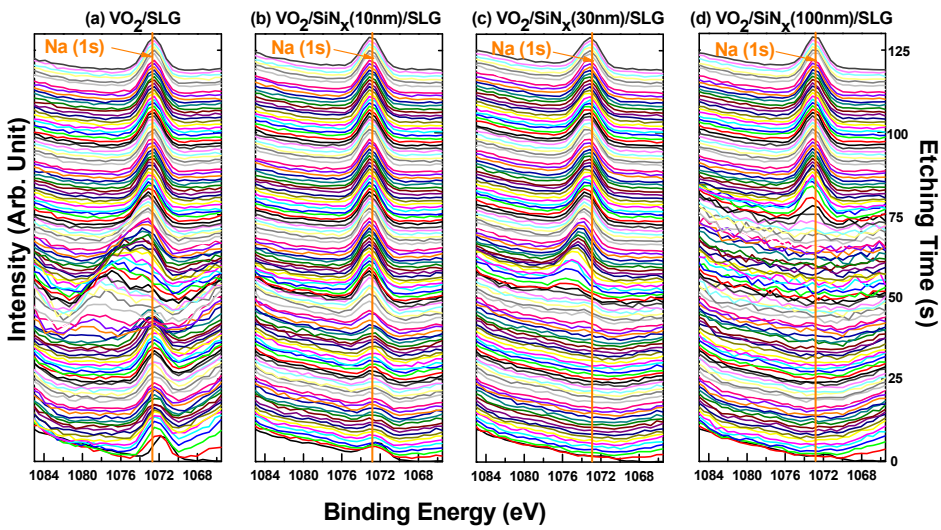

Figure 6-3. XPS depth profiling results of Na^+ ions in (a) VO_2/SLG, (b) VO_2/SiN_x(10nm)/SLG, (c) VO_2/SiN_x(30nm)/SLG, and (d) VO_2/SiN_x(100nm)/SLG.

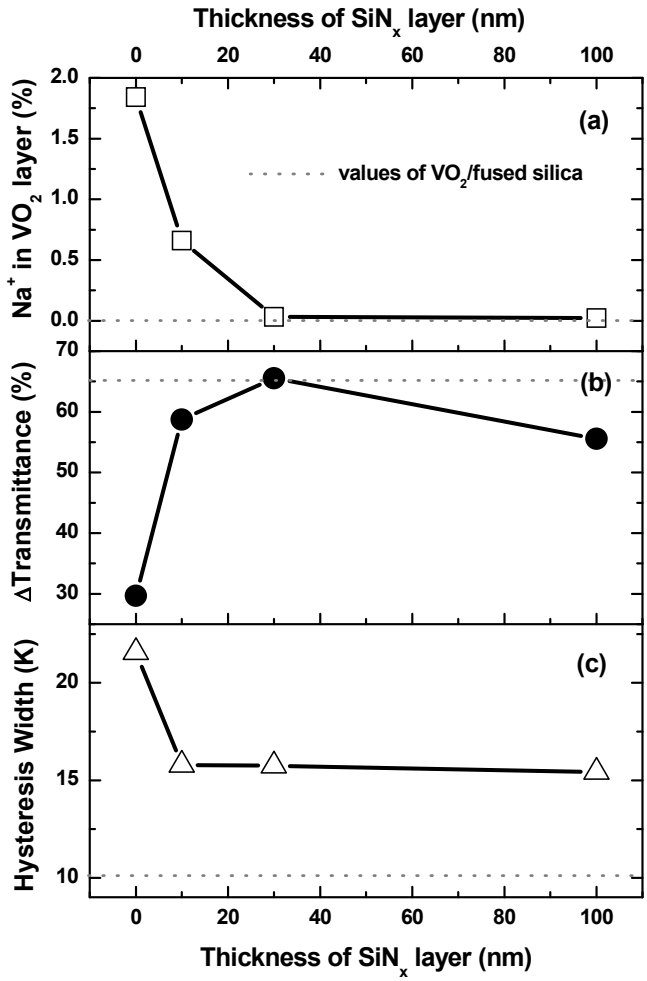

Figure 6-4. XPS depth profile analysis result of VO_2/SiN_x thin films on soda lime glass with and without SiN_x buffer layer: (a) the amount of sodium ion diffused in VO_2 layer, (b) infrared transmittance change at 2500nm wavelength from 80^oC to room temperature, and (c) hysteresis width of each sample

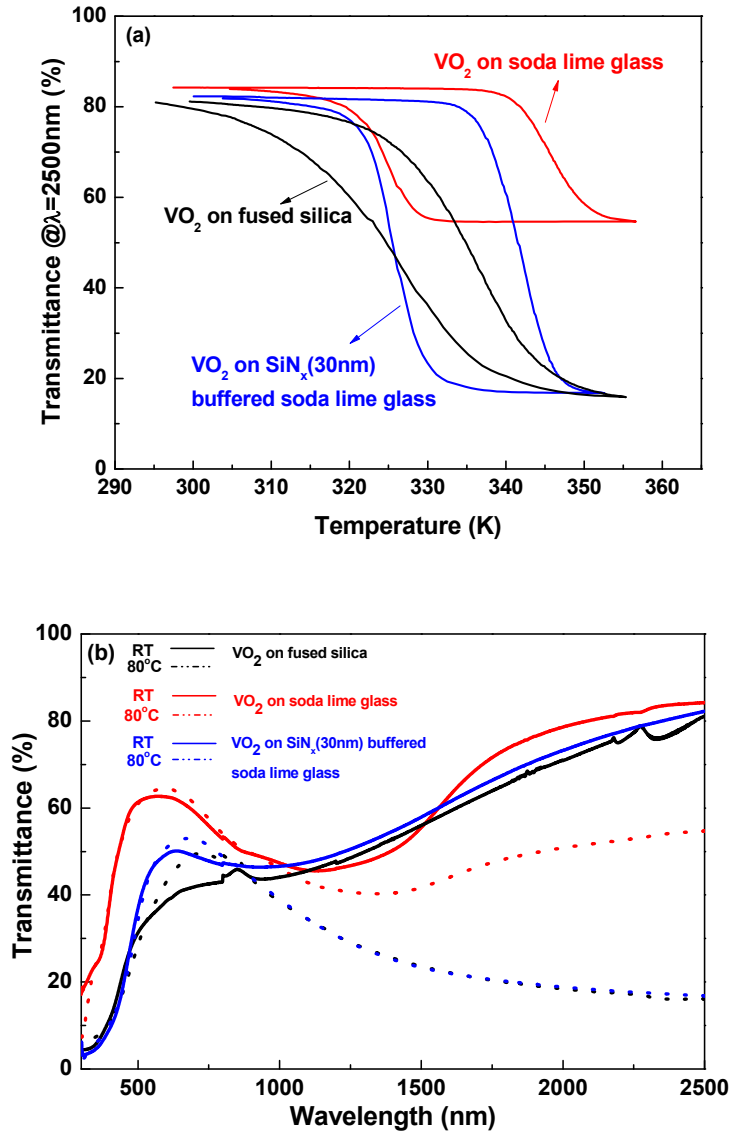

Figure 6-5. Optical transmittance of VO_2 thin films: (a) infrared transmittance change at 2500nm wavelength, (b) transmittance spectra at room temperature and 80°C

Table 6-1. Thermochromic properties of VO_2 + SiN_x films. (The thickness of VO_2 = 75±5nm).

substrate	T_c (K)	$\Delta T_{\lambda=2500nm,80°C-RT}$ (%)	Hysteresis Width (K)
fused silica	330	65.28	10.2
soda lime glass	336.5	29.56	21.5
10nm SiN_x buffered soda lime glass	334	58.72	15.7
30nm SiN_x buffered soda lime glass	333	65.52	15.9
100nm SiN_x buffered soda lime glass	334	58.81	15.8

Chapter 7. Effect of oxide buffer layer on the thermochromic properties of VO_2 thin films

7.1 Introduction

The increase of using heating/cooling system in buildings to maintain comfortable environments has led to the increase in the use of electricity and carbon dioxide emissions during the electricity generation process. As a result, global warming is becoming most serious environmental problem which the earth faces, and the efforts to use energy efficiently have been made by various methods.[1],[2] Many ways to reduce the energy consumption in buildings have been proposed, and applying smart coatings to window glass is one way to control the transmittance of the solar rays through windows in buildings.[3]-[5]

To use thermochromic smart window, which automatically changes its optical properties with temperature without consuming extra energy, is considered as a promising way to save energy used in heating/cooling system of buildings. Vanadium dioxide(VO_2) is considered to be the most promising material for

thermochromic smart window due to its abrupt change of reflectance in the infrared(IR) range near room temperature.[6],[7] At temperatures higher than the phase transition critical temperature T_c which is ~340K, it has tetragonal-rutile structure(VO_2(R)) with high electrical conductivity accompanied by high IR reflectance, while below T_c, it has monoclinic structure (VO_2(M)) with electrical insulating property accompanied by high IR transmittance.[6] Through this reversible metal-to-insulator transition(MIT) near room temperature, VO_2 is considered as a material having high potentials for various applications other than thermochromic smart coatings, which include optical switching/recording device, IR sensor, varistor, un-cooled microbolometer.[8]-[12]

In order for VO_2 thin film to be used in practical smart window application, several issues have to be addressed. First of all, controlling T_c is a critical issue. It has been found that T_c can be controlled by doping[13] or applying stress[14]. Secondly, visible light transmittance should be enhanced. Several reports[15],[16] revealed that the visible light transmittance can be improved by anti-reflective coating on the surface of VO_2 film. Reducing film thickness of VO_2 film can be another method to improve visible light transmittance.[17] Finally, the thermochromic VO_2 thin film should be easily grown on conventional soda lime glass with good optical properties. It has been reported that sodium ions from soda lime glass hinder the formation of thermochromic VO_2 thin film during the

deposition process.[18] Moreover, it is reported that sodium ions in soda lime glass can be diffused at room temperature.[19]

To use buffer layer between the VO_2 film and the soda lime glass substrate is a good method to improve the thermochromic properties of VO_2 films deposited at low temperature (< 400℃). Morever, it can modify the surface morphology of VO_2 film[20] and can also work as diffusion barrier[21]. Therefore, using buffer layer can help deposit VO_2 film with excellent thermochromic transition properties on soda lime glass. There, however, are few reports that have systematically studied the effects of buffer layer material on the growth and properties of VO_2 film. H. Miyazaki et al., used various metal buffer layer for successful VO_2(M/R) film deposition and concluded that the melting point of the metal buffer layer material is related with the formation of VO_2(M/R) phase.[22] Yet, there were no reports comparing thermochromic properties of VO_2 thin films on various oxide buffered soda lime glass substrates systematically. In this work, different oxide buffer layers were used in order to investigate the effect of buffer layer material on the formation and thermochromic properties of VO_2 film. The applied buffer layer materials were ZnO, SnO_2, TiO_2, and CeO_2. ZnO, which shows closed packed structure over (0001) plane, has been known as an efficient buffer layer material for depositing VO_2 thin film due to its easy crystallization on amorphous substrate[23] and the same surface symmetry with (010) VO_2(M) plane[24]. SnO_2 and TiO_2, which have same

tetragonal rutile structure as VO_2(R), were chosen to compare properties with those of ZnO buffered VO_2 film. CeO_2(cubic structure) buffer layers was used in order to observe and compare the effect of different surface symmetry on the formation of VO_2(M/R) thin film.

7.2 Experimental details

In order to deposit film on soda lime glass substrates, pulsed laser deposition(PLD) method was used. 1"Φ V_2O_5 pellet target was used for VO_2 film deposition, and the 1"Φ ZnO, TiO_2, SnO_2 and CeO_2 targets were used for buffer layers. The temperature and time of sintering of each target was 600^{o}C-12hrs, 1200^{o}C-10hrs, 1200^{o}C-10hrs, 1600^{o}C-5hrs, and 1200^{o}C-6hrs, for V_2O_5, ZnO, TiO_2, SnO_2, and CeO_2, respectively. The soda lime glass substrates with sizes of 10mm x 10mm x 1.6mm, were cleaned prior to the deposition process by washing with acetone, ethanol, and distilled water in ultrasonic bath for 10 minutes each and then blown with nitrogen. The films of VO_2 and buffer layers were deposited using PLD method using KrF excimer (248nm) laser. The base pressure was fixed at about 10^{-6} Torr using rotary pump and turbo-molecular pump, and the target-substrate

distance was 5 cm. The optimized deposition conditions for the VO_2 film and buffer layers were used; 370°C with P_{O2}=10mTorr for VO_2 and ZnO film, 490°C with P_{O2}=100mTorr for TiO_2 and SnO_2, and 370°C with P_{O2}=100mTorr for CeO_2. The deposition rates were 13nm/min, 11nm/min, 22nm/min and 16nm/min for ZnO, TiO_2, SnO_2 and CeO_2, respectively.

The X-ray diffraction patterns were obtained from Bruker D8Advance θ-2θ diffractometer using Cu-Kα radiation and Ge111 monochromator. Film thickness was determined by FE-SEM, observing a distinct edge between the film and the substrate. The temperature dependence of resistivity was measured using Hall measurement system based on the 4 probe stage and van der Pauw method with additional heating stage attached. In order to determine T_c of each sample accurately, the temperature during resistivity measurement was calibrated by attaching thermocouple on the surface of each substrate. The optical transmittance of the film samples was measured by Varian Cary5000 UV-VIS-NIR spectrometer with additional home-made heating stage.

7.3 Results and discussions

In order to study the effect of buffer layers on the thermochromic properties of VO_2 films, VO_2 films were deposited on soda lime glass substrate with buffer layers of ZnO, TiO_2, SnO_2 and CeO_2 at 370℃. By controlling deposition time considering deposition rate of each layer, the thicknesses of VO_2 film and buffer layers were fixed at 75nm and 50nm, respectively. Figure 7-1 shows the XRD patterns of VO_2 thin films with and without buffer layer at 370℃. Peaks corresponding to VO_2(B) (002) and VO_2(B) (003) are observed when VO_2 film was deposited on soda lime glass substrate directly. VO_2(B) is a metastable compound of VO_2 and has no phase transitions near room temperature. The formation of VO_2 (B) phase is believed to be caused by low deposition temperature, which is consistent with the results previous reported.[25]

When VO_2 films were fabricated on ZnO, TiO_2 and SnO_2, however, VO_2(M) peaks are observed without any peaks from VO_2(B). It has been found that an irreversible transformation from VO_2(B) to VO_2(R) can be affected by annealing of VO_2(B) in an inert atmosphere at 400-500℃[25]. The deposition temperature of VO_2 used in this study was fixed at 370℃, and the formation of VO_2(M) can be affected by the presence of buffer layers rather than transformed from VO_2(B). It indicates

that the crystallization temperature for VO_2(M) was reduced by using buffer layers. Similar phenomenon was reported by Zhang et al.[26], who observed the change of synthesis temperature of VO_2(M) when F-doped SnO_2 (FTO) glass substrate was used. It was believed that FTO buffer layer helped the formation of VO_2(M), which can result from the same crystalline structure and similar lattice parameters of FTO and VO_2(R). Similarly, applying TiO_2 buffer layer can also help the formation of VO_2(M) due to its structural similarity with VO_2(R) as shown in Table 7-1. However, even though the formation of VO_2(M) was identified after the film was deposited after the deposition of TiO_2 buffer layer, the presence of rutile TiO_2 phase in the film architecture has not been confirmed by XRD at this condition as shown in Figure 7-1. It has been generally known that TiO_2 films with pure rutile phase can be deposited at high temperatures of 700℃-800℃. Since the deposition temperature for TiO_2 buffer layer(490℃ in this work) was limited to 550℃, the glass transition temperature of soda lime glass, the TiO_2 layer may be amorphous or mixed phases of rutile and anatase TiO_2. If the TiO_2 buffer layer is amorphous, it can be expected that the buffer layer only acts as a diffusion barrier for sodium ion diffusion, and the crystallinity of VO_2(M/R) can be low compared to that on highly crystallized substrate. If the TiO_2 layer consists of mixed phases of rutile and anatase TiO_2, due to the large mismatch between anatase TiO_2 and VO_2(M/R), the formation of VO_2(M/R) may have been inhibited. For both occasion, the degree of

crystallization of VO_2 film can be smaller compared to that on highly crystallized substrate.

ZnO has hexagonal crystal structure which is similar with that of sapphire, and its thin film can be grown with the preferred orientation of [0001] even on glass substrate at 370^{o}C, which is lower than the glass transition temperature of soda lime glass, as shown in the XRD data. Therefore, ZnO can be a promising material for buffer layer that can help the formation of VO_2(M). And the result is in good agreement with the expectation that VO_2(M) was heteroepitaxially grown on ZnO buffer layer. Similar results have been previously reported.[24] On the other hand, the VO_2(B) was the dominant phase when VO_2 film was deposited on CeO_2 buffer layer. As shown in Table 1, the crystal structure of CeO_2 is cubic which is different from that of thermochromic VO_2(M/R). Therefore, the effect of CeO_2 buffer layer on the formation of VO_2(M) is limited. Thus, the results indicate that the structure of buffer layer is very important for the growth of VO_2 thin films below the glass transition temperature of soda lime glass, which is generally around 550^{o}C.

Figure 7-2 shows the variation of the electrical resistivity of VO_2 films deposited on soda lime glass with and without buffer layers as a function of temperature for both heating and cooling cycles. The VO_2 film on glass exhibits no MIT at the measured temperature range due to the formation of VO_2(B) as the dominant phase which has no MIT near room temperature. The film deposited on CeO_2 shows very

small change of resistivity from 30℃ to 90℃. It reveals that there exists a very small amount of VO_2(M), even though no VO_2(M) peak is observed in the XRD pattern. The characteristic VO_2 transition from the low-temperature semiconductor phases to the high temperature metallic phase is clearly observed when the VO_2 films were grown on ZnO, TiO_2 and SnO_2 buffer layers. Such abrupt changes in resistivity imply the formation of VO_2(M) in the films which has been confirmed in XRD spectra.

Figure 7-3 shows the spectral transmittance of VO_2 films deposited on different buffer layers for both semiconductor and metal phases. The IR transmittance changes of the VO_2 films are dependent on the buffer layer material used. When VO_2 film was grown on CeO_2 buffer layer, the IR transmittance change(@λ=2500nm) was only 7% which is consistent with the results that showed almost no resistivity change. The IR transmittance changes of VO_2 films deposited on the other three buffer layers, however, are larger than 40% which is comparable to the values reported for fully crystallized VO_2 films deposited on single crystal Si substrate at 300^{o}C [27].

The observed electrical and optical characteristics of VO_2 films deposited on ZnO, TiO_2, and SnO_2 buffer layers are summarized in Table 7-2. The transition temperature (T_c) is defined as the center of the derivative curve of the heating curve

in Figure 7-3. The sharpness of transition (ΔS) is characterized by the full width at half maximum (FWHM) of the derivative curve. And the hysteresis width (ΔH) is the difference between the T_c values measured during the heating and cooling cycles. Such thermochromic properties of a stoichiometric VO_2(M/R) film depend on stresses present, microstructure, and orientation of the films.

The T_c value of VO_2 films on ZnO, TiO_2 and SnO_2 are 64℃, 62℃ and 61℃, respectively. These value are slightly smaller than that of VO_2 bulk single crystal (68℃). The reduction of T_c is generally ascribed to the level of internal stress. The total stress in the film is a combination of thermal stress caused by the difference in thermal expansion coefficients between film and buffer layers and the internal stress produced by the lattice mismatch between film and buffer layers [14].

The amplitude of transition (ΔA) is defined as the resistivity changes(ΔR) and the IR transmittance changes(ΔT%) at λ=2500nm from room temperature to 90℃ in this work. The ΔR at temperatures from room temperature to 90℃ of VO_2 films depsoited on ZnO, TiO_2 and SnO_2 are 5.9×10^2, 1.2×10^2 and 4×10^2, respectively. It was reported that the degree of VO_2(M/R) crystallization is related with the amplitude of transition of VO_2 thin film.[24] The observed large ΔR values imply that thermochromic VO_2 thin films with high crystallinities delta R were successfully deposited on the buffer layers. However, compared with each other,

the ΔR of VO_2 deposited on ZnO buffer layer exhibited the highest value, and such was also the case in the ΔT%. ΔT% of VO_2 film on ZnO was larger than films deposited on any other buffer layers, and the film on TiO_2 has the smallest ΔT%, as shown in Table 7-2. The changes of optical and electrical properties observed in this work are consistent with each other.

It has also been found that the ΔA depends on the crystallinity of VO_2 film. The VO_2 on glass substrate with thickness of 80 nm showed no clear abrupt ΔR which is similar with the result of K. Kato et al..[24], However, by using ZnO buffer layer, the ΔR of 2 orders of magnitude was obtained , which can be attributed to the improved crystallinity of VO_2 film when deposited on ZnO buffer layer. It is well known that ZnO film can be easily crystallized on glass substrate with c-axis preferred orientation.[23] However, for TiO2 buffered sample, as mentioned above, due to the relatively low deposition temperature (490℃), XRD peaks from rutile TiO_2 has not been observed. The sample with SnO_2 buffer layer has SnO_2 peak while that with TiO_2 does not. Therefore, it can be assumed that the crystallinity of VO_2 film on ZnO is the highest and that on TiO_2 is the lowest, which leads to the largest and smallest ΔA values of VO_2 film on ZnO and TiO_2, respectively.

The sharpness of the transition (ΔS) appears to be related to the degree of misorientation between adjacent grains in the film.[28].[29] In single phase solids, the

crystallographic matching at grain boundaries permits the shear transformation front to propagate relatively unimpeded, producing a transformation width as low as 0.1℃[28]. However, the microstructure of the unoriented film was much more irregular due to the lack of constrained crystallization in the films. This lack of registry at grain boundaries can result in a discontinuous propagation of the transformation, requiring additional thermal energy to cross the boundaries. This leads to the broadening of the transformation width, which is commonly 5-10℃ in unoriented films and only 2-4℃ in the oriented films[29]. The ΔS values of VO_2 films on ZnO, TiO_2 and SnO_2 buffer layers are 7.5℃, 9.5℃ and 9.4℃, respectively. It is observed by XRD pattern that VO_2 film is grown on ZnO buffer layer with highly c-axis preferred orientation. Thus, the VO_2 film on ZnO buffer layer can be considered as out-of-plane textured. Therefore, the degree of grain boundary misorientation of VO_2 film on ZnO is smaller than that on TiO_2. The ΔS values of VO_2 films on SnO_2 and TiO_2 buffer layers are similar, which can be attributed to the similar degrees of grain boundary misorientation.

The hysteresis behavior in the transitions of VO_2 is found in both thin films and single crystals. In the single crystals, a ΔH of 1-2℃ is commonly reported. The hysteresis behavior in the transitions of VO_2 is due to the internal stresses and misorientation induced at the grain boundaries within the structure[30]. Electrical

switching curves reported in the literature have generally shown larger hysteresis for the thin films than for single crystals, which was attributed primarily to the unoriented nature of films. In this work, the ΔH of VO_2 films are 7℃, 10.5℃and 15℃ when deposited on ZnO, SnO_2 and TiO_2 buffer layers, respectively. J.Y. Suh et al.[31] found that the ΔH became larger when the grains grew in size. This contradiction was explained by the hypothesis that MIT in VO_2 can be described on the model of a martensitic transformation in which the density of heterogeneous nucleation centers, such as structural defects or oxygen vacancies, grain boundaries as well, plays the essential role in the phase transformation. Therefore, the ΔH becomes narrow in the films with small granules because the phase transition can easily occur in this highly defective structure. Moreover, a clear relationship between ΔH and degree of misorientation has also been observed. The degree of crystallographic misorientation between adjacent grains has been reported to be related to the sharpness of the transition. [29] Metallic regions can be effectively propagated without additional energy loss when the grain boundary misorientation angles are small, which can lead to narrow ΔH. Therefore, the difference of ΔH values of VO_2 films on different buffer layers can result from the combined effect of the grain size and the grain boundary misorientation.

By considering XRD result and thermochromic properties of each sample, it can be concluded that 1. Buffer layers with similar surface symmetry contribute to the

formation of highly crystallized VO_2 thin film, and 2. The crystallinity of VO_2 can be improved significantly by using highly crystallized thin film buffer layer as well.

7.4 Summary

In order to investigate the effect of buffer layers on the thermochromic properties of VO_2 thin film, different buffer layers were deposited on soda lime glass substrate using pulsed laser deposition method. VO_2 (B) instead of VO_2 (M) was formed when the films were deposited directly on soda lime glass substrate at low deposition temperature of 370℃. However, by using ZnO, TiO_2 and SnO_2 buffer layers, VO_2 (M) film could be successfully fabricated on soda lime glass at 370℃. On the contrary, VO_2 (B) is formed rather than VO_2 (M) when VO_2 film was deposited on CeO_2 buffer layer. The structure of buffer layer can play an important role in the growth of VO_2 films. Furthermore, the excellent thermochromic transition properties of VO_2(M) films were obtained by using ZnO, TiO_2 and SnO_2 buffer layers.

Compared with other buffer layer materials, the VO_2 film deposited on ZnO

buffer layer exhibits the best characteristics of thermochromic transition which shows the largest amplitude of transition and abruptness of transition with smallest hysteresis width. The difference in MIT characteristics has been explained to arise from the different buffer layer materials that can lead to different degree of grain boundary misorientations of VO_2 films. ZnO is easily grown on glass substrate with high degree of preferred orientation, which can lead to the VO_2 film with superior thermochromic properties compared to those on other buffer layer materials. These results suggest that deposition of VO_2 thin films on soda lime glass with excellent thermochromic properties can be achieved by considering the buffer layer material having structural similarity with VO_2, and ZnO can be one of the most effective buffer layer materials.

7.5 References

[1] B. O'Regan, M. Grätzel, A low-cost, high-efficiency solar cell based on dye-sensitized colloidal TiO_2 films, Nature 353 (1991) 737.

[2] O.J. Kwon, W. Jo, S. Yoon, D. Shin, H. You, K. Choi, J.S. Kim, C. Park,

Relation between Seebeck Coefficient and Lattice Parameters of $(Ca_{2y}Sr_yCoO_3)_xCoO_2$, J. Elec. Mat. 41 (2012) 1513-1518

[3] H.W. Heuer, R. Wehrmann, S. Kirchmeyer, Electrochromic Window Based on Conducting Poly(3,4-ethylenedioxythiophene)±Poly(styrene sulfonate), Adv. Funct. Mater. 12 (2002) 89-94.

[4] K.I. Jensen, J.M. Schultz, F.H. Kristiansen, Development of windows based on highly insulating aerogel glazings, J. Non-Cryst. Sol. 350 (2004) 351-357.

[5] J. Wu, X. Wei, N.P. Padture, P.G. Klemens, M. Gell, E. Garcia, P. Miranzo, M.I. Osendi, Low-Thermal-Conductivity Rare-Earth Zirconates for Potential Thermal-Barrier-Coating Applications, J. Am. Ceram. Soc. 85 (2002) 3031-3035.

[6] F.J. Morin, Oxides which show a metal-to-insulator transition at the Neel temperature, Phys Rev Lett 3 (1959) 34

[7] J.B. Goodenough, The two components of the crystallographic transition in VO_2, J. Solid State Chem. 3 (1971) 490

[8] C.H. Griffiths, H.K. Eastwood, Influence of stoichiometry on the metal-semiconductor transition in vanadium dioxide, J. Appl. Phys. 45 (1974) 2201.

[9] E.E. Chain, The infulence of deposition temperature on the structure and optical properties of vanadium oxide films, J. Vac. Sci. Technol. A4 (1986) 432.

[10] A. Razavi, L. Bobyak, P. Fallon, The effects of biasing and annealing on the optical properties of radio-frequency sputtered VO_2, J. Vac. Sci. Technol. A8 (1990) 1391.

[11] M. Fukuma, S. Zembutsu, S. Miyazawa, Preparation of VO2 thin film and its direct optical bit recording characteristics, Applied Optics 22 (1983) 265.

[12] I.P. Parkin, T.D. Manning, Intelligent Thermochromic Windows, J. Chem. Edu. 83 (2006) 3.

[13] C. Tang, P. Georgopoulos, M.E. Fine, J.B. Cohen, M. Nygren, G.S. Knapp, A. Aldred, Local atomic and electronic arrangements in $W_xV_{1-x}O_2$, Physical Review B 31 (1985) 1000.

[14] H. Koo, S. Yoon, O.J. Kwon, K.E. Ko, D. Shin, S.H. Bae, S.H. Chang, C. Park, Effect of lattice misfit on the transition temperature of VO_2 thin film, J. Mater. Sci. 47 (2012) 6397

[15] G.Xu, et al., Optimization of antireflection coating for VO_2-based energy efficient window, Solar Energy Materials & Solar Cells83 (2004) 29-37.

[16] P. Jin, et al., Design, formation and characterization of a novel multifunctional window with VO_2 and TiO_2 coatings, Appl. Phys. A77 (2003) 455-459.

[17] G. Xu, P. Jin, M. Tazawa, and K. Yoshimura, Thickness dependence of optical

properties of VO_2 thin films epitaxially grown on sapphire (0001), Applied Surface Science 244 (2005) 449.

[18] G. Guzman, R. Morineau, J. Livage, Synthesis of vanadium dioxide thin films from vanadium alkoxides, Materials Research Bulletin 29 (1994) 509.

[19] J.V. Fitzgerald, Anelasticity of Glass: II, Internal Friction and Sodium Ion Diffusion in Tank Plate Glass, A Typical Soda-Lime-Silica Glass, J. Am. Ceram. Soc. 34 (1951) 339-342

[20] K. Nagashima, T. Yanagida, H. Tanaka, and T. Kawai, Interface effect on metal-insulator transition of strained vanadium dioxide ultrathin films, J. Appl. Phys. 101 (2007) 026103

[21] H.Koo, H.W. You, K.E. Ko, O.J. Kwon, S.H. Chang, C. Park, Thermochromic properties of VO_2 thin film on SiNx buffered glass substrate, Appl. Surf. Sci. (2013) http://dx.doi.org/10.1016/j.apsusc.2013.04.031, in press.

[22] H. Miyazaki, I. Yasui, Effect of buffer layer on VO_x film fabrication by reactive RF sputtering, Appl. Surf. Sci. 252 (2006) 8367-8370

[23] J.J. Wu, S.C. Liu, Low-temperature growth of well-aligned ZnO nanorods by chemical vapor deposition, Adv. Mater. 14 (2002) 215

[24] K. Kato, P.K. Song, H. Odaka, and Y. Shigesato, Study on Thermochromic

VO_2 Films Grown on ZnO-Coated Glass Substrates for “Smart Windows”, Jpn. J. Appl. Phys. 42 (2003) 6523-6531.

[25] C. Leroux, G. Nihoul, G.V. Tendeloo, From VO_2(B) to VO_2(R): Theoretical structures of VO_2 polymorphs and in situ electron microscopy, Physical Review B 57 (1998) 5111-5121

[26] Z.T. Zhang et al., Solution-based fabrication of vanadium dioxide on F:SnO_2 substrates with largely enhance thermochromism and low-emissivity for energy-saving applications, Energy & Environmental Science 4 (2011) 4290-4297

[27] P. Jin, S. Tanemura, Formation and Thermochromism of VO_2 Films Deposited by RF Magnetron Sputtering at Low Substrate Temperature, Jpn. J. Appl. Phys. 33 (1994) 1478-1483

[28] D. Kucharczyk, T. Niklewski, Accurate X-ray determination of the lattice-parameters and the thermal-expansion coefficients of VO_2 near the transition-temperature, J. Appl. Cryst. 12 (1979) 370-373

[29] J.F. De Natale, P.J. Hood, A.B. Harker, Formation and characterization of grain-oriented VO_2 thin films, J. Appl. Phys. 66(1989) 5844-5850

[30] J.B. Macchesney, H.J. Guggenheim, Growth and electrical properties of vanadium dioxide single crystals containing selected impurity ions, J. Phys. Chem.

Solids 30 (1969) 225

[31] J.Y. Suh, R. Lopez, L.C. Feldman, R.F. Haglund Jr., Semiconductor to metal phase transition in the nucleation and growth of VO_2 nanoparticles and thin films, J. Appl. Phys. 96 (2004) 1209-1213.

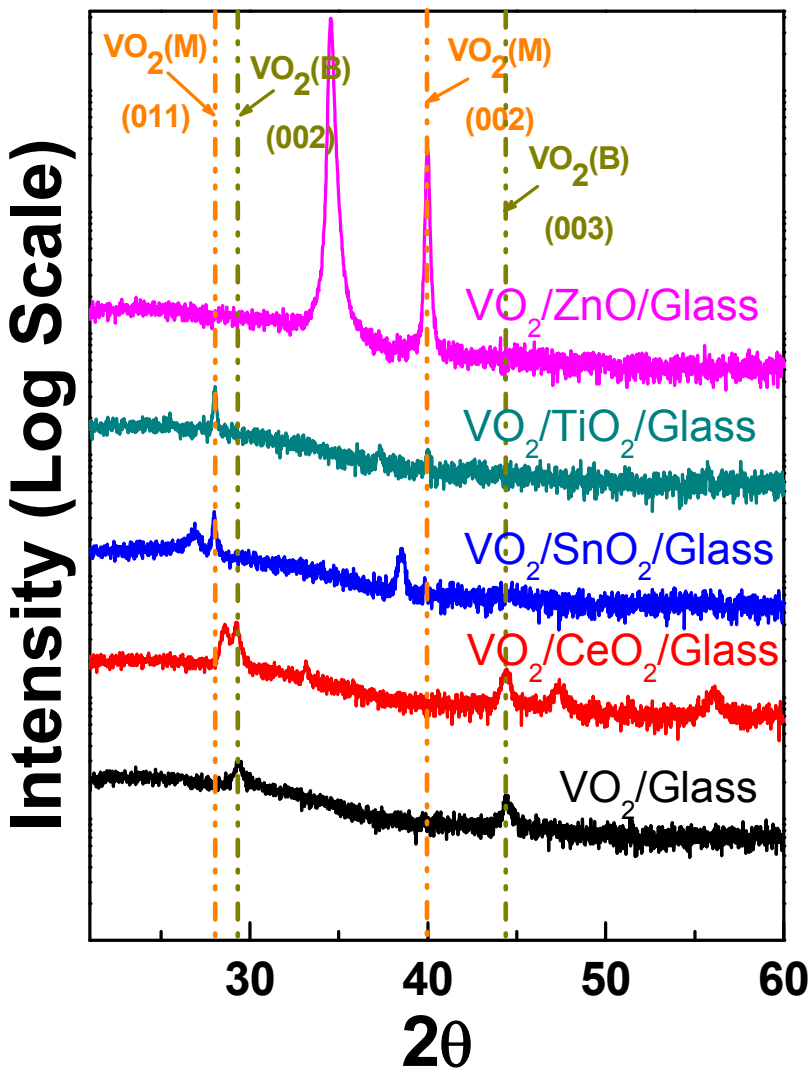

Figure 7-1. XRD spectra of VO_2 thin films with and without buffer layers

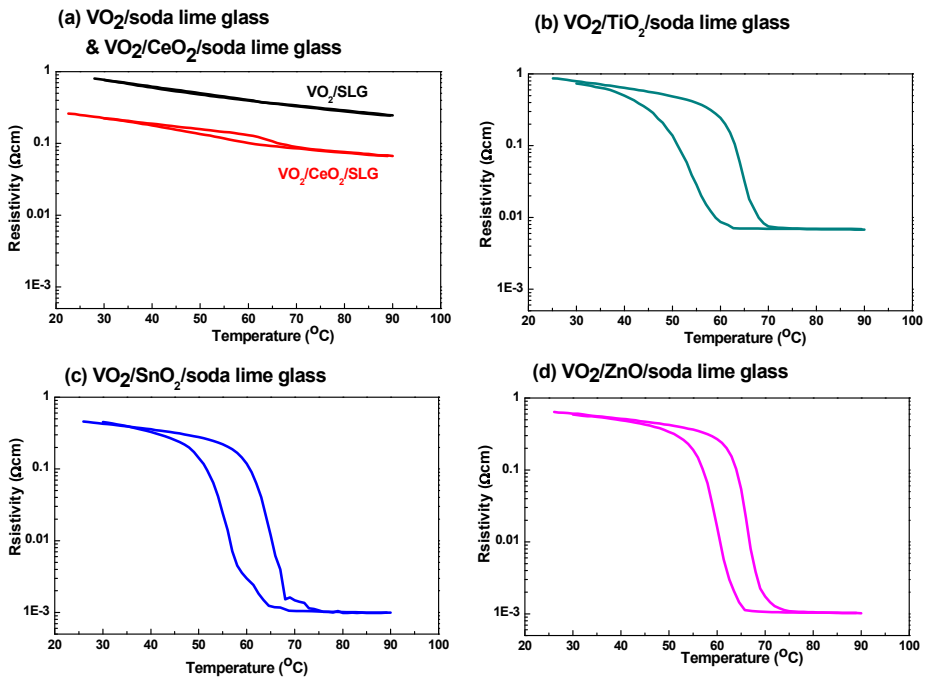

Figure 7-2. Resistivity spectra of VO_2 film deposited on soda lime glass substrate (a)without any buffer layer & CeO_2 , (b)TiO_2, (c)SnO_2, and (d)ZnO buffer layer

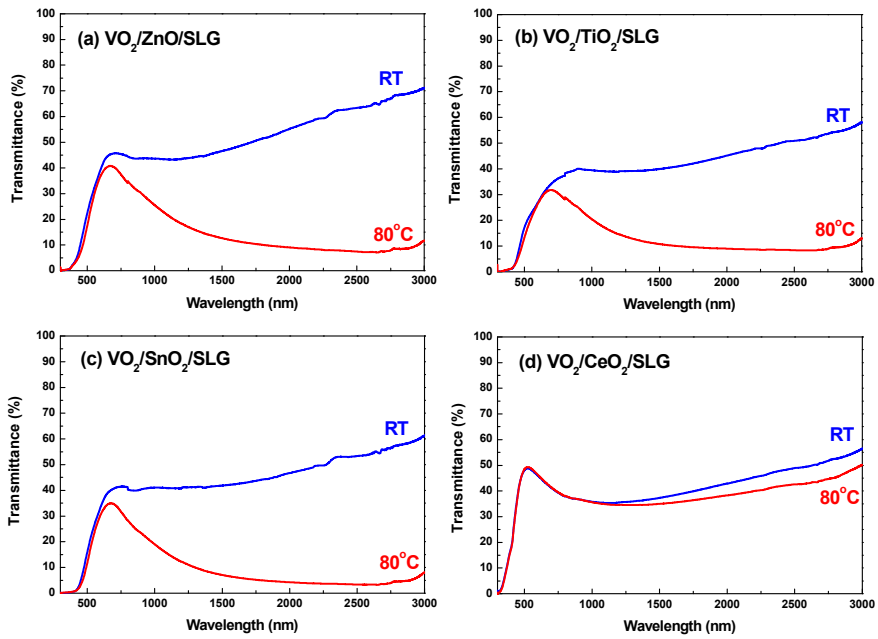

Figure 7-3. Spectral transmittance for the semiconductor phase at room temperature and metal phase at 80℃ of VO_2 films deposited on buffer layers

(a) ZnO; (b) TiO_2; (c) SnO_2; (d) CeO_2

Table 7-1. Structures and lattice parameters of buffer layers and VO_2

	Structure	**Lattice parameters (nm)**	**VO_2**
ZnO	Hexagonal	a 0.325; c 0.5201	Tetragonal a 0.4554 nm c 0.2856 nm
TiO_2	Tetragonal	R - a 0.4593; c 0.2959 A - a 0.3752; c 0.9514	
SnO_2	Tetragonal	a 0.4738; c 0.3187	
CeO_2	Cubic	a 0.5411	

Table 7-2. Thermochromic transition characteristics of VO_2 films deposited on ZnO, SnO_2 and TiO_2 buffer layers.

	ZnO	**SnO_2**	**TiO_2**
Transition temperature (T_c)	64℃	62℃	61℃
Resistivity change (ΔR)	6×10^2	4×10^2	1×10^2
IR transmittance change (ΔT%)	56%	49%	43%
Sharpness of transition (ΔS)	8℃	9℃	10℃
Hysteresis width (ΔH)	7℃	11℃	15℃

Chapter 8. Effect of deposition power on the thermochromic properties of VO_2 thin film by Sputtering

8.1 Introduction

Thermochromic smart window enables automatic solar/heat control in response to ambient temperature. For the materials, vanadium dioxide (VO_2) has been widely studied as the coating material of thermochromic smart window. The principle of thermochromic smart window is based on the structural phase transition of VO_2. At the phase transition temperature of ~68°C which is called critical temperature (T_c), VO_2 experiences a reversible structural transformation from low-temperature insulating monoclinic phase (VO_2(M)) to high temperature metallic rutile phase (VO_2(R)), which is called metal-insulator transition (MIT), first reported by Morin *et al*. in 1959[1]. This transition involves abrupt changes of electrical and optical properties of VO_2, which enables this material to be applied in thin-film form to not only thermochromic smart window, but many other devices including optical switch, optical recording device, field effect transistor (FET) and varistor [2-4].

To evaluate the appropriateness of electrical/optical properties of VO_2 thin films for practical application, four major factors are generally considered, which are

transtion temperature(T_c), amplitude of transition (ΔA), sharpness of transition (ΔS), and hysteresis width(ΔH). These characteristics of VO_2 thin films have been known to be a strong function of microstructure (grain size distribution and grain boundary characteristics) and chemistry (stoichiometry, dopant and/or other defects). However, the individual effect of these factors on the MIT parameters is not well understood as films studied in most of these cases were polycrystalline, includes oxide phases (e.g. V_2O_5 or V_2O_3), or dopants present in the films which is likely to produce a combined effect of all these parameters in modification of MIT characteristics.[5,6,7,8] Therefore, there is a major challenge in producing VO_2 thin films of correct structure, stoichiometry and controlled microstructures, especially high-quality single crystal films, which can be used to establish comprehensive structure-property correlations.

In this work, in order to induce microstructural difference between each sample, different RF power was applied. The influence of the microstructural difference on the thermochromic properties of the VO_2 thin films was analyzed. All the films were deposited on soda-lime glass (SLG) substrate by RF sputtering.

8.2 Experimental procedure

VO_2 thin films were deposited on 10mm x 10mm sized fused silica substrate by RF sputtering. The substrates were cleaned prior to the deposition process by washing with acetone, ethanol, and distilled water in ultrasonic bath for 10 minutes each which was followed by blowing with nitrogen. 3" Φ V_2O_5 target was used for the deposition with 200~400W of RF power applied at room temperature. The deposition time was varied in order to obtain films with similar film thicknesses, 30, 20, and 15minutes for 200W, 300W, and 400W respectively. During the deposition process, argon(Ar) gas was injected with 100sccm flow rate, maintaining 20mTorr of pressure in the chamber. The deposited films were post annealed at 550℃ with oxygen pressure of 10mTorr for 30 minutes.

After the annealing process, X-ray diffraction(XRD) patterns were obtained from Bruker D8-Advance θ-2θ diffractometer using Cu-Kα radiation and Ge111 monochromator. The thicknesses of the film and the deposition rates were determined by alpha step measurement, as shown in Figure 8-1 and Table 8-1. The grain size and the microstructure of VO_2 thin films were observed by transmission electron microscope(TEM).

The optical transmittance of the thin film samples was measured by VARIAN

CARY5000 UV-VIS-NIR spectrometer with additional home-made heating stage. In order to determine T_c of each sample accurately, the temperature during the measurement was calibrated by attaching a thermocouple on the surface of each substrate. T_c value of VO_2 thin film has been obtained by calculating the center of the derivative curve of the heating curve.

8.3 Results and discussions

Figure 8-2 shows the θ-2θ XRD patterns of the VO_2 thin films deposited with powers varying 200W, 300W, and 400W on fused silica substrates, respectively. All the samples had high intensity regardless of the power difference and the amorphous nature of fused silica substrate, showing preferred oriented growth of 2θ position near 27.8º which come from diffractions at (011) plane of VO_2(M) phase. No other peaks other than representing (011) plane were shown in the XRD analysis results from $10^o \leq 2\theta \leq 90^o$, which were not shown in Figure 8-2.

In order to estimate the grain size of the thin films, calculation was performed

using Scherrer's formula:

$$t = \frac{0.9\lambda}{B\cos\theta_B}$$

The calculated crystallite size of the each sample is shown in Table 8-1. As the deposition power increased from 200W to 400W, the calculated crystallite size decreased. Generally, when the number of particles that reach to the substrate from the target increases, the probability of the particles becoming to be nucleation sites increases, and the grain size can be small.[9,10] When deposition power increases two main factors can be changed. One is the energy of the particles from the target, and the other is the number of particles from the target. Therefore, it can be said that the number of particles from the target increases with increasing deposition power, and thus the grain size of the high-power deposited film can be smaller compared to that of low-power deposited film. It has been reported that the grain size of ZnO thin film decreased with increasing RF sputtering power.[9] It is speculated that with high RF power, the zinc atoms have more opportunity to reach the substrates and increase the probability of forming nuclei. More nuclei existing on the substrate implies more sites for grain growth. It means a large number of small grains can grow simultaneously and finally result in small grain structure.

The actual grain size of the VO_2 thin film of each sample was confirmed by TEM

analysis, as shown in Figure 8-3. As the deposition power increased from 200W to 400W, the grain size decreased from approximately 50nm to 25nm. The linear relationship between the calculated crystallite size and the actual grain size from TEM analysis is plotted in Figure 8-4.

The optical transmittance of each sample with increasing temperature is shown in Figure 8-5. The observed thermochromic properties of VO_2 films deposited by applying 200W, 300W, and 400W of RF power are summarized in Table 8-1. The transition temperature (T_c) is defined as the center of the derivative curve of the heating curve in Figure 8-5. The sharpness of transition (ΔS) is characterized by the full width at half maximum (FWHM) of the derivative curve. And the hysteresis width (ΔH) is the difference between the T_c values measured during the heating and cooling cycles. As the deposition power increased, the hysteresis width of the VO_2 thin film decreased. J.Y. Suh et al.[11] found that the ΔH became larger when the grains grew in size. This contradiction was explained by the hypothesis that MIT in VO_2 can be described on the model of a martensitic transformation in which the density of heterogeneous nucleation centers, such as structural defects, oxygen vacancies, or grain boundaries as well, plays the essential role in the phase transformation. Therefore, the ΔH becomes narrow in the films with small granules because the phase transition can easily occur in this highly defective structure. Moreover, a clear relationship between ΔH and degree of misorientation has also

been observed. The degree of crystallographic misorientation between adjacent grains has been reported to be related to the sharpness of the transition.[12] Metallic regions can be effectively propagated without additional energy loss when the grain boundary misorientation angles are small, which can lead to narrow ΔH.

As shown in Figure 8-6 and by considering all the results above, it can be concluded as follows; the grain size can be controlled by changing deposition power applied to the target, and the grain size can affect the hysteresis width of the VO_2 thin film.

8.4 Summary

The VO_2 films were deposited on fused silica with different sputtering power. The grain size of each sample was calculated and measured using XRD, Scherrer's formula, and TEM analysis. As the sputtering power increases, the grain size of VO_2 film decreased. Hysteresis width can be affected by the grain size of the VO_2 film. Hysteresis width tends to decrease while increasing sputtering power. The results suggest that grain size can be controlled by changing sputtering power, and can effectively control the hysteresis width of the VO_2 film.

8.5 References

[1] F. Morin, *Oxides which show a metal-to-insulator transition at the Neel temperature*, Physical Review Letters, 3 (1959) 34-36.

[2] M. Soltani, M. Chaker, E. Haddad, R.V. Kruzelesky, *Thermochromic vanadium dioxide smart coatings grown on Kapton substrates by reactive pulsed laser deposition*, J Vac Sci Technol A, 24 (2006) 612-617.

[3] B.J. Kim, Y.W. Lee, S. Choi, S.J. Yun, H.T. Kim, *VO_2 Thin-Film Varistor Based on Metal-Insulator Transition*, Ieee Electron Device Letters, 31 (2010) 14-16.

[4] W. Burkhardt, T. Christmann, S. Franke, W. Kriegseis, D. Meister, B.K. Meyer, W. Niessner, D. Schalch, A. Scharmann, *Tungsten and fluorine co-doping of VO_2 films*, Thin Solid Films, 402 (2002) 226-231.

[5] Y.L. Wang, M.C. Li, L.C. Zhao, *The effects of vacuum annealing on the structure of VO_2 thin films*, Surface and Coatings Technology 201 (2007) 15

[6] O. Ya. Berezina, A.A. Velichko, L.A. Lugovskaya, A.L. Pergament and G.B. Stefanovich, *Metal-semiconductor transition in nonstoichiometric vanadium dioxide films*, Inorganic Materials 43 (2007) 505

[7] W. Yin, S. Wolf, C. Ko, S. Ramanathan, and P. Reinke, *Nanoscale probing of*

electronic band gap and topography of VO_2 thin film surfaces by scanning tunneling microscopy, J. Appl. Phys. 109 (2011) 024311

[8] G. Fu, A. Polity, N. Volbers, B.K. Meyer, *Annealing effects on VO_2 thin films deposited by reactive sputtering*, Thin Solid Films 515 (2006) 2519

[9] Y.M. Lua, W.S. Hwang, W.Y. Liu, J.S. Yang, *Effect of RF power on optical and electrical properties of ZnO thin film by magnetron sputtering*, Materials Chemistry and Physics 72 (2001) 269

[10] A Zendehnam, M Ghanati and M Mirzaei, *Study and comparison of deposition rates, grain size of Ag and Cu thin films with respect to sputtering parameters, and annealing temperature*, Journal of Physics: Conference Series 61 (2007) 1322

[11] J.Y. Suh, R. Lopez, L.C. Feldman, R.F. Haglund Jr., Semiconductor to metal phase transition in the nucleation and growth of VO_2 nanoparticles and thin films, J. Appl. Phys. 96 (2004) 1209-1213.

[12] J.F. De Natale, P.J. Hood, A.B. Harker, Formation and characterization of grain-oriented VO_2 thin films, J. Appl. Phys. 66(1989) 5844-5850

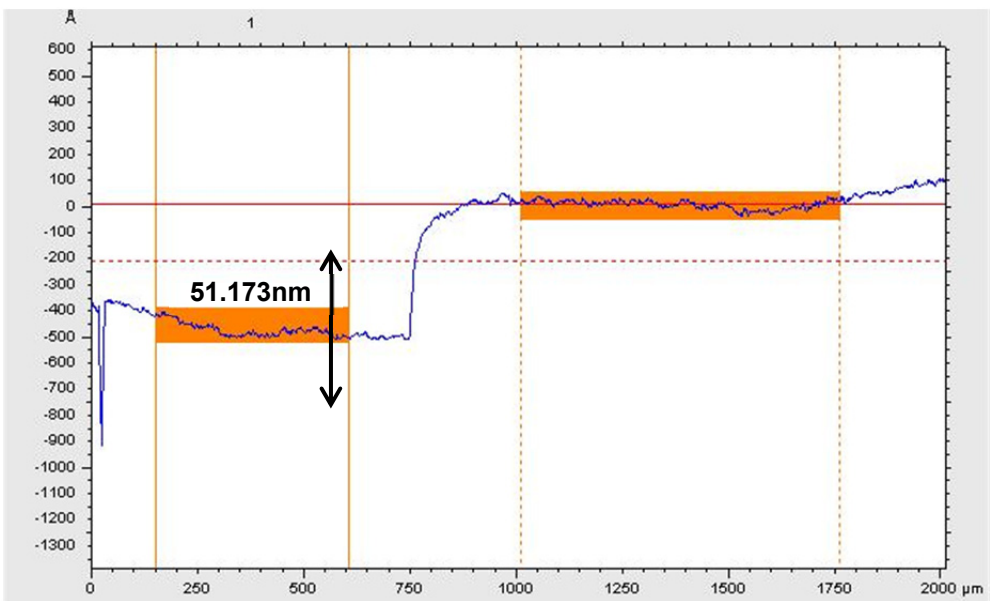

Figure 8-1. Alpha-step measurement result of VO_2 thin film deposited by applying RF power of 300W.

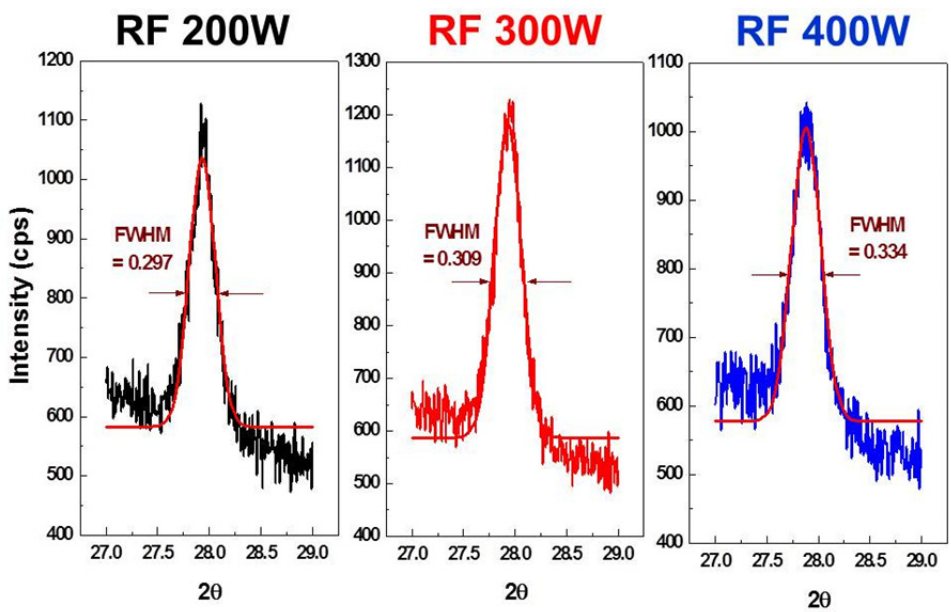

Figure 8-2. XRD analysis results of VO_2 thin films on fused silica substrate deposited by (a) 200W, (b) 300W, and (c) 400W of RF sputtering.

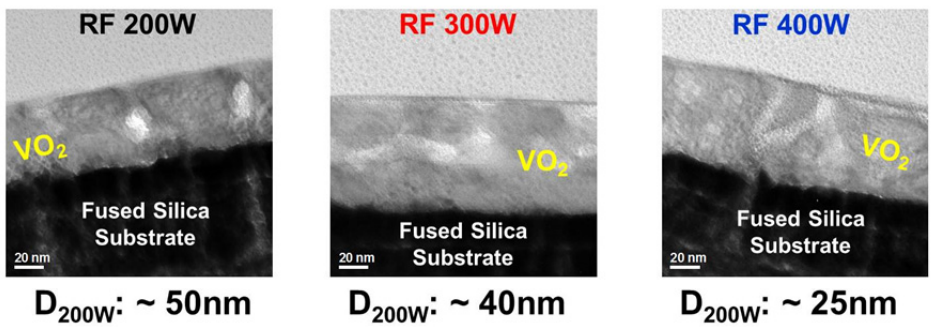

Figure 8-3. Transmission electron microscope(TEM) images of VO2 thin films on fused silica substrate deposited by (a) 200W, (b) 300W, and (c) 400W of RF sputtering.

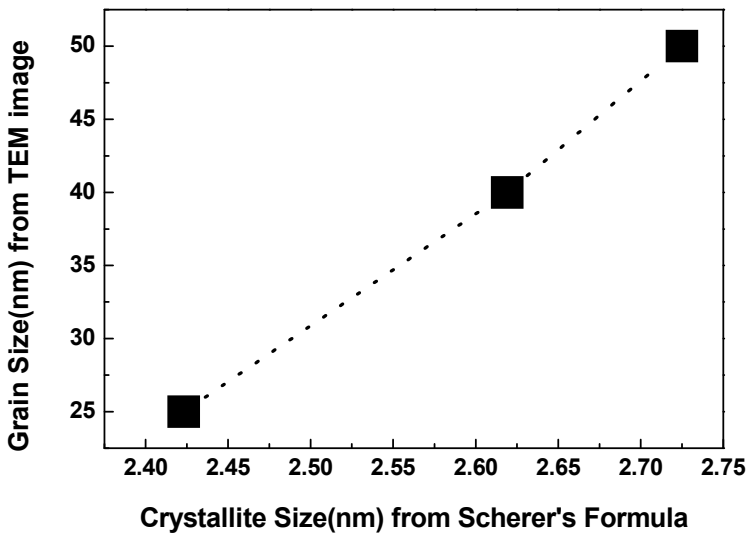

Figure 8-4. The linear relationship between the calculated crystallite size and the observed grain size of the VO_2 thin films

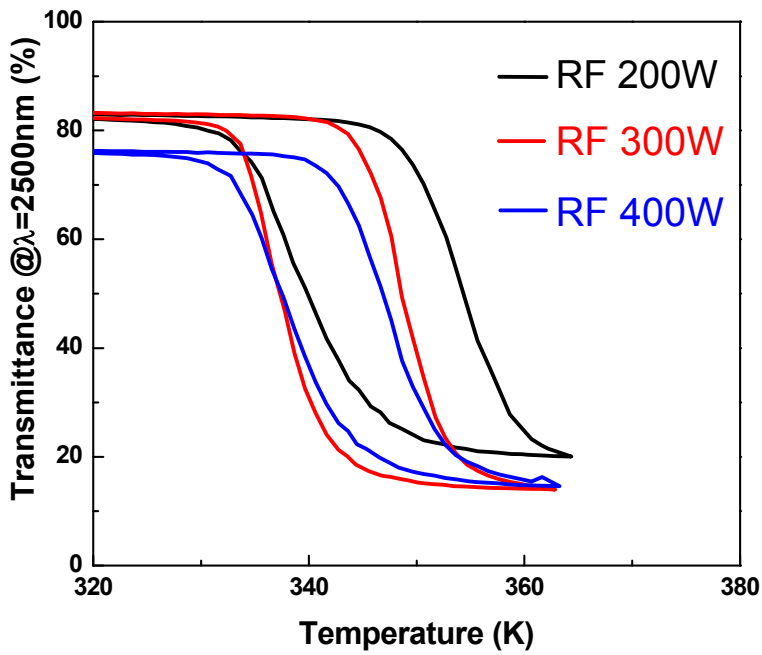

Figure 8-5. Optical transmittance(@λ=2500nm) of VO_2 thin films deposited by applying 200W, 300W, and 400W of RF power.

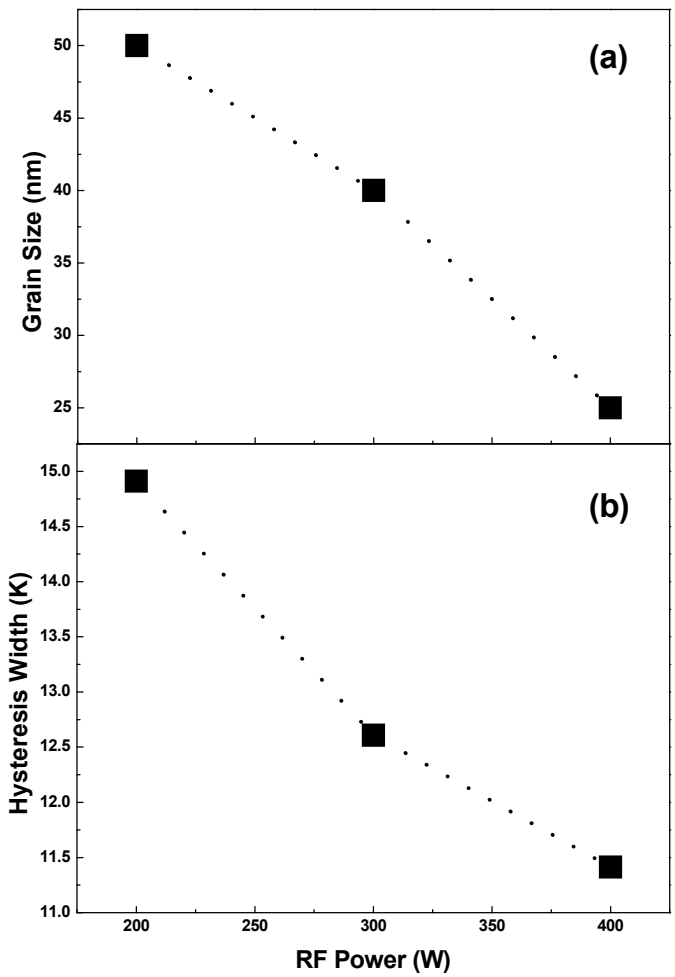

Figure 8-6. (a) Grain size and (b) hysteresis width of the VO_2 thin films with respect to deposition power

Table 8-1. Film thickness and deposition rate with RF power from 200-400W

RF Power	Deposition time	Film thickness	Deposition Rate
200W	30min	48.304nm	1.61nm/min
300W	20min	51.173nm	2.56nm/min
400W	15min	49.621nm	3.31nm/min

Table 8-2. Crystallite size and thermochromic properties of VO2 thin films deposited by RF sputtering of 200, 300, and 400W

RF Power (W)	**Calculated crystallite size (nm)**	**Observed grain size (nm)**	**Transition Temperature (K)**	**Amplitude of Transition (%)**	**Hysteresis Width (K)**
200W	2.76	50	346.7	59.7%	14.91
300W	2.61	40	343.7	67.3%	12.61
400W	2.42	25	343.5	62.4%	11.41

Chapter 9. Summary and suggestions for future work

The research presented in this dissertation focused on controlling thermochromic properties of vanadium dioxide (VO_2) by selecting appropriate substrate or buffer layer materials and controlling processing parameters. The metal-to-insulator transition in VO_2 and associated drastic changes in resistance render VO_2 very interesting scientifically and technologically for applications in thermochromic smart windows. Therefore, the integration of VO_2 on the soda lime glass substrate, the mainstay substrate of glass industry, has significant merit towards realization of commercial usage. In the present study, pulsed laser deposition (PLD) technique was used to epitaxially grow VO_2 on MgO (111), c-Sapphire, and soda lime glass substrates with ZnO, TiO_2, SnO_2, and CeO_2 buffer layers. Also, radio frequency magnetron sputtering was used to deposit highly crystallized VO_2 thin film on fused silica and SiN_x buffered soda lime glass substrates. The crystal structure of VO_2 transforms from high-temperature rutile to low-temperature complex monoclinic structure involving pairing of V-atoms along rutile c-axis. Therefore, integrating and achieving high-quality monoclinic VO_2 films on hexagonal or cubic substrates were also an achievement of this research work. We have investigated the effect of lattice misfit between the thin film and the substrate on the transition

temperature of VO_2 thin film by depositing VO_2 thin films on c-cut sapphire and MgO (111) substrate using pulsed laser deposition method. All vanadium dioxide thin films showed heteroepitaxial growth with (002) preferred orientation. VO_2/c-sapphire and VO_2/MgO(111) had different transition temperatures, regardless of the thickness, orientation, and deposition conditions of the thin film. These results suggest that considering lattice mismatch between thin film and substrate is another promising option for controlling transition temperature of VO_2 thin films.

To implement the transition temperature controlled VO_2 thin film on soda lime glass, however, VO_2 thin films should be deposited on soda lime glass substrates. To successfully deposit highly crystallized VO_2 thin films on soda lime glass, preventing sodium ion diffusion is necessary. Therefore, silicon nitride thin film was introduced as a diffusion barrier. SiN_x layers with thicknesses over 30 nm were found to successfully prevent sodium ion diffusion in VO_2 thin film and also contribute to the formation of VO_2 thin film, which was confirmed by XRD spectra and XPS measurements. The change of infrared transmittance at 2500 nm wavelength with temperature change from room temperature to 80^{o}C was increased significantly, and the optical hysteresis width of the sample decreased by almost 6K as well. The results suggest that applying diffusion barrier can improve the thermochromic properties of the VO_2 films for energy-saving smart coatings, and silicon nitride can be one of the effective materials to prevent sodium ion diffusion.

By considering both results mentioned above, it can be concluded that the selection of appropriate buffer layer material is very important. By comparing the thermochromic VO_2 thin films on different buffer layers, we have studied the relationship between the VO_2 thin film and the buffer layer. VO_2 thin films were deposited on soda lime glass substrates with ZnO, TiO_2, SnO_2 and CeO_2 thin films applied as buffer layers between the VO_2 films and the substrates in order to investigate the effect of buffer layer on the formation and the thermochromic properties of VO_2 film. Buffer layers with thicknesses over 50 nm were found to affect the formation of VO_2 film, which was confirmed by XRD spectra. By using ZnO, TiO_2 and SnO_2 buffer layers, monoclinic VO_2 (VO_2(M)) film was successfully fabricated on soda lime glass at 370^{o}C. On the contrary, films of VO_2 (B) which is known to have no phase transition near room temperature was formed rather than VO_2 (M) when the film was deposited on CeO_2 buffer layer at the same film deposition temperature. The excellent thermochromic properties of the films deposited on ZnO, TiO_2 and SnO_2 buffer layers were confirmed from the temperature dependence of electrical resistivity from room temperature to 80^{o}C. Especially, due to the tendency of ZnO thin film to grow with high degree of preferred orientation on soda lime glass at low temperature, the VO_2 film deposited on ZnO buffer layer exhibits the best thermochromic properties compared to those on other buffer layer materials used in this study. These results suggest that

deposition of VO_2 films on soda lime glass at low temperature with excellent thermochromic properties can be achieved by considering the buffer layer material having structural similarity with VO_2. Moreover, the degree of crystallization of buffer layer is also related with that of VO_2 film, and thus ZnO can be one of the most effective buffer layer materials.

Finally, we studied the effect of deposition power on the microstructure and thermochromic properties of VO_2 thin films. To correlate the property changes with change in grain size upon deposition power, the thickness, crystallinity, and phase purity of the VO_2 thin film was preserved. We observed the hysteresis width decrease as the deposition power increased. The increment of deposition power also led to modification of transition temperature change. From the literature review and on the basis of research work presented here, some suggestions for the further work can be made. They are as follows:

1. Potential of other buffer layer materials can be explored and further understanding of structure-property correlations can be established. In this research, only silicon nitride was studied as a diffusion barrier, and most of the buffer layer materials applied in this dissertation were oxide materials. However, it is possible that nitrides can be good buffer layer materials as well. For example, titanium nitride (TiN) is one of buffer layers that can be used to grow epitaxial VO_2 films. Furthermore, TiN can be deposited on soda lime glass and subsequently, it can be

partially oxidized to form epitaxial TiO_2 which can be used as a template to grow epitaxial VO_2 films.

2. It will be worthwhile to manufacture large area deposited VO_2 based thermochromic glass utilizing VO_2/buffer layer/soda lime glass heterostructure with buffer layer working as a diffusion barrier as well and VO_2 as a thermochromic layer. The thermochromic properties of VO_2 films deposited on small sized substrate have been studied widely. However, depending on the deposition conditions, uniformity can be a problem for successful deposition of VO_2 thin film on large sized substrates. Layer thicknesses and growth conditions can be further optimized to achieve the best uniformity and thermochromic properties.

3. The effect of deposition power on the doping level of tungsten in $W_xV_{1-x}O_2$ thin film should be studied further. By far, tungsten doping is known as the most effective method of controlling transition temperature of VO_2 thin film. According to the results from our work (which were not introduced in this dissertation) and recently reported literatures, doping level of thin films using sputtering can be affected by deposition power. Detailed experiments are worth performing to extract information about deposition power in tungsten doped VO_2 thin film deposition.

4. The direct comparison of energy saving efficiency between VO_2 based thermochromic window and other energy saving windows should be made. Up to

now, most of the literatures have used the amplitude of transition to be the main factor that affects the energy saving efficiency. Recently, some of the literatures have suggested the methods of evaluating the energy saving efficiency of VO_2 based thermochromic glass. However, systematic experiments and analyses are required to apply VO_2 thin film to thermochromic smart coating practically.

Publications

1. **Hyun Koo**, Lu Xu, Kyeong-Eun Ko, Seunghyun Ahn, Se-Hong Chang, and Chan Park, “Effect of oxide buffer layer on the thermochromic properties of VO_2 thin films,” Journal of Materials Engineering and Performance, Submitted (2013)

2. Seunghyun Ahn, **Hyun Koo**, Sung-Hwan Bae, Chan Park, GuYoung Cho, IkWhang Chang, Suk-Won Cha, Young-Sung Yoo, “Effect of nickel contents on the microstructure of mesoporous nickel oxide/gadolinium-doped ceria for the anode of solid oxide fuel cells,” Functional Materials Letters , Submitted (2013)

3. **Hyun Koo**, Dongmin Shin, Sung-Hwan Bae, Kyeong-Eun Ko, Se-Hong Chang, and Chan Park, “The effect of CeO_2 antireflection layer on the optical properties of thermochromic VO_2 film for smart window system,” Journal of Materials Engineering and Performance, Submitted (2013)

4. Sung-Hwan Bae, Sangmin Lee, **Hyun Koo**, Long Lin, Bong Hyun Jo, Chan Park and Zhong Lin Wang, "Single VO_2 nanowire based memristor and switch controlled by self heating," Advanced Materials, Accepted (2013)

5. Seunghyun Ahn, **Hyun Koo**, Sung-Hwan Bae, Ikwhang Chang, Sukwon Cha, Young-sung Yoo, and Chan Park, “The Grain Growth Behavior of NiO in

Thermally-stable Mesoporous Gadolinium-doped Ceria Network for Intermediate Temperature SOFC Anode Materials," Journal of Nanoscience and Nanotechnology, Submitted (2012)

6. **Hyun Koo**, HyunWoo You, Kyeong-Eun Ko, O-Jong Kwon, Se-Hong Chang, and Chan Park, "Thermochromic Properties of VO_2 thin film on SiN_x buffered glass substrate," Applied Surface Science, 277 (2013) 237-241

7. **Hyun Koo**, Sejin Yoon, O-Jong Kwon, Kyeong-Eun Ko, Dongmin Shin, Sung-Hwan Bae, Se-Hong Chang, Chan Park, "Effect of lattice misfit on the transition temperature of VO_2 thin film," Journal of Material Science, 47 (2012) 6397-6401

8. Il Hwan Yoo, Sung-Hwan Bae, **Hyun Koo**, O-Jong Kwon, Jaeun Yoo, Sukill Kang, Chan Park, "Electrical and Optical Properties of Amorphous (In,Sn)-Ga-Zn-O Thin Film," Journal of Nanoscience and Nanotechnology, 12 (2012) 3673-3676

9. O-Jong Kwon, Wook Jo, Kyeong-Eun Ko, Jae-Yeol Kim, Sung-Hwan Bae, **Hyun Koo**, Seong-Min Jeong, Jin-Sang Kim, Chan Park, "Thermoelectric properties and texture evaluation of $Ca_3Co_4O_9$ prepared by a cost-effective multisheet cofiring technique," Journal of Materials Science, 46 (2011) 2887-2894

10. O-Jong Kwon, Jonglo Park, Ju-Hyuk Yim, **Hyun Koo**, Jae-Yeol Kim, HyunWoo You, Sung-Hwan Bae, Jin-Sang Kim, Chan Park, "The effect of

microstructure on the thermoelectric properties of Bi_2Te_3-PbTe alloy," Current Applied Physics, 11 (2011) S242-S245

국문 초록

기판과 공정변수가 스마트 윈도우 적용을 위한 이산화바나듐 박막의 열변색 특성에 미치는 영향

구 현

공과 대학 재료공학부

서울대학교

기판과 공정변수가 이산화바나듐(VO_2) 박막에 미치는 영향을 알아보기 위하여, VO2 박막을 pulsed laser deposition법과 radio frequency magnetron sputtering법에 의하여 다양한 단결정과 완충층이 적용된 유리 기판 위에 증착하였다.

먼저, 격자 불일치가 VO_2 박막의 상전이 온도에 미치는 영향을 알아보

기 위하여, VO_2 박막을 c-cut sapphire와 MgO(111) 단결정 기판위에 pulsed laser deposition법을 사용하여 증착하였다. 모든 VO_2 박막은 (002)면과 평행하게 heteroepitaxial 한 성장을 보였다. Sapphire와 MgO에 증착된 VO_2 박막은 동일한 두께, 배향성, 그리고 증착조건에서 제조되었음에도 불구하고, 각각 다른 상전이 온도를 보였다. 이러한 결과는 박막과 기판간의 격자 불일치를 고려하는 것이 VO_2 박막의 상전이 온도를 조절하는 방법 중 하나임을 제시하는 것으로 볼 수 있다.

두번째로, 알칼리 이온의 확산을 방지하는 것이 VO_2 박막의 상 형성에 어떠한 영향을 미치는 지 알아보기 위하여, 질화규소 박막이 증착된 soda lime glass위에 VO_2 박막을 증착하였다. 30nm 이상의 질화규소 박막이 확산 방지층으로 적용된 soda lime glass기판을 사용하였을 경우, XRD와 XPS 분석을 통하여 알칼리 이온의 확산이 성공적으로 방지되었고 이에 따라 VO_2 박막의 성공적인 증착에 기여하였음을 알 수 있었다. 상온에서부터 80^{o}C 까지 온도를 변화시키며 2500nm 파장의 적외선 투과도 변화 폭이 크게 증가하였고, hysteresis width 역시 6 ^{o}C 정도 줄어들었다. 이러한 결과는 확산 방지층을 적용하는 것이 VO_2 박막의 열변색 특성을 개선하여 에너지 절약형 스마트 코팅에 적용하기에 적합하도록 기여하고, 질화규소 박막이 확산방지층으로 적합한 재료임을 보여준다.

세번째로, ZnO, TiO_2, SnO_2, CeO_2 박막을 완충층으로 적용한 soda lime glass위에 VO_2 박막을 증착하여 산화물 완충층이 VO_2 박막의 상형성과 열변색 특성 변화에 미치는 영향을 알아보았다. 50nm이상의 완충층은 VO_2박막의 상형성에 영향을 미치는 것이 XRD분석을 통하여 확인되었다. ZnO, TiO_2, SnO_2의 경우 열변색을 보이는 VO_2(M) 상을 형성하는데 크게 기여하였지만, CeO_2의 경우에는 열변색을 보이지 않는 VO_2(B) 형성을 도운 것으로 확인되었다. ZnO, TiO_2, SnO_2완충층 적용 시, VO_2박막의 열변색 특성은 우수하였으며, 특히, ZnO의 경우 높은 결정성과 함께 가장 우수한 열변색 특성을 가졌다. 이러한 결과는 VO_2박막을 soda lime glass위에 증착함에 있어서, 완충층의 구조적 유사성이 VO_2박막 형성에 기여하고, 결정성이 좋은 완충층일수록 VO_2 박막의 결정성과 열변색 특성을 크게 향상시킨다는 것을 의미한다.

마지막으로, 공정변수가 VO_2 박막의 열변색 특성에 미치는 영향을 알아보기 위하여, 증착 파워를 달리하여 VO_2 박막을 증착하였다. VO_2 박막의 결정립 크기는 XRD측정 및 Scherrer의 식을 활용한 계산과 TEM 분석을 통하여 측정되었다. 증착파워가 증가함에 따라 VO_2박막의 결정립 크기는 감소하였고, hysteresis width는 결정립 크기에 비례하여 변화하였다. 이러한 결과는 RF sputtering으로 VO_2 박막을 증착할 경우, 증착파워

를 조절함에 따라 VO_2박막의 hysteresis width를 효과적으로 조절할 수 있음을 의미한다.